DAA/LEWIS

R84-926376-15

NASA

DEMONSTRATION TEST OF BURNER LINER STRAIN MEASURING SYSTEM

by
Karl A. Stetson

UNITED TECHNOLOGIES RESEARCH CENTER

PREPARED FOR

NATIONAL AERONAUTICS AND SPACE ADMINISTRATION

NASA Lewis Research Center
Contract NAS 23690

NAS3-23690

Unclassified

SECURITY CLASSIFICATION OF THIS PAGE *(When Data Entered)*

REPORT DOCUMENTATION PAGE

READ INSTRUCTIONS BEFORE COMPLETING FORM

1. REPORT NUMBER: R84-926376-15 CR-174743	2. GOVT ACCESSION NO.
3. RECIPIENT'S CATALOG NUMBER	
4. TITLE *(and Subtitle)*: Demonstration Test of Burner Liner Strain Measuring System	5. TYPE OF REPORT & PERIOD COVERED: Draft Final Report
	6. PERFORMING ORG. REPORT NUMBER: 926376
7. AUTHOR(s): Karl A. Stetson	8. CONTRACT OR GRANT NUMBER(s): NAS3-23690
9. PERFORMING ORGANIZATION NAME AND ADDRESS: United Technologies Research Center, Silver Lane, East Hartford, CT 06108	10. PROGRAM ELEMENT, PROJECT, TASK AREA & WORK UNIT NUMBERS
11. CONTROLLING OFFICE NAME AND ADDRESS: NASA-Lewis Research Center, 21000 Brookpark Road, Cleveland, Ohio 44135	12. REPORT DATE: June, 1984
	13. NUMBER OF PAGES: 90
14. MONITORING AGENCY NAME & ADDRESS *(if different from Controlling Office)*: Same as above	15. SECURITY CLASS. *(of this report)*: Unclassified
	15a. DECLASSIFICATION/DOWNGRADING SCHEDULE

16. DISTRIBUTION STATEMENT *(of this Report)*

17. DISTRIBUTION STATEMENT *(of the abstract entered in Block 20, if different from Report)*

18. SUPPLEMENTARY NOTES

Project Manager: Frank G. Pollack
NASA Lewis Research Center;
Cleveland, Ohio 44135

19. KEY WORDS *(Continue on reverse side if necessary and identify by block number)*

High temperature strain measurement
Kanthal A-1 gages
Speckle photography

20. ABSTRACT *(Continue on reverse side if necessary and identify by block number)*

A demonstration test was conducted for two systems of static strain measurement that had been shown to have potential for application jet engine combustors. A modified JT12D combustor was operated in a jet burner test stand while subjected simultaneously to both systems of instrumentation, i.e. Kanthal A-1 wire strain gages and laser speckle photography. A section of the burner was removed for installation and calibration of the wire gages, and welded back into the burner. The burner test rig was modified to provide a viewing port

DD FORM 1 JAN 73 1473 EDITION OF 1 NOV 65 IS OBSOLETE
S/N 0102-LF-014-6601

Unclassified

SECURITY CLASSIFICATION OF THIS PAGE *(When Data Entered)*

JUL

for the laser speckle photography such that the instrumented section could be observed during operation. Six out of ten wire gages survived testing and showed excellent repeatability. The extensive precalibration procedures were shown to be effective in compensating for the large apparent strains associated with these gages. Although all portions of the speckle photography system operated satisfactorily, a problem was encountered in the form of optical inhomogeneities in the hot, high-pressure gas flowing by the combustor case which generate large and random apparent strain distributions.

ABSTRACT

A demonstration test was conducted for two systems of static strain measurement that had been shown to have potential for application jet engine combustors. A modified JT12D combustor was operated in a jet burner test stand while subjected simultaneously to both systems of instrumentation, i.e. Kanthal A-1 wire strain gages and laser speckle photography. A section of the burner was removed for installation and calibration of the wire gages, and welded back into the burner. The burner test rig was modified to provide a viewing port for the laser speckle photography such that the instrumented section could be observed during operation. Six out of ten wire gages survived testing and showed excellent repeatability. The extensive precalibration procedures were shown to be effective in compensating for the large apparent strains associated with these gages. Although all portions of the speckle photography system operated satisfactorily, a problem was encountered in the form of optical inhomogeneities in the hot, high-pressure gas flowing by the combustor case which generate large and random apparent strain distributions.

FOREWORD

The work documented in this report was performed by the United Technologies Research Center for the National Aeronautics and Space Administration under Contract NAS3-23690. The principal investigator was K. A. Stetson, and the program was carried out in collaboration with T. J. Rosfjord of UTRC and with H. P. Grant and W. L. Anderson of the Pratt and Whitney Group.

Demonstration Test of Burner Liner Strain Measuring System

TABLE OF CONTENTS

Demonstration Test of Burner Liner Strain Measuring System

1.0 INTRODUCTION

1.1 Background

The components of the hot section of an aircraft engine are subjected to large transients in temperature and stress for durations of a few seconds to one or two minutes. These occur during engine startup and shutdown and during the engine accelerations and decelerations encountered in takeoff, landing, and other extreme maneuvers. During these transients, hot section components such as burner cans experience excursions of metal surface temperature through several hundred degrees to peak temperatures between 800K and 1300K. Strain due to loading and thermal distortion may range from 1000 to 10,000 microstrain which may briefly exceed the yield point of the metal. Repeated exposure to these transients may result in significant local plastic flow, work hardening, cracking, and catastrophic failure. This is described as low-cycle fatigue failure to differentiate it from other failure modes such as creep to rupture under steady loading or failure after millions of cycles of elastic vibration.

Improvement of low-cycle fatigue life through better design has been hampered by lack of any means, above about 650K, to measure large non-isothermal strains on small areas of components such as burner cans during the testing phase of engine development. The device most commonly employed to measure local strain is the small (1 mm to 3 mm length) resistive wire strain gage. Wire gages made from materials that are mechanically durable above 650K (noble metal alloys and alloys such as NiCr and FeCrAl that form self protective oxides) all suffer from extreme variations or anomalous behavior of electrical resistance with temperature and are also limited to a range of a few thousand microstrain. Historically, these gages have been used for measurement of low-amplitude dynamic (isothermal) strain amplitude at temperatures as high as 1350K. They have not been successfully employed, however, for the measurement of large, static (non-isothermal) strain of the type experienced by the hot section of a jet engine during low-cycle fatigue testing.

1.2 Objective

The objective of this program was to perform a demonstration test of two methods of strain measurement with potential for application to low-cycle fatigue testing of jet engine combustor liners. The potential had been established in laboratory tests under NASA Contract NAS3-22126. One method

employed Kanthal A-1 wire (0.025 mm dia) strain gages together with extensive precalibration procedures and the other employed laser speckle photographs and an interferometric photocomparator. The practical problems and limitations of these techniques were to be determined by testing them on an operating combustor in a high-pressure jet burner test stand. If either or both methods were successful, useful data would be obtained for the distributions of thermomechanical strain on a representative jet engine combustor.

1.3 Program Tasks and Management

The program consisted of six tasks that are listed as follows:

Task 1: Experiment Design and Test Plan Formulation
Task 2: Review of Experiment and Test Plan
Task 3: Preparation of the Experiment
Task 4: Test Performance and Analysis of Results
Task 5: Review of Test Results
Task 6: Preparation of Reports

1.4 Summary of Results

1.4.1 Speckle Photogrammetry - All systems associated with the speckle photography operated successfully. This included an optical quality window on the burner for illumination and observation of the burner, a telecentric lens, an open cavity pulsed laser synchronized to a camera shutter and a photographic plate transport. The photogrammetry system also performed successfully and provided automatic readout of strain distributions from speckle photographs. The major difficulty of the technique was identified as blurring and distortion of the speckle patterns due to inhomogeneities of the high pressure gas within the burner. This caused random values of high apparent strain to appear in the output and also caused decorrelation of the laser speckle patterns.

1.4.2 Kanthal A-1 Wire Strain Gages - The installation and calibration procedures for the Kanthal A-1 wire (0.025 mm dia.) strain gaging were successfully demonstrated. The special feature of the calibration procedure was the measurement of the change in strain gage resistance due to temperature (with no stress applied) during rapid cooling transients of spatially uniform temperature. These cooling rates were in the range to be encountered in the planned combustor tests and typical of low-cycle fatigue testing in engines (less than one minute). This procedure was employed to allow compensation for the strong dependence of Kanthal A-1 strain gage resistance change on the rate of change of temperature. To assure stress-free uniform cooling during these

tests the procedure involved removal of a section from the burner for installation of the gages and thermocouples, thermal measurement of apparent strain as a function of temperature and cooling rate for the installed gages, and welding the section back into the burner. Gage factors were successfully determined by separate gages fastened to a constant-strain calibration bar which was thermally cycled. Six of the ten gages installed on the burner liner survived all testing, with repeatability of strain change measurements generally better than ±200 microstrain at temperatures up to 950K (1250°F). The other four gages failed when accidentally exposed to an overtemperature of 1040K (1410°F). Comparison of measured strain changes to analytically predicted values showed general agreement in direction of changes, but only fair agreement in magnitudes (typically 700 microstrain disagreement). Temperature measurements of several additional locations are recommended in future tests to permit a more detailed analytical prediction of the strain field.

2.0 EXPERIMENT DESIGN AND TEST PLAN FORMULATION (TASK 1)

2.1 Preliminary Considerations

2.1.1 Selection of the Burner Can to be Tested - A version of a burner can designed for the P&W JT12 engine was selected for the present test (Fig. 1). This design is a type widely used in the industry and an existing test rig was available that required only minimal modification. Methods of analysis for predicting nonlinear strain had been developed under Contract NAS-21836 at P&W for this type of burner structure. The selection of this burner design presented an opportunity to compare predicted and measured strains in a program of reasonable cost. The performance of this burner can and the distribution of outside liner temperature were well documented in the previous contract (Fig. 2), and strains in the vicinity of a knuckle had been predicted (Fig. 3).

2.1.2 Definition of Test Area Location on the Burner Can - An area for the location of the strain gages and the speckle photo-grammetry was defined with respect to the burner configuration, previously measured temperature profiles, and estimated strain levels. Centering it approximately upon the knuckle of the third section (Fig. 4) and between four cooling holes would allow the 62 mm diameter field of view of the camera to cover an area from the midpoint of Section 2 to the midpoint of Section 3 and span about 1/6 of the burner circumference. Viewing access to the louver lip would be obtained through a hole in the burner. The peak temperatures were expected to be in the order of 755K on the knuckle, 950K at the end of Section 2, and nearly 1145K on the louver lip under the knuckle. Largest hoop strains were expected to be found on the knuckle, (location B), with magnitude of about 1/4 percent tensile.

2.1.3 Determination of the Number of Gages and Their Location - The number and location of the wire gages were to be chosen to allow duplication of each gage measurement for redundancy and for back-up in case of failure. Three axial locations were considered for mounting ten gages as described in Appendix A. The locations had to be picked to satisfy requirements for restricting the gage temperatures to less than 950K. Thermocouples were needed near each gage and on the louver lip. The lead wires had to be routed to keep them as much as possible out of the field of view of the speckle photography.

2.1.4 Ground Rules for Static Strain (Non-Isothermal) Measurement with Kanthal A-1 Strain Gages - The experiments carried out under NASA contracts NAS3-22126 and NAS3-23169 established a methodology for fabrication and calibration of static strain gages of Kanthal A-1 alloy wire. The alloy is stable

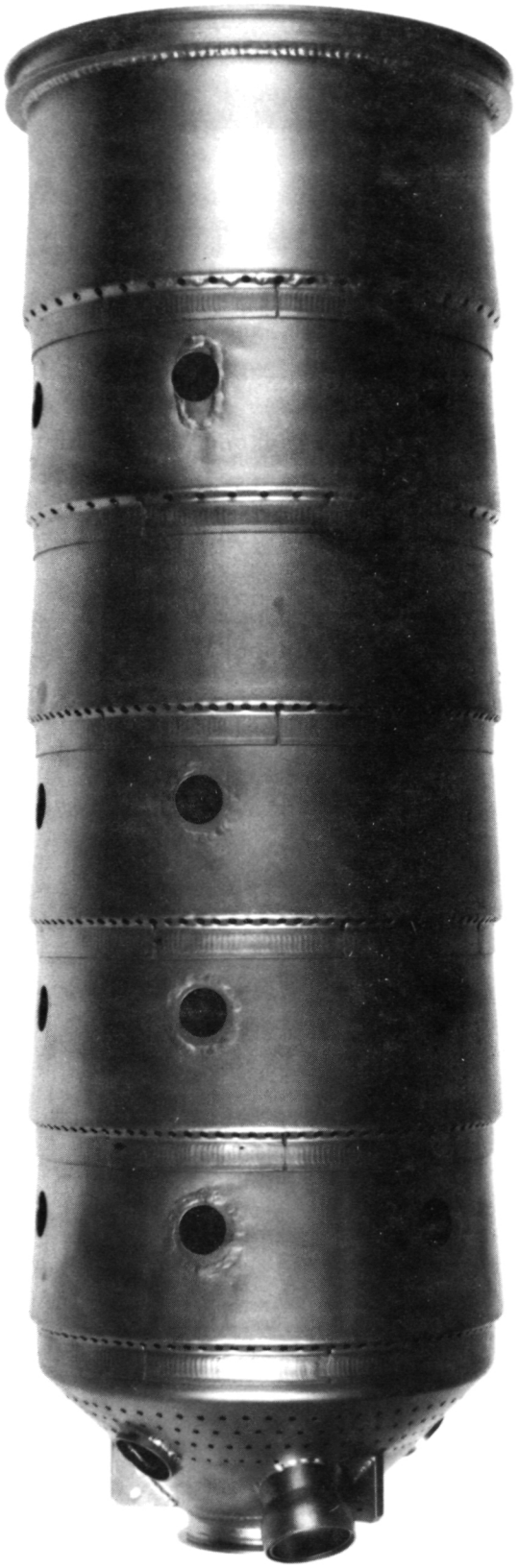

FIG. 1 JT12 BURNER CAN

FIG. 2 SURFACE TEMPERATURE PROFILES MEASURED ON JT12D BURNER LINER PROPOSED FOR NAS3-23690 TESTS

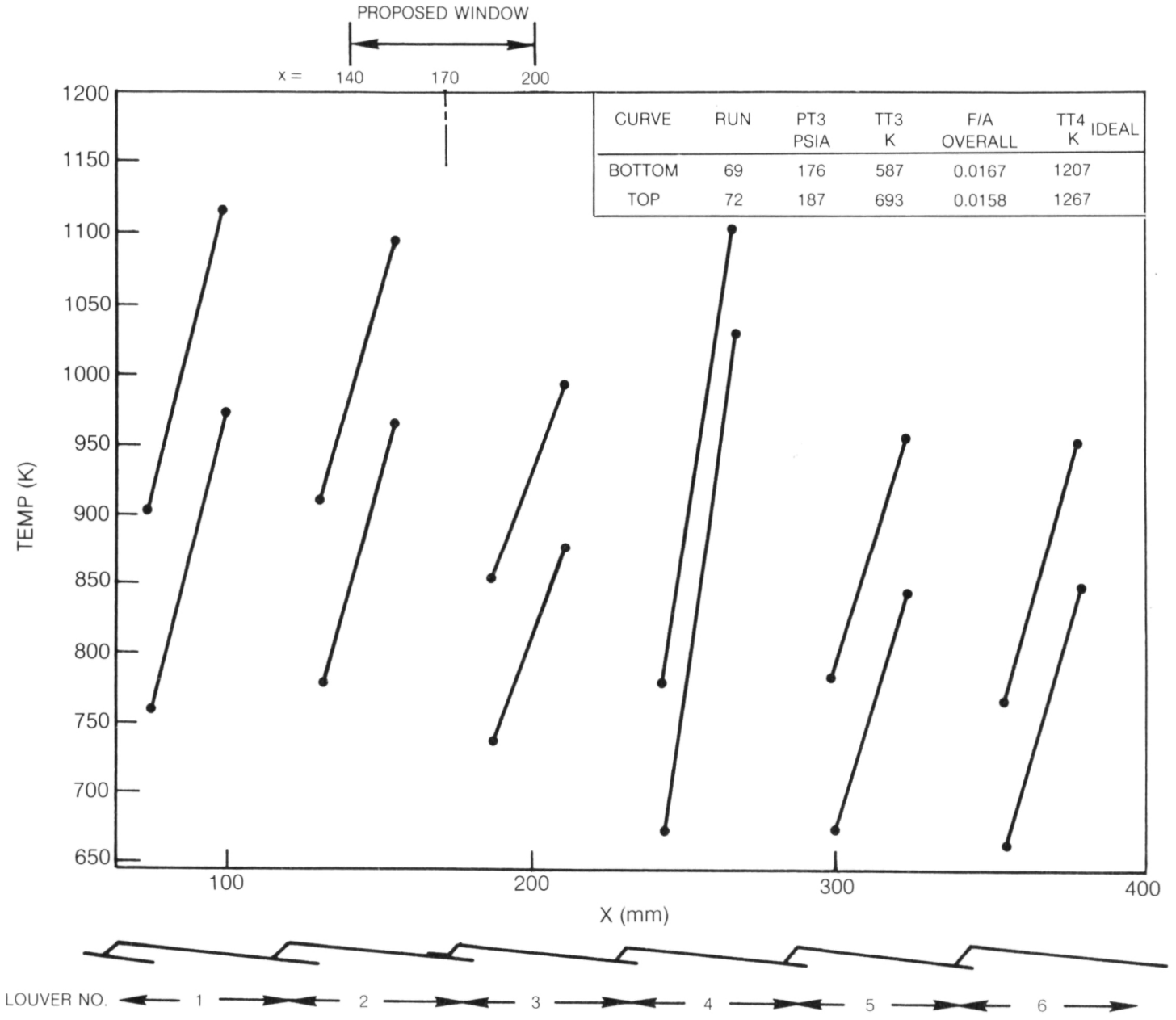

84-4-18-2

FIG. 3 STRAINS ESTIMATED FOR JT12D BURNER LINER IN VICINITY OF THIRD KNUCKLE

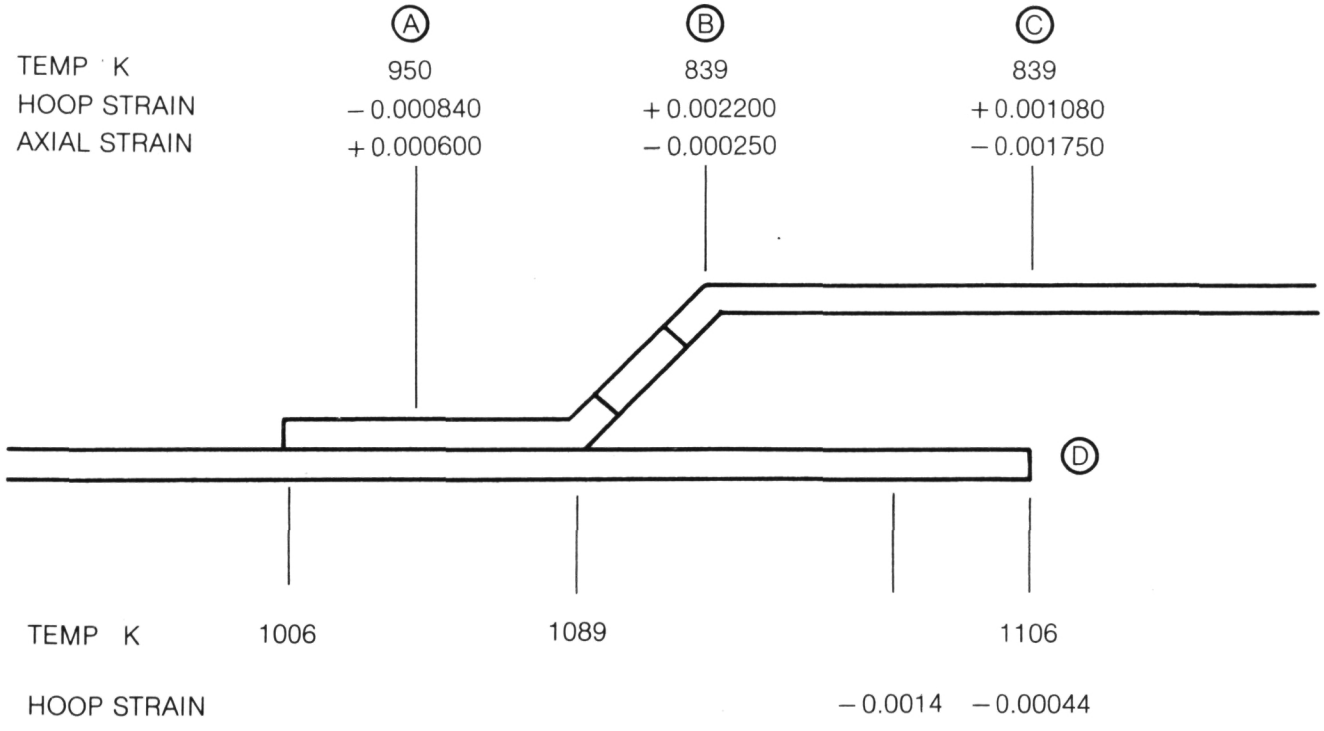

84–4–18–3

FIG. 4 JT12D BURNER LINER STRAIN MEASUREMENT LOCATIONS

ALL DIMENSIONS IN MM

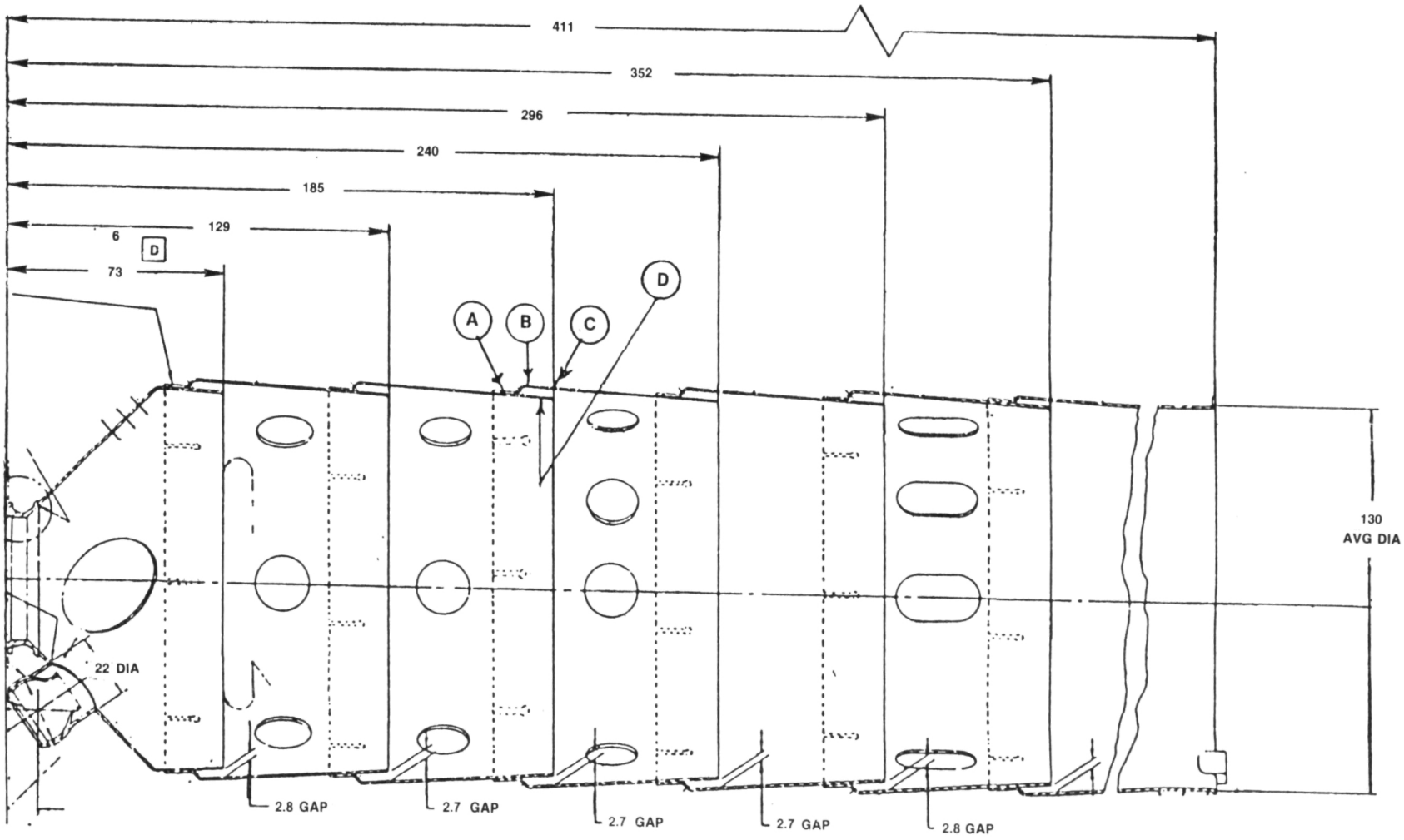

and oxidation resistant at any constant temperature from room temperature to 973K (1300°F). In this range, the apparent strain due to temperature is fairly large (6000 microstrain) but quite repeatable (±100 microstrain) from test to test as long as all tests are conducted at the same fixed heat-up rate and cool-down rate.

The problem in using Kanthal A-1 wire gages for static strain measurement centers on the strong effects (2000 microstrain) of changes in the cool-down rate and (to a lesser extent) the heat-up rate and the cycle end-point temperatures on the apparent strain due to temperature of the Kanthal A-1 wire.

The detailed behavior of the eighteen gages employed in the present program is presented in a later section, showing the effects of temperature and time during thermal cycles at various rates between various end-point temperatures. These tests confirm previous data of the reference contracts, which impose the following ground rules for accurate static strain measurement with Kanthal A-1 strain gages in engine tests at high temperatures:

a) The temperature of each strain gage must be monitored (±20K) by installing a nearby thermocouple.

b) The strain measurements must be confined to engine cycles in which the upper temperature of the strain gages does not exceed 977K (1300°F).

c) Above 500K, non-isothermal static strain measurement should be confined to measurement of strain change during fast cool-down only (one minute or less). Corrections for apparent strain due to temperature are smallest and most repeatable during fast cool-downs.

d) Each strain gage should be preconditioned by baking at 977K for about one hour. The apparent strain due to temperature for each strain gage should then be measured during uniform-temperature cool-down tests covering the range of cool-down rates and end-point temperatures expected in the engine test.

e) In the engine test each engine cycle should be repeated two or three times in succession to establish repeatability of all measurements.

These ground rules were taken into consideration in the design of the test program described below.

2.1.5 Determination of Viewing Port Construction and Location - A commercial source of window ports was located and a unit identified that was

compatible with an optical quality window. It would require sizing of a commercially available window, but at considerably less cost than fabrication of the port itself. Locating the window as close to the burner as possible would minimize aberrations. Illumination of the burner would be possible without significant shadowing, and reflections from the window surface would not pass through the telecentric lens.

2.1.6 Determination of Laser Operation Mode and Synchronization - Preliminary experiments established that open-cavity operation of a pulsed ruby laser provided laser pulses of adequate coherence and energy to record proper quality specklegrams on heat blackened Hastelloy X. This mode of operation would greatly enhance reliability and simplify alignment. It was also determined that the shutter located within the telecentric lens had a flash output that could be used to synchronize the firing of the ruby laser.

2.1.7 Characterization of Thermal Cycling - The general procedures for the thermal cycling were determined by the requirements for speckle photography and the temperature limitations of the Kanthal gages. Isothermal heating of the burner to about 700K by pre-heating the inlet air would be required for the specklegram recordings to provide continuity from ambient temperature to 700K. Spontaneous combustion would occur with the introduction of fuel at which time the logging of strain gage data would begin. Specklegrams would be recorded after ignition and periodically during the test cycling. The minimum time between specklegram recordings would be limited by the charging time for the laser to about 30 seconds.

2.2 Formulation of the Experiment Design and Test Plan

The considerations above resulted in the formulation of a design for the experiment and a formulation of the test plan. The complete plan is presented in Appendix A.

3.0 REVIEW OF THE EXPERIMENT DESIGN AND TEST PLAN (TASK 2)

A presentation was made at NASA Lewis Research Center on 25 March 1983 in which the details of the entire program were reviewed. The discussion included the following:

1. The choice of the JT12D burner
2. The test facility
3. The viewing port design and layout
4. Laser power and stability requirements
5. Optics layout and checkout procedures
6. The test cycling sequences
7. Specklegram data reduction
8. Anticipated strain and temperature profiles
9. Detailed strain gage and thermocouple layout
10. Strain gage data acquisition
11. Precalibration and post test analysis procedures

4.0 PREPARATION FOR THE EXPERIMENT (TASK 3)

4.1 UTRC Aerothermosciences Group Activities

A JT12D burner was procured for use in this test program. It was modified according the experiment plan to be identical to the burner used in NASA Contract NAS3-23167. The burner was 127 mm in diameter and contained a 45 degree dome and six sheet metal louver sections. The performance of this burner and the distribution of outside liner temperatures were well documented in the contract mentioned above and it was expected to provide strain levels of interest. After modification, the burner was delivered to the participating group at P&W for strain gage instrumentation.

A viewing port for observation of the burner was procured and delivered to the Electro-Optics and Applied Physics Group for modification. The glass window with which the unit was delivered was to be replaced by an optical-quality, fused-quartz etalon, 25 mm thick, to provide a nearly 75 mm diameter viewing area.

The hardware required to support the test effort was designed and fabricated. The test chamber was a 152 mm pipe spool section with appropriate provisions for mounting the combustor and fuel supply duct, and for permitting a sliding seal at the combustor exit. The test section also contained a boss for mounting the viewing port. As the components became available, they were assembled and tested in preparation for the test.

4.2 P&W Activities

4.2.1 Preparation of the Burner Can - Upon receipt of the modified burner from UTRC, the exact location and shape of the piece to be cut from the JT12 burner can (for instrumenting) were specified. The burner was sent to Turbine Engine Services of East Granby, Connecticut, and the selected section was cut out for instrumentation and testing. Dimensions of the cut out section were approximately 71 mm X 145 mm and the locations of the cuts are shown in sketch SKH-16557 (Fig. 5).

A 7.1 mm diameter viewing hole was drilled in the knuckle area, as shown in Fig. 6. The hole permitted line-of-sight viewing of the louver lip for the specklegram recording system. The lip extended past the edge of the hole by 0.25 mm to avoid direct exposure of the optical system to glare from the luminous gas flowing within the burner.

FIG. 5 BURNER CAN WITH CUTOUT FOR INSTRUMENTATION

ALL DIMENSIONS IN MM

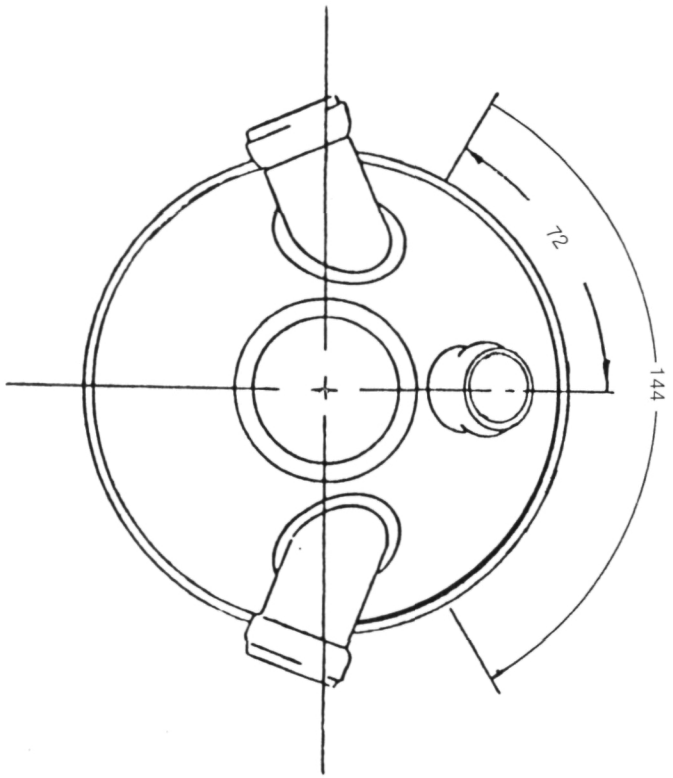

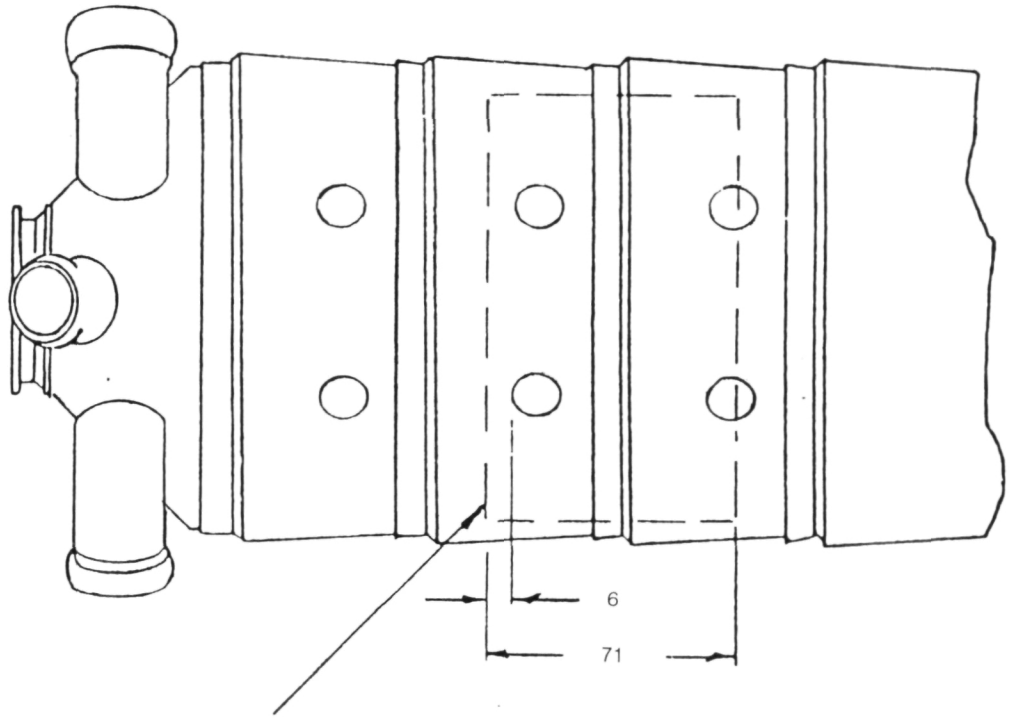

SECTION FOR CUT OUT

FIG. 6 STRAIN GAGE & THERMOCOUPLE LOCATIONS

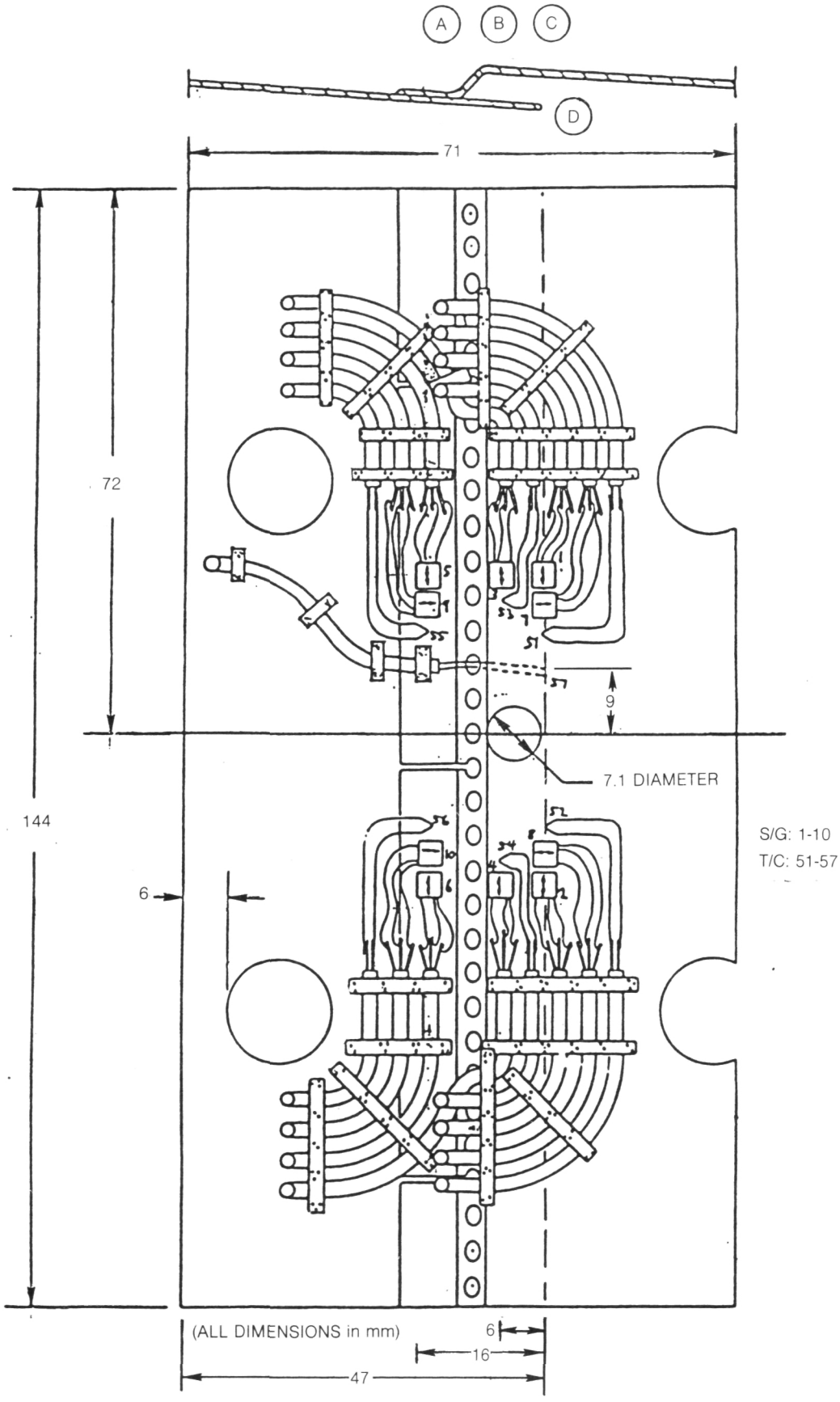

84–4–18–6

4.2.2 Strain Gage Fabrication Procedure - The Kanthal A-1 wire static-strain gages were installed using the flame-spray aluminum-oxide precoat and SermeTel™ P-1 ceramic cement overcoat technique. The design is shown in Fig. 7. In a previous contract, NAS-3-22126, strain gages installed using this technique proved to be durable to 1000K (1340°F) in laboratory tests at UTRC and P&W Engineering. An x-ray photograph of a preliminary sample gage installation, Fig. 8, shows that the configuration of gage loops and lead wire attachments, under the overcoat layer of ceramic cement, conformed well to the design.

A critical step in the installation of the gages is the application of the overcoat of ceramic cement. Good adherence is required everywhere between the gage grid and the ceramic cement and between the ceramic cement and the flame-sprayed precoat. The cement is applied to two steps using the ladder-taping method. A strip of tape is placed over the gage grid to hold the gage in position while the end loops are cemented in place. After the cement has dried the tape is removed, the gage grid area is cleaned of tape residue, and cement is applied to the gage grid area. If the cleaning of the gage wire is not thorough or the cement layer is applied too thickly, then the result may be a gage only partially bonded (internal voids in the cement), or even completely unbonded (floating inside a cement envelope).

4.2.3 Installation of Strain Gages and Thermocouples on the Burner Liner - Ten Kanthal A-1 gages and seven Type K (Chromel-Alumel) thermocouples were installed on the piece cut from the burner can at the locations A, B, and C shown in the layout drawing, Fig. 6. This arrangement provided the following five strain measurements with 100 percent redundancy: 1) the axial strain on the flange forward of the knuckle, 2) the hoop strain at the same location, 3) the axial strain at a location aft of the knuckle just over the edge of the louver lip, 4) the hoop strain at the same location, and 5) the hoop strain only on the knuckle (axial strain was predicted to be small at the knuckle and was not measured).

The thermocouples provided temperature measurements at each axial station, with 100 percent redundancy, and in addition, provided one temperature measurement on the louver lip, D, at a location about 9 mm circumferentially away from the centerline of the viewing hole. The thermocouple junctions at locations A, B, and C were formed of 0.13 mm diameter bare thermocouple wires welded together (but not welded to the burner can) and embedded in SermeTel P-1 ceramic cement. The junction on the louver lip was formed of 0.13 mm diameter bare wires routed through a louver cooling hole and welded to the louver lip at the point of measurement. The bare lead wires were then embedded in ceramic cement. The bare wires were spliced to the 0.13 mm conductors of the sheathed extension cables as shown in Fig. 6. This arrangement kept all extension cables out of the field of view of the speckle photography as much as possible.

FIG. 7 GAGE INSTALLATION

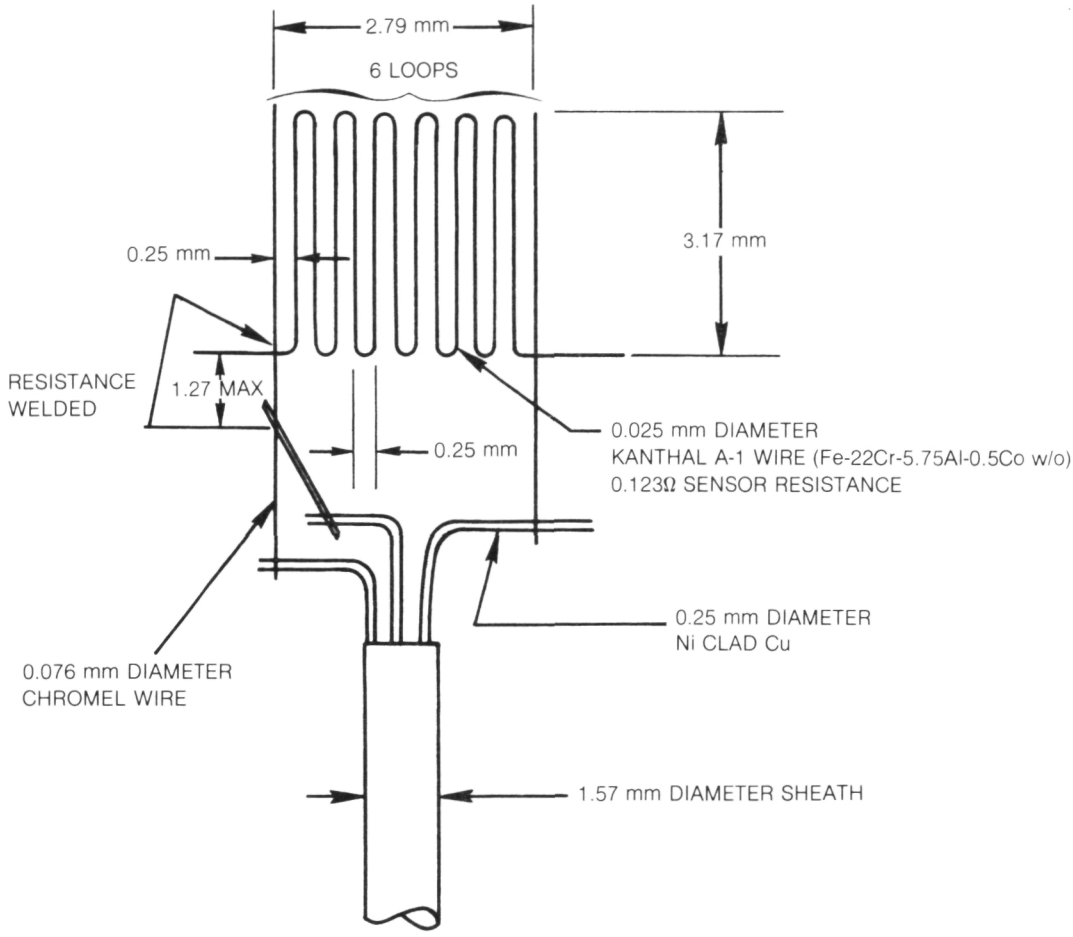

INSTALLATION

SURFACE PREPARATION: NiCrAl (METCO 443) FLAME SPRAYED, ABOUT 0.127 mm THICK

PRECOAT: Al_2O_3 (ROKIDE "H") FLAME SPRAYED, ABOUT 0.127 mm THICK

OVERCOAT: AlP_4 (SERMETAL P-1) CERAMIC CEMENT, ABOUT 0.127 mm THICK

EXTENSION LEADS: 3c Ni CLAD Cu WIRE WITH 1.57 mm DIAMETER
S/S SHEATH AND 0.025 mm DIAMETER CONDUCTORS
CABLE IS STRAP WELDED TO SUBSTRATE AND SPLICES
ARE BRAZED WITH NICROBRAZE 50 (AWS BNi-7)

84–4–18–7

FIG. 8 X-RAY PHOTOGRAPH OF STRAIN GAGE

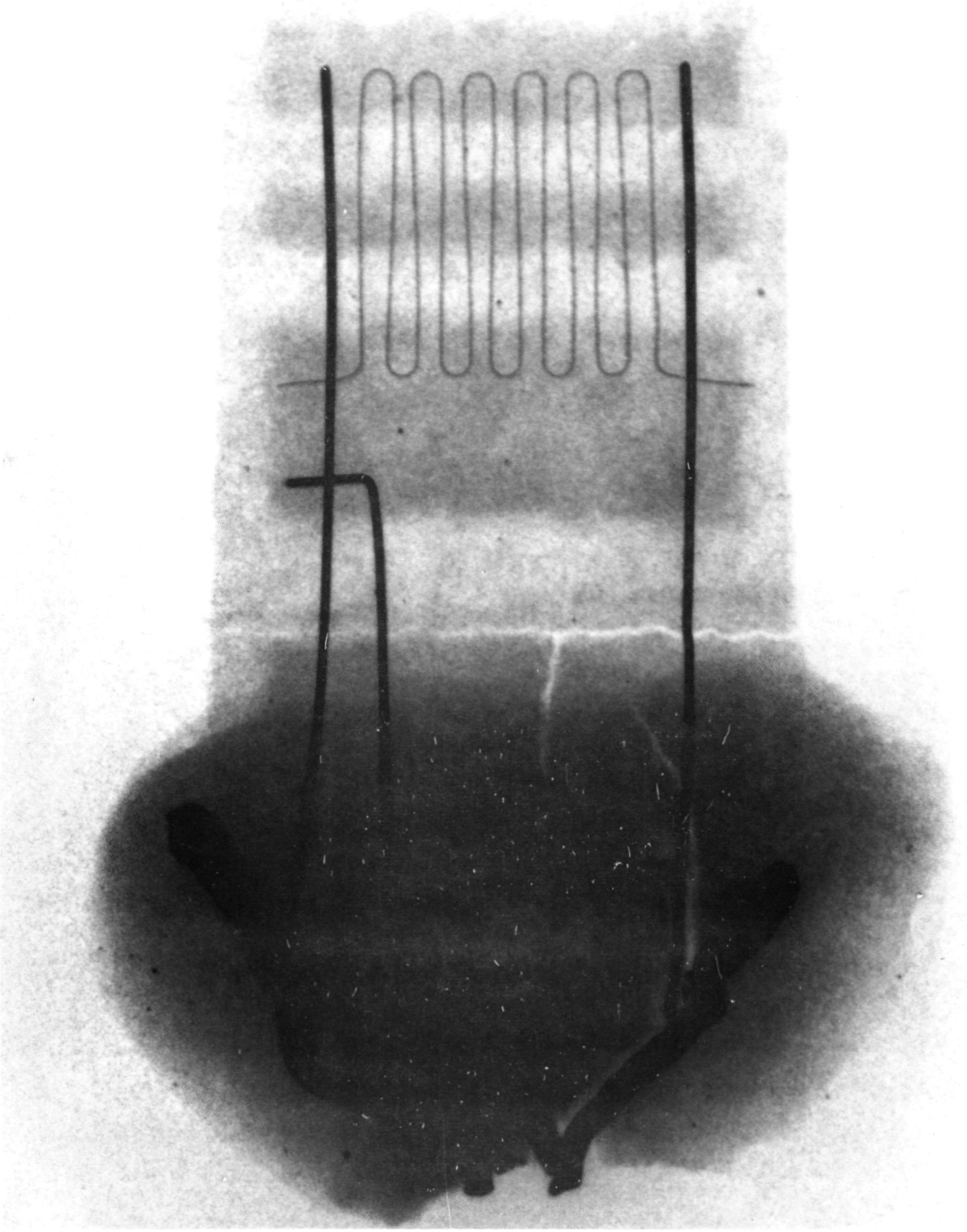

Figure 9 is a photo of the burner can with the instrumented piece removed. Figure 10 is a photo of the removed piece, after the installation of the ten strain gages and the six thermocouples on the outside surface. Figure 11 shows the burner can with the instrumented section welded back in place. After the apparent strain testing described in the next section was completed, the piece was welded back into the burner can. The thermocouples were monitored during the welding and the highest temperature recorded was about 420K (300°F). The seventh thermocouple was then installed on the louver lip.

4.2.4 Apparent Strain Testing - The instrumented segment from the burner liner was heat treated and tested as follows to establish correction curves for apparent strain versus temperature at several cooling rates:

1. The initial heat treatment was in air at 960K (1270°F) for two hours.

2. The change of gage resistance with temperature was measured for each of the ten gages during cool-downs from 950K to near room temperature, with eight different cooling rates. The cooling rate was characterized by the time, t_c (seconds), from 810K (1000°F) to 727K (850°F) during each cool-down. The literature indicates that the time-dependent metallurgical changes affecting the temperature coefficient of gage resistance occur mainly in this temperature range. t_c was varied from 11 seconds to 95 seconds. The fast cooling was attained by moving the test piece from the oven into a stream of cooling air.

3. Drift in gage resistance with time at 960K (1270°F) was measured after completion of the apparent strain tests.

Strain gage data were acquired through a precision Wheatstone bridge circuit connected to each gage, as diagrammed in Fig. 12, using the three-wire gage connection method that minimizes the effects of lead-wire resistance. A constant-voltage 1.5V power source was used. The adjustable resistor R_1 was set to produce bridge null at an initial reference condition.

The recorder indicated in Fig. 12 is a digital data acquisition system, controlled by a desktop computer, providing acquisition and storage of bridge output voltage and power source voltage on manual command. It also provided subsequent automatic data reduction and output in the form of tables and plots of calculated resistance change and temperature versus time for each strain gage.

FIG. 9 BURNER CAN WITH SECTION CUT OUT

(83C2782-002)

84-4-18-13

FIG. 10 INSTRUMENTED SECTION OF BURNER CAN

(83C2479-003)

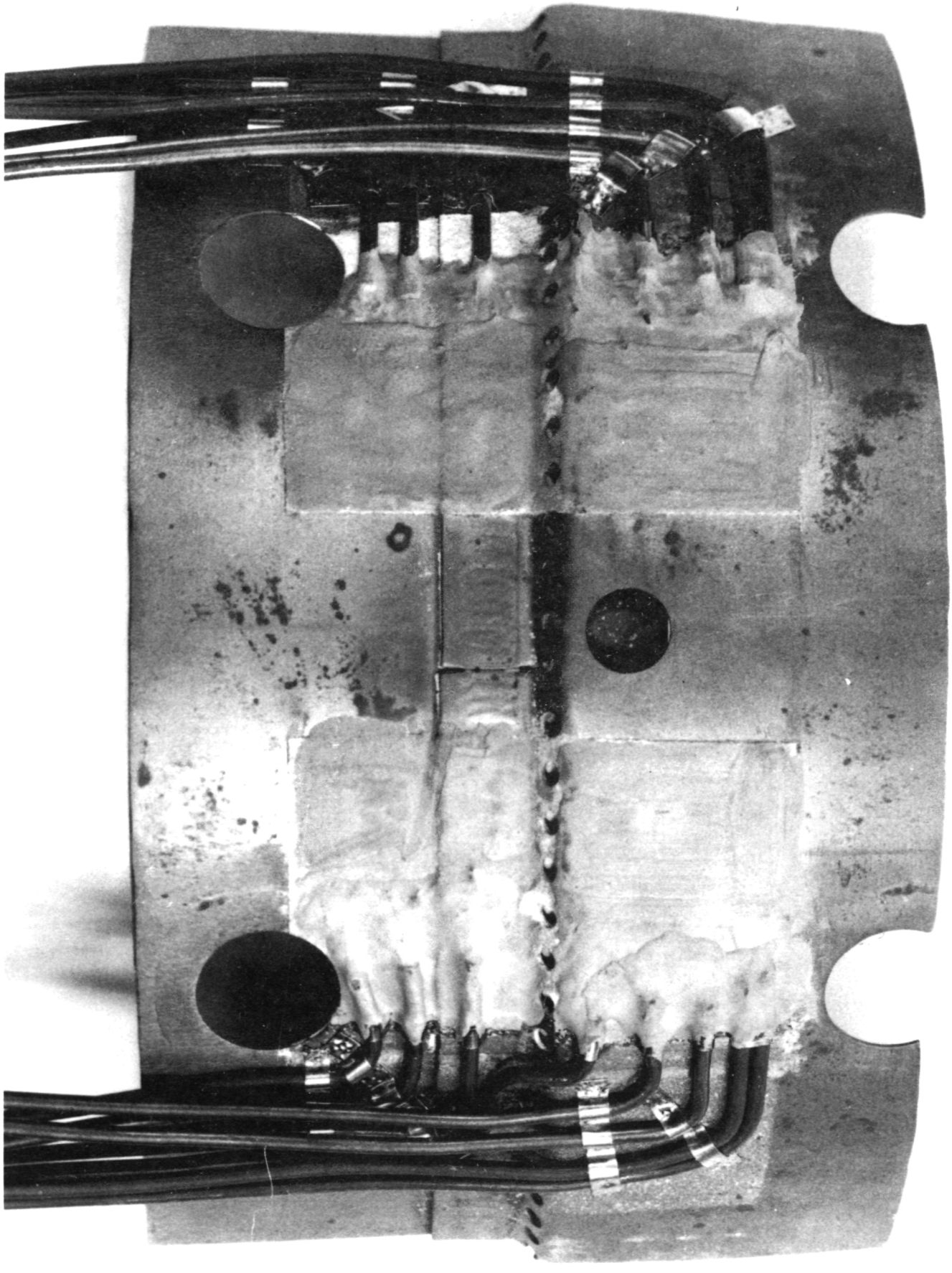

FIG. 11 BURNER CAN WITH INSTRUMENTED SECTION REINSTALLED

(83C2816-001)

FIG. 12 STRAIN GAGE BRIDGE CIRCUIT

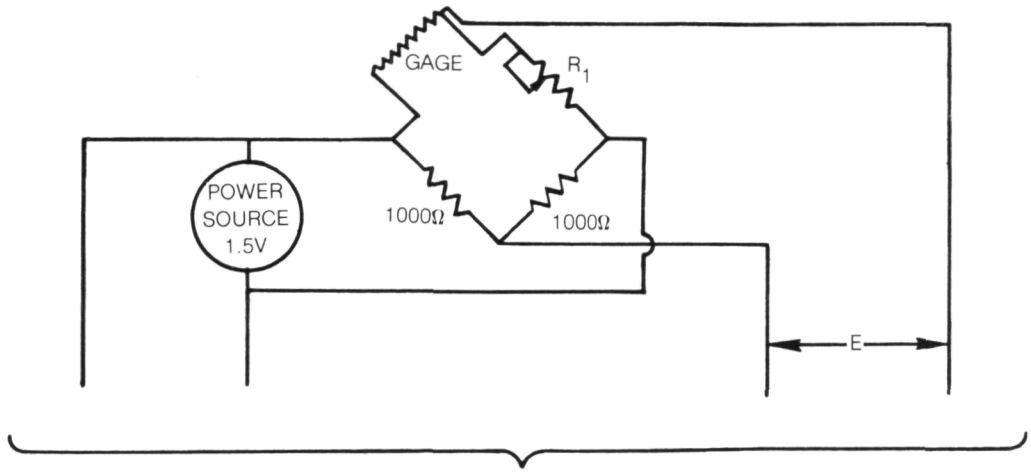

84–4- 18–16

Thermocouple data were acquired by the same digital data acquisition system through an interface module providing a reference cold junction and providing translation to engineering units through the standard Type K thermocouple curve. The data system was programmed to acquire and store sample measurements of temperature and gage resistance once every three seconds.

Overall accuracy of temperature measurement was within 3K, including uncertainties in the calibration of the thermocouple wire and in the calibration of the data system. Overall accuracy of gage resistance dimensionless change $(R-R_o)/R_o$ was within 20 parts per million over the range of ±20,000 parts per million, including uncertainties in the bridge linearity, zero stability, and initial resistance of the gage.

After the completion of the burner tests in the high pressure combustor, the instrumented section of the burner can was again cut out and further tests of gage resistance versus temperature were performed. These were carried out to determine the effect of the extensive burner cycling on the gage behavior and to determine the resistance versus temperature during temperature cycles closely duplicating the actual burner test history at each gage location.

4.2.5 Gage Factor Determinations - Two Hastelloy X test bars (Fig. 13) were each instrumented with four Kanthal A-1 strain gages plus a reference commercial gage and a thermocouple. These installations were tested to determine gage factor of sample Kanthal A-1 strain gages fabricated and installed at the same time as the gages on the burner can, and by the same technician.

The gage factor was measured at room temperature and at approximately 400K, 550K, 700K, 800K, and 950K, and then again at room temperature. Gage factor was determined by the cantilever bending method of ASTM E251-67, using a P&W fatigue testing machine to apply bending stress to the test bars of Fig. 13. A heated environment was provided by a split Marshall oven fitted over the test bar and mounted in the fatigue machine. The oven is capable of 1250K operation and has an 8 cm diameter cylindrical interior 30 cm long. Special end fixtures are used to isolate the region of high strain. Previous tests have shown that room temperature strain is uniform within five percent and that temperature is uniform within 5K (at temperatures to 1100K) over the 6 cm active portion in the center of a test bar with the static test bar shape of Fig. 13. The amplitude of deflection is determined by the eccentricity of a motor-driven crank arm. The eccentricity is manually selected before each test and is repeatable within one percent.

A Hastelloy test bar instrumented with four commercial strain gages on one side was used to determine the overall accuracy of the automated test system (including the reference strain gage), at room temperature. Repeatability was within one percent when several repetitions of a strain measurement were made without changing the test conditions, and within two percent

FIG. 13 GAGE FACTOR TEST BAR

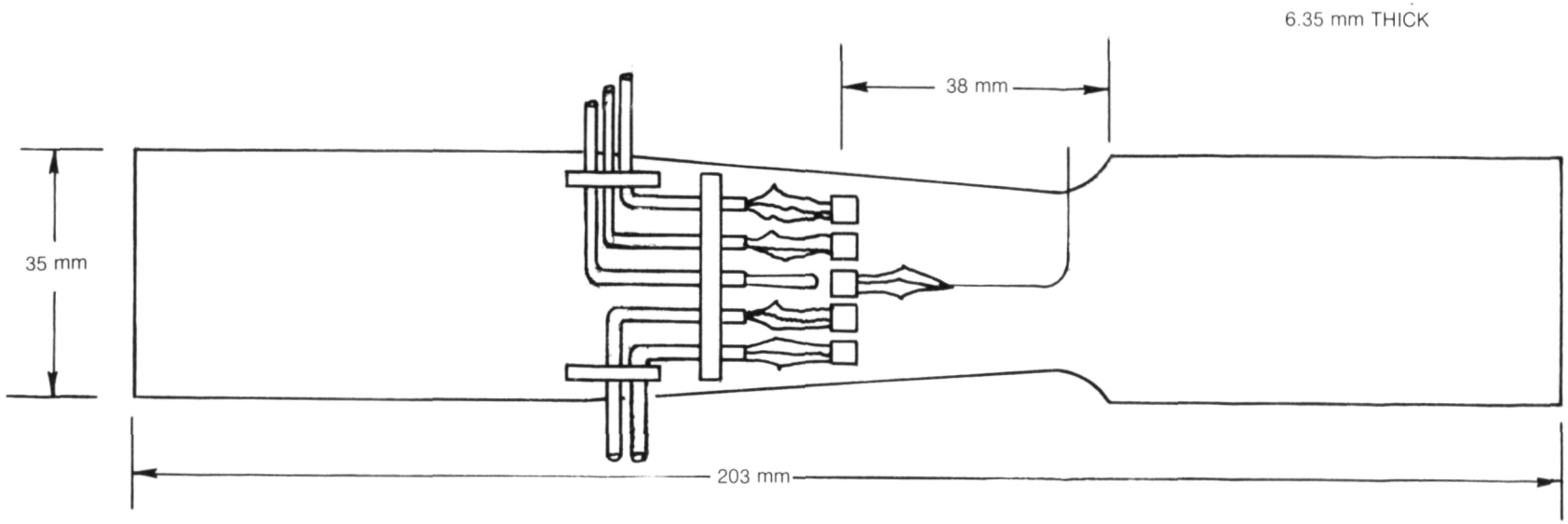

4 TEST GAGES
1 REFERENCE GAGE (FOIL)
1 THERMOCOUPLE (TYPE K)

BAR MATERIAL: HASTELLOY X

when the bar was removed from the fixture and reinstalled between measurements. Agreement gage-to-gage among the four gages was within two percent, gage factors in tension and compression, at 500 microstrain and at 1000 microstrain, were the same within two percent. Agreement with the manufacturers specified gage factor was also within two percent, as determined by comparing indicated and calculated strain (all percentage figures are two-sigma error bands, based on at least four repetitions of each measurement).

Before the start of the gage factor testing, each test bar was aged for two hours at 960K in air, to duplicate the initial heat treatment of the burner can installations. In addition, gage factor tests were repeated on one test bar after a further heat treatment for 200 hours at 950K in air.

The gage factor measurement procedure was as follows: For each strain level and temperature, the bar was deflected (strained) twice in each direction (tension and compression) in a 0, +, 0, -, 0, +, 0, -, 0 sequence. The sequence was run first at a 500 microstrain level and then at a 1000 microstrain level. This test was conducted at each temperature. For each strain gage, an average gage factor was calculated for each direction, strain level, and temperature based on four measurements (from the deflection sequence). The standard deviation was also calculated for the four measurements.

The temperature of the bar was indicated by the wire thermocouple attached to the bar (Fig. 13). The strain level was determined from the commercial gage at temperatures up to 550K (limit of the commercial gage). The same deflections were then employed at higher temperatures and the same strain was assumed to occur. The laboratory digital data system was used to acquire, store, process, and plot data.

Overall accuracy of gage factor determinations were estimated to be within ±3 percent, including uncertainty in reference gage strain indication at room temperature, uncertainty in test bar strain variation with temperature (due to oven temperature gradients at constant bar deflection), bridge circuit repeatability, and data acquisition uncertainty. Accuracy of temperature determination was estimated to be within 3K in these isothermal steady-state tests.

4.3. UTRC Electro-Optics and Applied Physics Activities

4.3.1 Procurement - Three major items procured:

A) A fused silica window was procured for the viewing port on the test section. It was 25.4 mm thick by 81 mm diameter, 1 arc sec. parallelism, 1/4 wave flatness, and antireflection coated on both sides for 694 nm wavelength.

B) 100 photographic plates, AGFA-Gevaert 10E75, were procured for recording the pulsed laser specklegrams.

C) A honeycomb core pallet was procured as a mounting surface for the laser and the optical components.

4.3.2 Component Fabrication - A number of items were fabricated for use in the test program:

A) A device was built to hold a pair of overlaid specklegrams so that their correlation could be checked by observation of halo fringe contrast. The holder provided adjustment for rotation and 2-D translation of one specklegram relative to the other.

B) A three-digit, LED numeric display was built with a counter and display timer for photographically exposing code numbers onto the plates. This made it possible to number the specklegrams in sequence according to each test run before loading them into the automatic plate changer.

C) A fixture was fabricated to connect the Automatic Plate Changer to the Telecentric Lens System and provide both a light baffle and bellows arrangement.

D) A solenoid actuator was constructed for tripping the camera shutter, and forty-foot cables were made for each of the components that required remote operation: the camera shutter, the plate changer, and the pulsed laser.

E) A stand was constructed to support the optics pallet at the burner facility. Provision was made for adjusting the height of each leg so that it could be leveled and centered on the viewing port.

F) A cover was made for the laser and illuminating optics with provision for dry nitrogen purge. This avoided possibility of contamination of the laser or optics by airborne dirt.

4.3.3 Automation of the Interferometric Photocomparator - A number of items were acquired as capital equipment in order to automate the interferometric photocomparator, and the final system was used for data processing under this contract. These items included: a computer controllable x-z translation stage for positioning the pairs of specklegrams, a computer controlled gimbaled etalon for translating the input beam, and a multiplex scanner for sampling a 24 channel detector array. These items were incorporated into the photocomparator, checked out, and a program written for automatic operation of the system.

4.3.4 Preparation of the Viewing Port - The conventional window that was shipped with the viewing port was removed and a spacer ring fabricated to allow mounting of the fused silica window. A second gasket was procured to provide a proper seal on either side of the spacer ring. After assembly, the port was tested for shadowing of the illumination beam and found to be satisfactory.

4.3.5 Assembly of the Optics Pallet for the Test Stand - The equipment to be used at the burner test stand was mounted on the optics pallet. The telecentric lens and the automatic plate changer were mounted together with the solenoid for operating the lens shutter. High energy mirrors and a diverging lens were used to direct the illumination beam onto the surface of the burner. The pulsed laser was mounted on adaptor plates designed to hold it at the proper height. Figure 14 shows the layout of the components on the optics pallet.

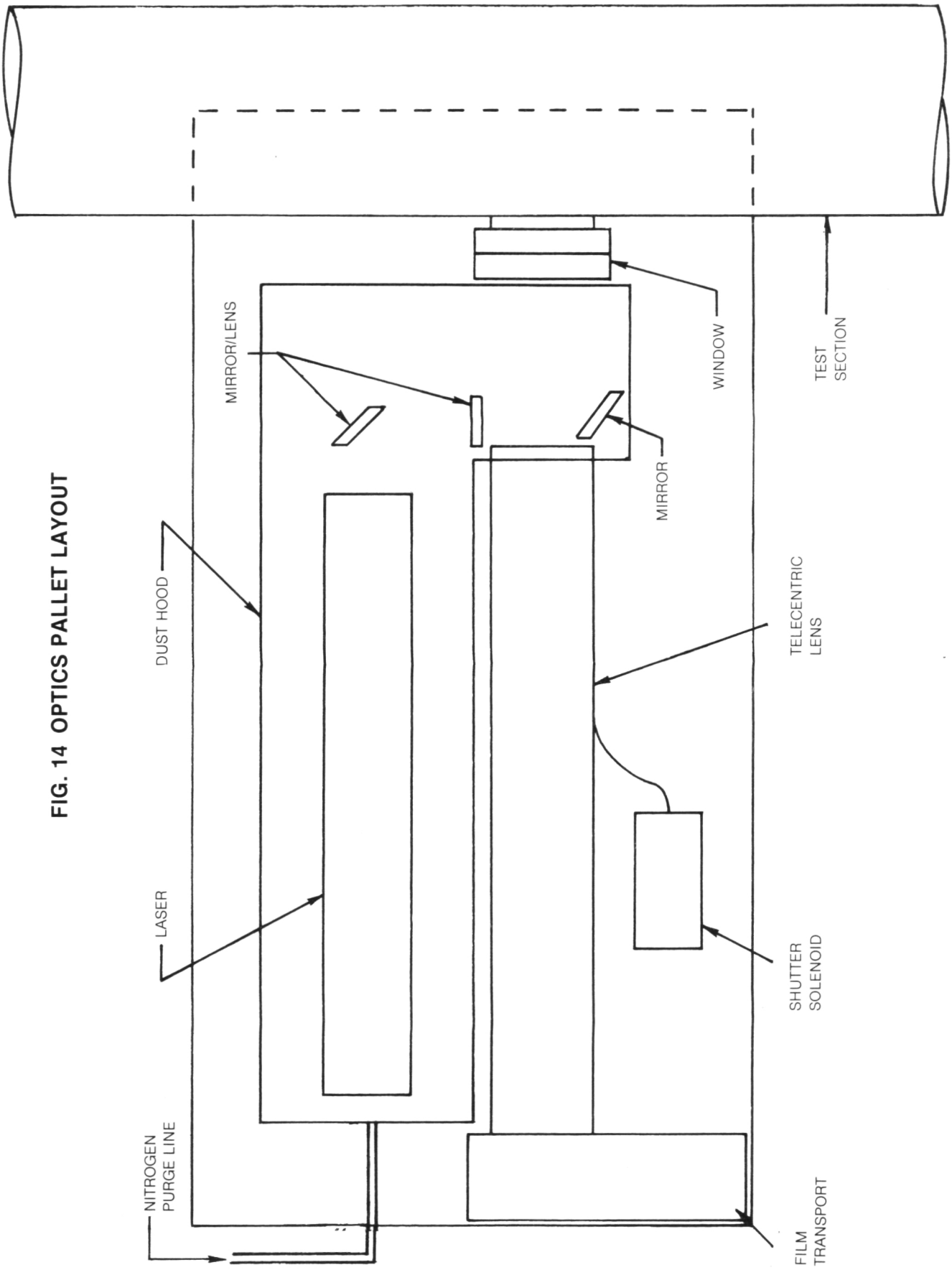

FIG. 14 OPTICS PALLET LAYOUT

84–4–18–9

5.0 TEST PERFORMANCE AND ANALYSIS OF RESULTS (TASK 4)

5.1 Experiment Set Up and Test Execution

5.1.1 Aerothermosciences Activities

5.1.1.1 Setting Up of the Combustor Test Rig - The combustor test rig was set up for the burner liner strain measurement test program. The modified JT12D combustor, instrumented by P&W with ten strain gages and seven thermocouples, was installed in the test section with the instrumented area visible through the quartz window in the side of the test section housing. The test section was installed in the burner rig with window oriented so that the optical system could be properly aligned. The instrumentation required to document the rig operation was put in place, and cables were prepared to connect the strain gages and bridge completion networks to the automatic data acquisition system.

The UTRC WISARD (Wide-band System for Acquisition and Recording of Data) system was used for acquisition of resistive strain gage data. This system has a main scanner and can incorporate subscanners to accommodate various types of data signals, such as temperature, pressure and strain. The acquisition rate was about five seconds per reading for the parameters needed in the burner test. The WISARD system data processing capability was used to convert raw data to engineering units, to compensate for apparent strain due to temperature, and to provide printout and plot data.

A strain gage bridge and balance console was provided by P&W Commercial Engineering, using 1.5 volts excitation in a Wheatstone bridge and producing about ± 9 mv output for $\pm 10{,}000$ microstrain full scale. Amplifiers (Preston Scientific, Inc.) were used in the WISARD system to increase the signals to the required 9 v input level. Overall accuracy of the data acquisition system in this application was estimated to be within ± 1 percent in indicated strain and ± 2K in temperature.

A channel was also provided on the WISARD system to mark when the speckle photographs were recorded so that strain gage readings could be compared with specklegram data.

5.1.1.2 Operation of the Test Stand - During the performance of the test program, the Aerothermosciences group was responsible for all aspects of test stand operation. They provided consultation on the most practical test sequences, scheduled test runs with respect to other test stand commitments, executed start up and shut down procedures, and controlled the burner operation during the test runs. This group also provided the primary data processing via computer readout of the WISARD system.

5.1.2 P&W Activities

5.1.2.1 Assembly of Experimental Apparatus - A static strain gage console was delivered by P&W which provided bridge completion networks, DC excitation, and balance potentiometers for the strain gages. The strain gages and thermocouples on the burner can were wired to connectors at the test stand and cabled to the static strain gage console. An excitation of 1.5 volts was used which resulted in output signals ranging from -10 mv to +10 mv. These signals were amplified to the levels required by the UTRC WISARD data system. The entire system was checked out and found to operate satisfactorily.

5.1.2.2 Support During Test Runs - P&W personnel provided support during the test by monitoring data output and periodic inspection of the strain gages and thermocouples. Between the third and fourth test runs, the burner can was removed and two faulty thermocouples repaired. After completion of the test the burner was removed and a post-test analysis of the strain gages was performed.

5.1.3 Electro-Optics and Applied Physics Group Activities

5.1.3.1 Final Laboratory Check - Before the instrumented burner can was installed at the burner stand, it was set up in the laboratory for preliminary speckle photographs with the pulsed ruby laser. This provided a check of the entire system before it was installed in the test stand. It also determined whether the window would vignette the illumination beam and whether the cement covering the strain gages and thermocouples had similar reflectivity to the hastelloy X burner can. The resulting photographs showed that the illumination covered the area of interest and that the cement was only marginally more reflective than the hastelloy X under red light. The two photographs that were recorded were stored for later use in assessment of minimum strain detectability. The burner can was then returned to the Aerothermosciences group for mounting in the burner rig.

5.1.3.2 Burner Stand Installation - After the can was mounted in the burner test rig, the optics pallet, stand, and pulsed ruby laser were moved to that location and the system was set in place. After the optics were properly oriented and aligned, a pair of pulsed laser specklegrams were recorded of the burner can at ambient temperature, again to check the alignment and provide reference data. These specklegrams showed excellent alignment and good correlation. The cables for the remote operation of the system were connected and routed to the control room.

5.2 Test Runs and Results

5.2.1 Checkout

5.2.1.1 Checkout Run - With all preparations complete, an initial checkout was performed with isothermal heating of the combustor by the electric air heater. The camera lens aperture had been set to f/20 and ten photographic plates loaded in the automatic plate changer. The first two specklegrams were recorded without air flow and with 1.8 kg/sec flow at 10 atmospheres, at ambient temperature. The other eight were recorded with 1.1 kg/sec air flow at the following temperatures: 494K, 666K, 494K, 308K, 442K, 565K, 667K, and 568K. This sequence allowed comparison between two rates of heating to determine any effect upon specklegram correlation. Strain gage and thermocouple readings were examined and found to be well-behaved; however, data was not logged on the WISARD system.

The photographic plates were removed from the test stand and developed for evaluation. Photographic densities were excellent, and use was made of a process for converting them to dichromated gelatin images which diffracted light more efficiently than photographic silver. The speckle photographs were examined to determine the effects of isothermal heating on speckle correlation.

5.2.1.2 Checkout Results - No significant loss of correlation was observed between specklegrams recorded at ambient temperature with and without air flow. The first temperature cycle, however, showed severe loss of correlation, especially on the cement that covered the strain gages and thermocouples. The second cycle showed a definite improvement over the first and suggested that a more gradual heating sequence should be used. It was decided to begin taking specklegrams at about 422K on subsequent runs which would allow smaller temperature changes before ignition without requiring more photographs.

5.2.2 First Test

5.2.2.1 First Test Run - The first test run was performed with three accel/decel cycles according to the initial plan, with the exception that the first specklegram was recorded at 411K rather than at ambient temperature. The thermocouple on the louver lip was monitored and the indicated temperature was manually recorded when specklegrams were exposed. The WISARD system logged data during the run.

Specklegrams were recorded at the following temperatures:

TABLE 1. First Run Specklegrams

Plate #	Temperature	Remark
1	411K	Isothermal heating
2	558K	
3	703K	
4	735K	
5	857K	Ignition
6	964K	First cycle start
7	1083K	
8	1063K	
9	889K	
10	797K	
11	814K	Second cycle start
12	934K	
13	1047K	
14	1056K	
15	898K	
16	787K	
17	839K	Third cycle start
18	906K	
19	1068K	
20	1080K	
21	900K	
22	793K	
23	699K	Fuel off
24	563K	

5.2.2.2 First Test Run Results - The specklegrams showed severe loss of correlation which was particularly bad on the cement covered areas. The transition from isothermal heating to fuel combustion was particularly bad and involved loss of correlation on most areas of those two specklegrams. Only those specklegrams that involved little if any temperature change showed good correlation. The data was of such poor quality that strain measurements could not be made in many cases and in most other cases only with poor accuracy. There was also a loss of laser power after the burner had been ignited which showed up as weak exposure of the specklegrams.

Strain gage readings appeared to be reasonable and well-behaved; however, thermocouples #5 and #6, on the weld area appeared to be functioning improperly.

Post-test inspection indicated that the optics did not experience excessive heating or other deterioration. Contact was noticed between the protective cowl that covered the laser and optics and the burner rig. It was presumed that vibration from the rig may have interfered with proper operation of the laser and caused the drop in output power. This was corrected. Also, the focal ratio of the lens was increased to f/27 by reducing the aperture which increased the depth of focus to 2 mm. This would improve correlation if it were lost due to displacement of the burner toward the lens. It was decided also that the next run should consist of a single cycle during which a large number of specklegrams would be taken to minimize temperature transitions. Acceleration and deceleration rates would be slower also to help improve correlation.

5.2.3 Second Test

5.2.3.1 Second Test Run - A second run was performed with the camera lens set to f/27, increased laser pumping power, and no contact between the rig and the optics pallet. A single accel/decel cycle was performed at a slower rate (about 2 min transition times) which allowed three specklegrams during the transitions. The WISARD system was logging data during the entire run.

Specklegrams were recorded at the following temperatures:

TABLE 2. Second Run Specklegrams

Plate #	Temperature	Remark
1	412K	Isothermal heating
2	491K	
3	580K	
4	643K	
5	704K	
6	842K	Ingition
7	896K	
8	959K	
9	1029K	
10	1082K	
11	1088K	
12	1090K	
13	1057K	
14	941K	
15	850K	
16	843K	

TABLE 2. Second Run Specklegrams (Cont'd)

Plate #	Temperature	Remark
17	842K	
18	714K	Fuel off
19	707K	
20	629K	
21	592K	
22	506K	
23	452K	
24	452K	

5.2.3.2 Second Test Run Results - Laser power remained constant during the entire run, and this indicated a correct diagnosis of the previous difficulty. Specklegram correlation, however, did not improve dispite the longer focal length and smaller temperature transitions. Again only those specklegrams between which the temperature did not change showed good correlation, and again the cemented areas showed particularly bad correlation. It was observed that the metal regions about midway between the adjacent knuckles seemed to have the best correlation when all other areas were poor.

It was reasoned that the burner might be warping due to the axial variation in temperature and that this might tilt the burner surface sufficiently to destroy correlation. For this condition, the lens aperture should be increased rather than decreased to provide greater tolerance to tilting of the input field. This would be tried on the next test run.

The strain gages appeared to operate in a reasonable manner. Thermocouples #5 and #6 were confirmed to be defective and their loss made it impossible to correct strain gage data on the weld area for either run #1 or #2. These gages were at the regions of highest temperature.

Post-test examination showed thermocouples #5 and #6 to be open circuited at the connectors just outside the burner. Also, strain gage #10 showed an open circuit on one wire. It was decided to conduct one more run with further adjustments to the speckle photography system and then remove the burner can from the test rig to repair the thermocouples.

5.2.4 Third Test

5.2.4.1 Third Test Run - A third test run was performed with the camera lens set to a larger aperture (F/14) to provide the speckle photographs with greater tolerance against tilting of the burner can surface. Photographs were recorded under isothermal heating starting from 407K. Ignition occured

at 700K, and a single accel/decel cycle was recorded. This was followed by fuel shut-off and isothermal cooling to 497K. Twenty-four specklegrams were recorded and the WISARD system was logging data during the entire run.

Specklegrams were recorded at the following temperatures:

TABLE 3. Third Run Specklegrams

Plate #	Temperature	Remark
1	407K	Isothermal heating
2	500K	
3	581K	
4	622K	
5	702K	
6	828K	Ignition
7	819K	Start accel
8	881K	
9	919K	
10	956K	
11	983K	
12	1016K	High Temp Dwell
13	1021K	
14	1040K	
15	1049K	Start Decel
16	996K	
17	889K	
18	833K	Idle Dwell
19	808K	
20	808K	
21	685K	Fuel off
22	639K	
23	581K	
24	497K	

5.2.4.2 Third Test Run Results - The problems of speckle decorrelation were not improved by the system modifications employed during this run. Observation of the specklegrams revealed two major difficulties. First, it was noticed that the entire test section of the burner rig shifted laterally downstream during the test run. Re-examination of photos from the two earlier runs showed that this motion had occurred on those runs also. Between initial and peak temperatures, the translation amounted to about 10 mm. Review of the

mounting arrangements confirmed that the translation was due to thermal expansion of the rig which was fastened nearly seven meters or more upstream, near the heater.

Much of the decorrelation between speckle photographs could have resulted from the combination of this translation and the divergence of the illumination beam. As the burner can surface translates, the angle of illumination is changed for every object point and this generates an angular change in the reflected field similar to the effect of tilting the object surface.

The second difficulty could be seen in the halos of the speckleograms. Observation of the speckleogram halos showed irregularities in their size and shape. The halos would often appear oblong and shift randomly in orientation with translation of the speckleogram. This indicated possible speckle blurring due to moving air gradients. The speckleograms were further observed and photographed through an aperture in a Fourier-transform filtering system (Fig. 15) which allowed them to function like schlieren photographs. These results showed patterns of speckle blurring in the photographs that looked very much like gas inhomogeneities. These blur patterns differed randomly from photograph to photograph and in some cases even seemed to show stream lines. Typical examples are shown in Fig. 16. Similar observation of previously recorded speckleograms established that the speckle blurring did not occur except when the temperature was elevated, even in the presence of 1.8 kg/sec air flow.

5.2.5 Final Test

5.2.5.1 Final Test Run - In preparation for the final test run, the burner was removed from the rig and the two faulty thermocouples were repaired. One strain gage was determined to be defective but could not be repaired. The burner has been re-installed in the rig and the strain gages and thermocouples reconnected. A bellows was mounted before the test section on the rig and the test section itself was immobilized. The telecentric lens system was set to f/20.

The first portion of the test consisted of recording eight speckleograms under various isothermal conditions to determine the effects of temperature, pressure, and air flow on speckle blurring. The second portion of the test consisted of recording speckleograms during one final ignition/accel/decel cycle. The final portion of the test consisted of performing four rapid accel/decel cycles for the benefit of the wire strain gages. The last four cycles ranged from 10 to 20 sec for each temperature transition with about 1 min dwells at each extreme.

The speckleograms were recorded at all combinations of two mass flows, two pressures, and two temperatures, namely: 0.9 kg/sec and 1.4 kg/sec, 3 atm

FIG. 15 FOURIER TRANSFORM SYSTEM

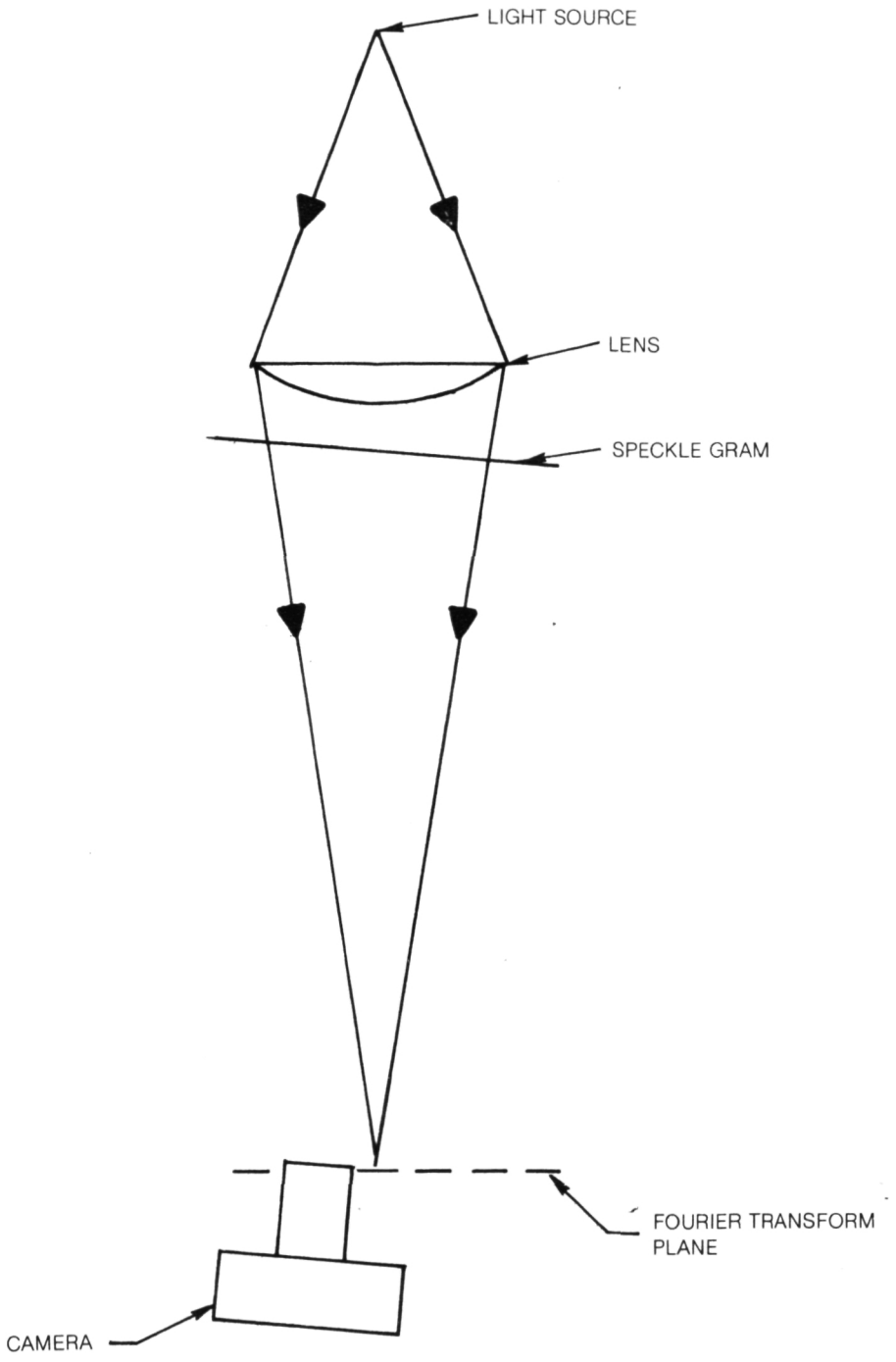

84–4–18–10

FIG. 16a SPECKLEGRAM IMAGES WITH FOURIER TRANSFORM FILTERING

NO FLOW

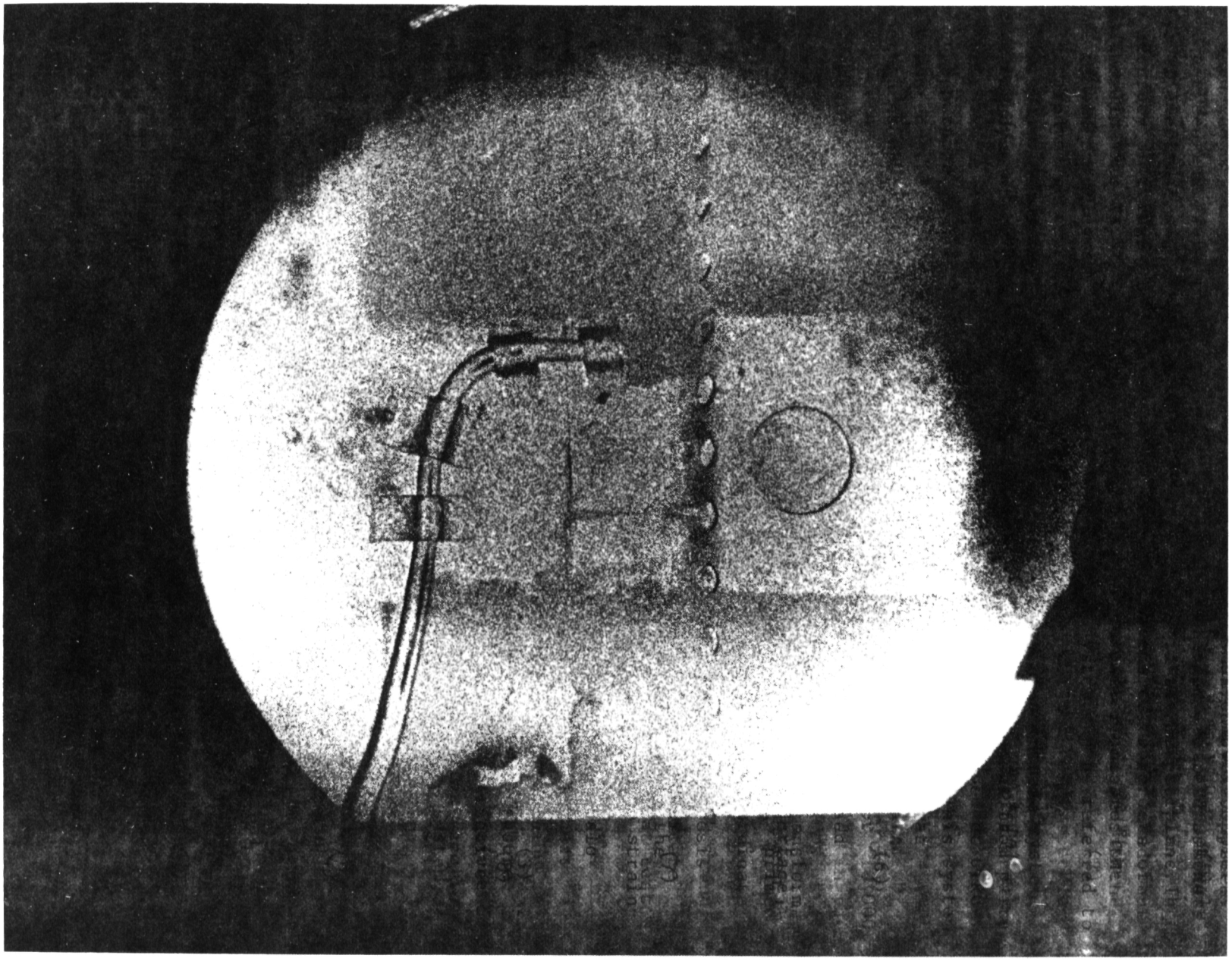

FIG. 16b SPECKLEGRAM IMAGES WITH FOURIER TRANSFORM FILTERING

RUN 3 #12

FIG. 16c SPECKLEGRAM IMAGES WITH FOURIER TRANSFORM FILTERING

RUN 3 #4

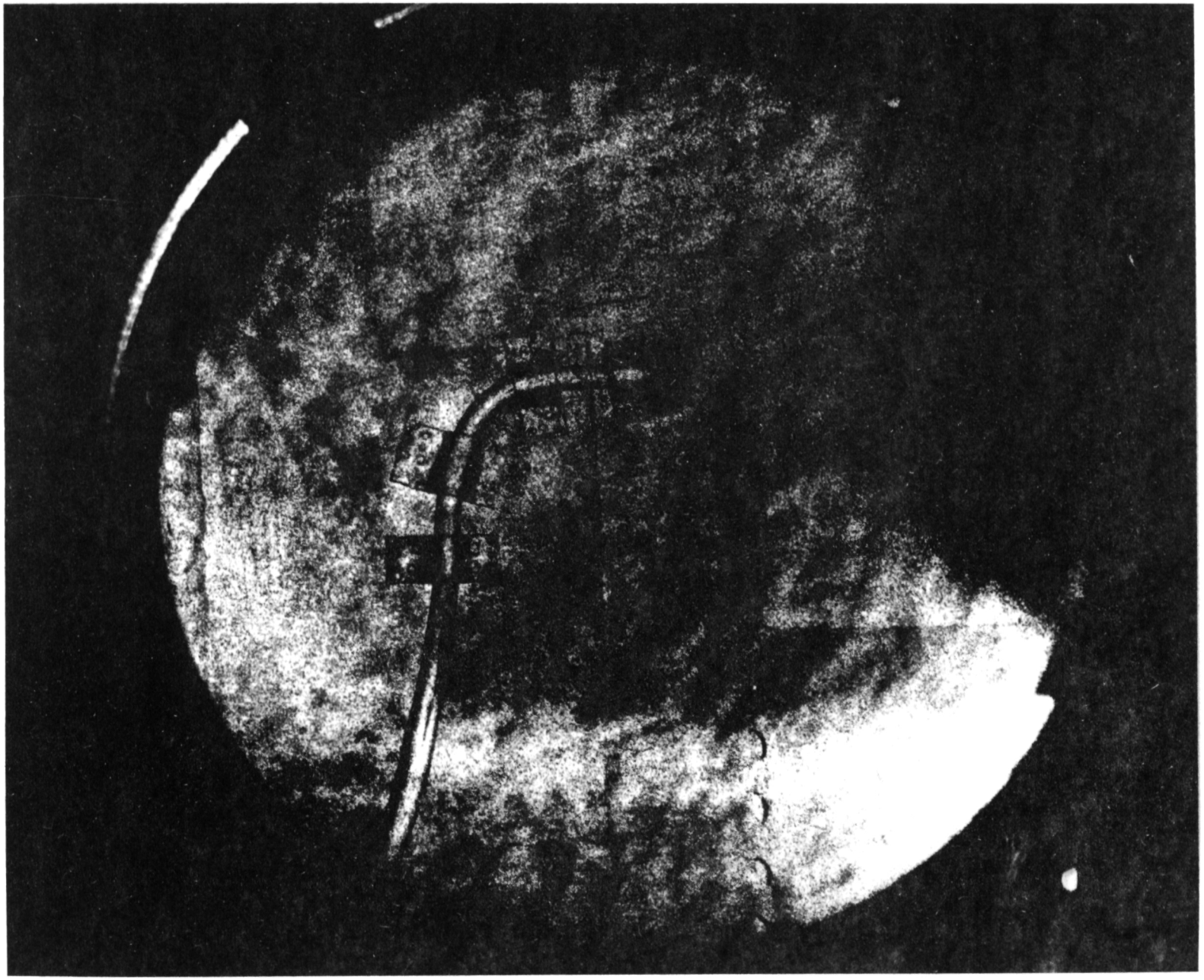

FIG. 16d SPECKLEGRAM IMAGES WITH FOURIER TRANSFORM FILTERING

RUN 2 #11

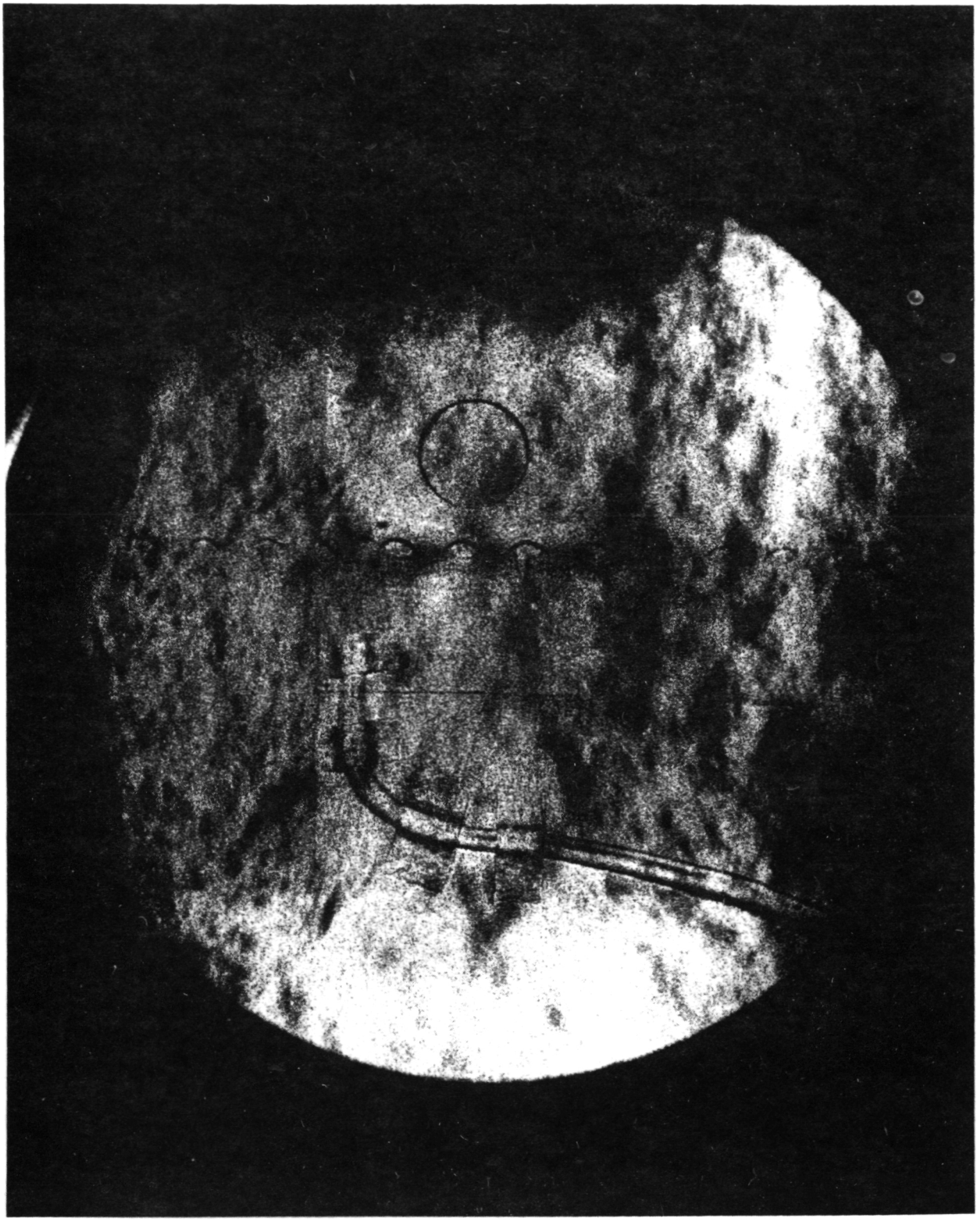

and 6 atm, and 422K and 589K. Three specklegrams were recorded at an isothermal, pre-ignition condition of 1.6 kg/sec flow, 9 atm pressure, and 736K. These should have been substantially identical and processing them on the photocomparator gave a measure of the apparent strain associated with the inhomogeneities of the gas in the burner rig for that condition. The thirteen remaining plates were used to record the final ignition/accel/decel cycle. The transition times were in the order of one minute and there was an approximately two minute dwell at the peak temperature. The temperature of the louver lip was recorded manually and ranged from 856K to 1078K. Single data scans were recorded on the WISARD system after each of the first eight specklegrams were recorded. The system was allowed to run continuously during the final fourteen specklegram recordings and during the final four accel/decel cycles.

The conditions for the specklegram recordings are as follows:

TABLE 4. Fourth Run Specklegrams

Plate #	Temperature	Remark		
1	422K	0.9 kg/sec	3 atm	
2	429K	0.9 kg/sec	6 atm	
3	587K	0.9 kg/sec	6 atm	
4	588K	0.9 kg/sec	3 atm	
5	424K	1.4 kg/sec	3 atm	
6	599K	1.4 kg/sec	3.5 atm	
7	592K	1.4 kg/sec	6 atm	
8	432K	1.4 kg/sec	6 atm	
9	736K	1.6 kg/sec	8.9 atm	
10	736K	1.6 kg/sec	8.9 atm	
11	736K	1.6 kg/sec	8.9 atm	
12	856K	1.9 kg/sec	10 atm	Ignition
13	913K			
14	1017K			
15	1067K	one min till next		
16	1068K	one min till next		
17	1078K			
18	1017K			
19	883K			
20	847K			
21	843K			
22	844K			
23	842K			
24	844K			

5.2.5.2 Final Test Results - Specklegram decorrelation was present in the results of this test to essentially the same degree as before, especially during the ignition/accel/decel cycle. Fourier-transform observation of the specklegrams indicated that the speckle blurring correlated more closely with pressure than with temperature or flow. This was consistent with theory which indicated that such problems should increase in direct proportion to pressure. The lack of improvement of speckle correlation with the bellows in place indicates that the apparent strain generated by the thermal lenslets in the hot gas within the burner rig may itself cause the decorrelation.

5.3 Data Reduction

5.3.1 Specklegram Data - Data reduction was performed on the three specklegrams recorded before ignition (#9, #10, and #11) to determine the extent to which the speckle distortions influenced strain evaluation. Twelve points were located on the specklegrams as shown in Fig. 17. Because the temperature, air flow, and pressure were the same for all three, comparisons should have yielded no apparent strain. Table 5 presents the results obtained comparing (a) #9 and #10, and (b) #10 and #11. Data reduction yields values of the four partial derivatives of the axial and circumferential displacements, and, in Table 5, these are resolved into principle strains as outlined in Appendix B. This is done in order to obtain the peak values of apparent strain, rather than presenting only the axial and circumferential components.

The apparent strains shown in Table 5 vary randomly in direction and in magnitude by several thousand microstrain. It is possible to compute the average of these strains over the twelve locations, as well as their standard deviations. The average and standard deviations are computed for the partial derivatives in the original x,y coordinate system, and the results are transformed into a principal coordinates for a compatible presentation in Table 5. The values of principal strains for the standard deviations are ambiguous because the values obtained refer to statistical variations plus or minus relative to the average values. For simplicity, only plus values were used, which results, as seen, in a nearly uniaxial strain at 45°. The magnitude of this 45° strain is representative of the variance of the values obtained in it exceeds three thousand microstrain. As expected, the average apparent strain over the twelve locations is considerably less than that value.

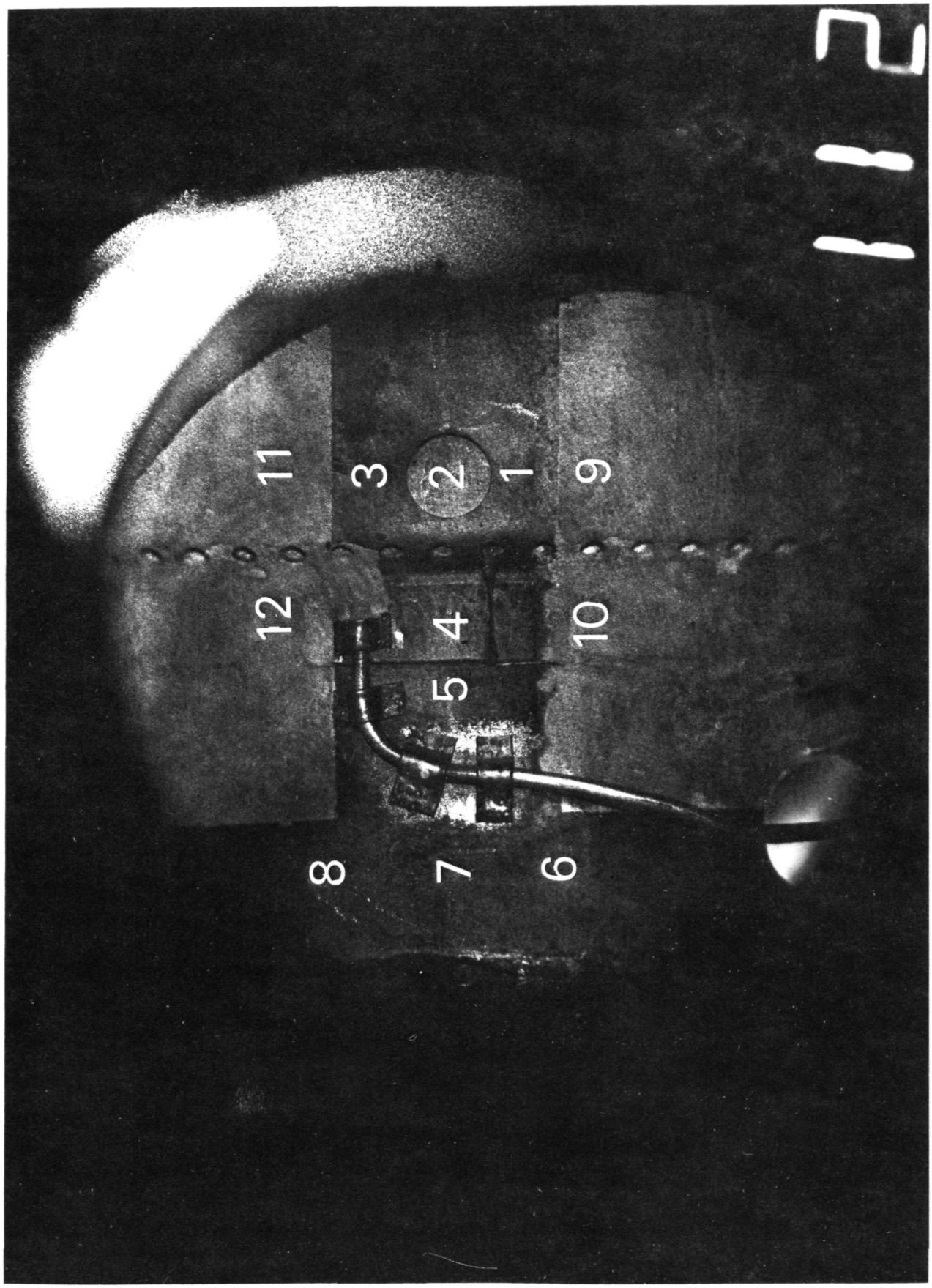

FIG. 17 LOCATIONS OF STRAIN MEASUREMENTS ON SPECKLEGRAM IMAGE

84-4-18-11

TABLE 5. Apparent strain for specklegram pairs. Pnt# indicates the location, ang is the angle from horizontal to the PX axis, PX is the principal X strain and PY is the principal Y strain.

(a) #9 and #10

pnt#	ang deg	PX με	PY με
1	-43	-2609	1907
2	24	3932	839
3	32	-231	917
4	13	-824	-3302
5	-12	904	3017
6	-28	1812	-1878
7	30	-2012	1103
8	14	-2643	-613
9	-37	-3490	-7
10	44	1970	-1127
11	35	2238	-1182
12	44	2508	-1900
average	44	600	-656
std dev	44	3037	83

(b) #10 and #11

pnt# με	ang deg	PX με	PY με
1	-35	699	-1335
2	28	-1804	-747
3	8	-1952	-590
4	-26	-3209	2002
5	-38	-1738	-2717
6	7	-3999	3113
7	-26	-246	4705
8	-14	-1709	1672
9	-18	1868	-1383
10	30	-3176	112
11	4	-262	-2023
12	36	-662	3373
average	8	-1094	260
std dev	-42	290	3282

For comparison, the two specklegrams recorded at ambient conditions before the checkout run were processed for apparent strain at the same twelve locations. These results are presented in Table 6.

TABLE 6. Apparent strain for specklegrams recorded under ambient conditions.

Pnt#	ang deg	PX με	PY με
1	2	385	221
2	-3	468	333
3	-6	485	227
4	-2	532	55
5	-23	396	-7
6	-16	278	-327
7	-14	141	-96
8	-11	258	89
9	-4	492	269
10	-20	352	96
11	-5	471	284
12	-2	446	98
average	-10	387	109
std dev	-36	70	228

The peak values of apparent strain shown in Table 6 are considerably less than those shown in Table 5. The major principal component derived from the standard deviations of the values in Table 6 is more than an order of magnitude less than the corresponding major value in Table 5. Clearly, the turbulent gas flow creates a pattern of randomly oriented apparent strains of very significant magnitude.

5.3.2 Strain Gage Data Analysis and Results

5.3.2.1 Data Reduction Procedure - The following relationship was used to determine the change in strain on the burner liner surface as the burner operating point was changed:

$$\varepsilon_1-\varepsilon_2 = \left[K(E_1-E_2) - (r_{T1}-r_{T2})/R_o - (G_1-G_2)\varepsilon_2\right]G_1, \qquad (1)$$

where ε = strain
E = bridge output voltage (volts)
G = gage factor (a function of temperature)
K = a bridge constant (volts^{-1}), equal to the ratio of the fractional change in the resistance of the strain gage to the change in the bridge output. $K = r/ER_o$
R_o = resistance (ohms) of the gage at an initial reference condition (room temperature, no strain)
r = change in resistance (ohms) of the gage from the reference value ($r=0$ at room temperature, no strain)
r_T = Change in resistance (ohms) of the gage due solely to temperature, as determined by calibration of gage resistance versus temperature.

Subscripts 1 and 2 designate two successive operating points during the burner test.

The relationship was derived as follows. The output of the strain gage bridge circuit was assumed to be proportional to the fractional change r/R_o in resistance of the gage. (Nonlinearity in the bridge, on the order of $(r/R_o)^2$ was neglected.) The change, r, was further assumed to be the sum of r_T, a contribution due to temperature, and r_s, a contribution due to strain. That is

$$r/R_o = (r_T + r_s)/R_o. \qquad (2)$$

The contribution due to strain, r_s, was expressed in terms of strain ε by introducing the definition of gage factor, G.

$$G = r_s/\varepsilon R_o \tag{3}$$

Substituting this relationship into Eq. (2) for each operating point, and subtracting, gives Eq. (1).

If ε_2 is known (or zero), Eq. (1) completely determines the strain change, $\varepsilon_1-\varepsilon_2$, between any two successive points during the burner test because all other quantities on the righthand side of Eq. (1) are known or measured. If ε_2 is unknown, then the possible error due to change in G with temperature is given by the last term on the right, i.e.

$$\varepsilon_2(G_1-G_2)/G_1$$

This term vanishes if the gage factor is independent of temperature so that $G_2 = G_1$.

The accuracy of the measurement depends critically upon the accuracy and repeatability of laboratory calibrations which determine the gage resistance change $(r_{T1} - r_{T2})/R_o$ due to temperature and the gage factor versus temperature. The results (including uncertainty analysis) of the laboratory tests which provided these determinations are described in the next section after which follows the presentation and analysis of the final results of the burner tests.

5.3.2.2 Results of Calibration Tests

Change of Gage Resistance due to Temperature

The main features of the observed behavior of resistance versus temperature for the Kanthal A-1 gages are shown in Fig. 18 which is a plot of resistance ratio versus temperature during a series of tests performed on gage No. 2 on the burner liner. Three principal features should be noted:

1. When the gage is heated to 950K, the gage resistance always returns to the same value. Drift of resistance with time is very slow at 950K, on the order of 20 X 10^{-4} percent per hour.

FIG. 18 EFFECT OF INITIAL TEMPERATURE AND DWELL ON CHANGE IN RESISTANCE RATIO

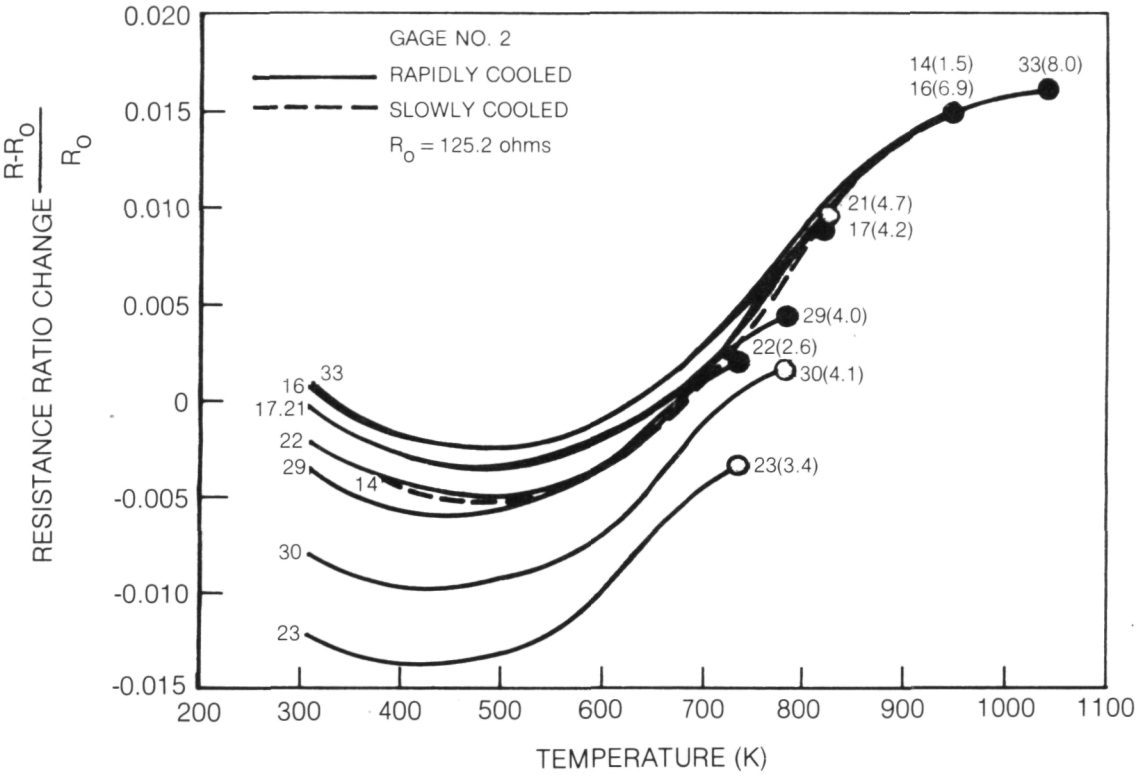

RESISTANCE RATIO CHANGE VERSUS TEMPERATURE OF KANTHAL A-1 STRAIN GAGE NO. 2 DURING RAPID COOLING FOR VARIOUS STARTING TEMPERATURES AND VARIOUS DWELL TIMES AT THE STARTING TEMPERATURE. A SOLID SYMBOL INDICATES DWELL TIME OF FIVE TO TEN MINUTES. AN OPEN SYMBOL INDICATES DWELL TIME OF TWENTY TO THIRTY MINUTES. THE NUMBER ON THE CURVE IS THE RUN NUMBER OF TABLE 8, AND THE NUMBER IN PARENTHESES IS THE COOLING RATE (K/sec.) IN THE 800K TO 700K RANGE.

84–4–18–30

2. When the gage is cooled from 950K to room temperature, the path it traces on the resistance-temperature plane depends strongly on cooling time. Rapid cooling from 950K (6.9 K/sec, curve 16) results in much smaller change in gage resistance than slow cooling from 950K (1.5 K/sec, curve 14). In the example shown in Fig. 18, the difference is on the order of 0.4 percent which is equivalent to an apparent strain difference of about 2000 microstrain. Reheating to 950K returns the gage to the original resistance. The path during heating is not shown in Fig. 18. During heating, the gage appears to retrace approximately the same path it took on the last cool-down.

3. When the gage is cooled from 950K to a temperature between 700K and 800K, and then held for some time at this intermediate temperature, the gage resistance continues to drop slowly. Examples in Fig. 18 are the dwell at 730K before run 23 and the dwell at 780K before run 30. If the cooling is then resumed, the subsequent path still depends on cool-down time, but less strongly than before the dwell at an intermediate temperature. In Fig. 18, as an example, the path of rapid cooling from 730K to room temperature, curve 23, (after a dwell at 730K) is little different from the path of slow cooling from 730K (not shown).

All of the curves in Fig. 18 are presented exactly as recorded except for one adjustment noted here. Just before run 28 the operator changed all of the strain gage bridge offset voltages by unknown amounts in order to produce zero output at room temperature. To correct for this offset, the last three curves in Fig. 18 (runs 29, 30, 33) have been translated vertically by the fixed amount required to make the 950K point of run 33 coincide with the 950K point of run 16. This procedure is based on experience with the Kanthal A-1 gages which has shown repeatedly that gage resistance always returns to nearly the same value at 950K.

The changes due to cooling time, dwell time and starting temperature of cool-down illustrated in Fig. 18 are believed to be associated with reversible metallurgical changes in the structure of the Kanthal A-1 alloy. Two possibilities are: order-disorder transformations in the atomic lattice, and precipitation of phases. A search of the literature has not allowed identification of specific metallurgical processes in FeCrAl alloys that explain the observed behavior, but this behavior is much like that reported by Bertodo in Ref. 1 for NiCrAl (Karma) alloy strain gages. The NiCrAl behavior is attributed by Bertodo to the appearance of an ordered Ni_3Cr phase during cooling, with the transformation occurring at about 813K. Since a relaxation time is required for completion of the transformation, the dwell time near 813K (or the cooling rate through 813K) strongly affects the result.

A small part of the change in gage resistance with temperature in Fig. 18 is due to the mismatch in coefficients of linear thermal expansion between the Kanthal gage and the Hastelloy substrate. This mismatch is not known precisely, but is believed to be about 1 ppm/K. For a Poisson ratio of 1/3, the resulting change in gage resistance from room temperature to 950K due to this mismatch would be about 0.1 percent. This represents only 4 percent of the change observed.

The main features of Fig. 18 are evident in the detailed measurements of resistance versus temperature for each of the ten Kanthal A-1 gages on the burner liner and the eight on the gage-factor test bars. These test results are presented in Figs. 19, 20, 21, 22, 23, 24, 25, 26, and 27, and are discussed in the remainder of this section. These results also confirmed the need to calibrate each gage individually in order to determine the correction $(r_{T1}-r_{T2})/R_o$ due to temperature to be applied in Eq. (1) for the cool-down portion of each combustor cycle for each gage.

Initial testing of the ten gages on the burner liner, before the combustor tests, consisted of measurements of resistance versus temperature during cool-downs from 950K to room temperature at eight cooling rates. Temperature versus time for the series of eight tests is presented in Fig. 19. The temperature plotted in Fig. 19 is the reading of thermocouple No. 101, adjacent to gage No. 1. All five thermocouples on the burner liner were monitored and temperature was uniform to within 3K.

Resistance versus temperature for one gage is plotted in Fig. 20 for the various cooling rates. It is evident that shorter cooling times generally resulted in smaller resistance changes from 950K to room temperature, as expected. A close examination of Figs. 19 and 20 reveals that during any one test the cooling rate (K/second) varied considerably, and that total change in resistance in Fig. 20 does not correlate simply with total cooling time from 950K to room temperature in Fig. 19. Instead, the cooling time from about 800K to 700K appears to dictate the shape of the entire curve of resistance versus temperature from 950K to room temperature in Fig. 20. The cooling time from 811K (1000°F) to 727K (850°F) was adopted, therefore, as the parameter of interest. This cooling time was denoted t_c. Its value is indicated in Fig. 19 and Fig. 20 for each test. In the fastest test t_c was 11.1 seconds and in the slowest it was 95.2 seconds.

Each of the ten gages showed a monotonic increase in resistance change with increasing t_c. The results for all ten gages in these initial cool tests are compared in Fig. 21, where overall resistance change is plotted against t_c. It is notable that the gage-to-gage scatter in Fig. 21 is large enough (about 2000 ppm) to require each gage to be individually calibrated. Further indication of this gage-to-gage scatter is presented in Fig. 22 and

FIG. 19 COOL-DOWN TESTS FOR BURNER LINER GAGES

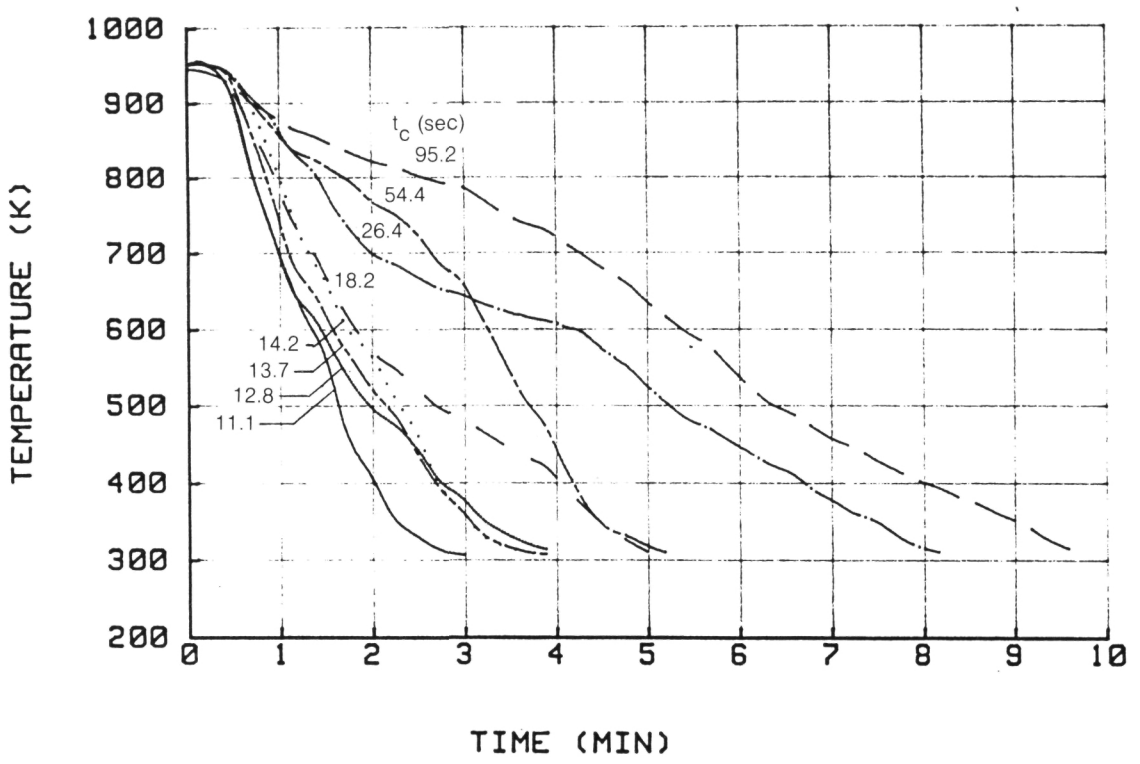

TEMPERATURE VERSUS TIME DURING EIGHT COOL-DOWN TESTS OF THE KANTHAL A-1 GAGES MOUNTED ON THE PIECE CUT FROM THE BURNER LINER, BEFORE BURNER TESTS.

84–4–18–21

FIG. 20 GAGE RESISTANCE RATIO FOR 8 COOLING RATES

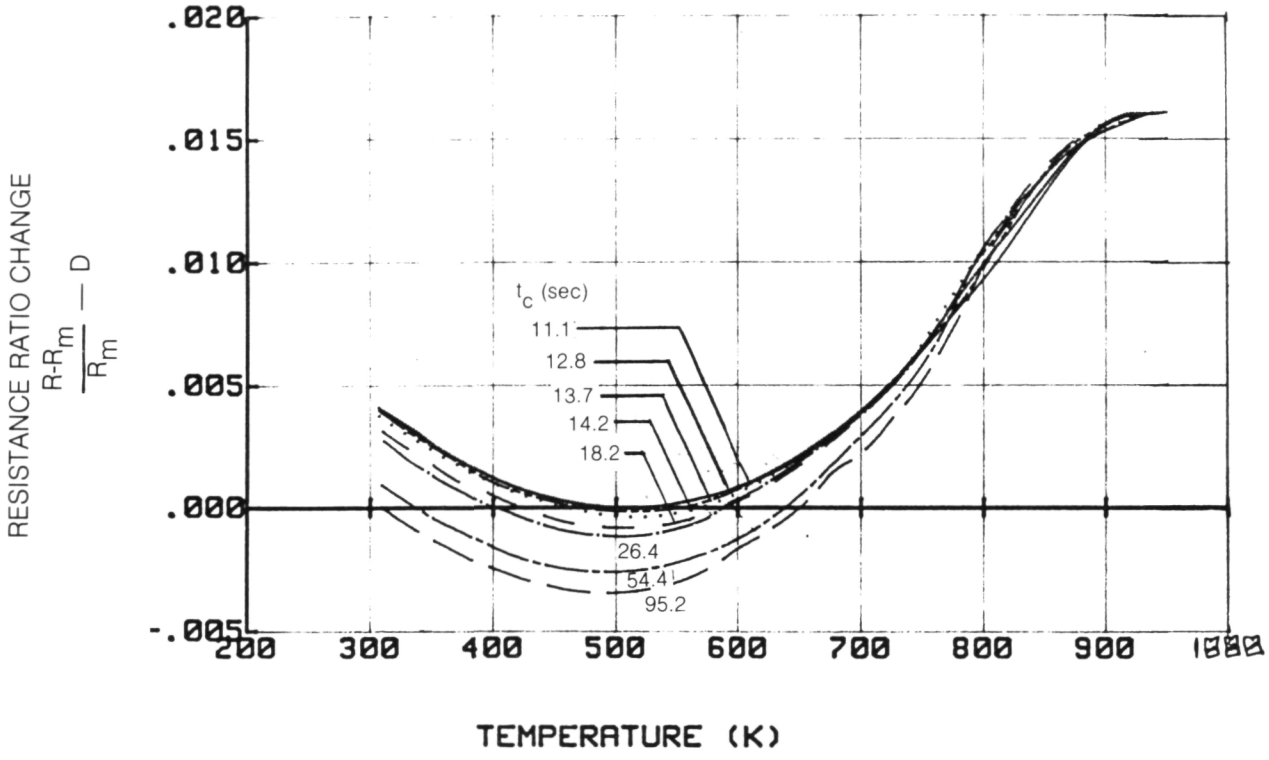

GAGE RESISTANCE RATIO CHANGE VERSUS TEMPERATURE FOR ONE GAGE ON THE BURNER LINER, AT EIGHT COOLING RATES, BEFORE THE COMBUSTOR TESTS. THE QUANTITY D IS AN ARBITRARY OFFSET ADJUSTMENT TO SUBTRACT THE EFFECTS OF SMALL DRIFTS AT 950K FROM ONE TEST TO ANOTHER SO THAT ALL CURVES PASS THROUGH THE SAME POINT AT 950K.

R = GAGE RESISTANCE

R_m = MINIMUM RESISTANCE DURING FASTEST TEST (t_c = 11.1 seconds)

t_c = COOLING TIME FROM 811K (1000°F) TO 727K (850°F)

84–4–18–22

FIG. 21 GAGE RESISTANCE CHANGE VS t_c

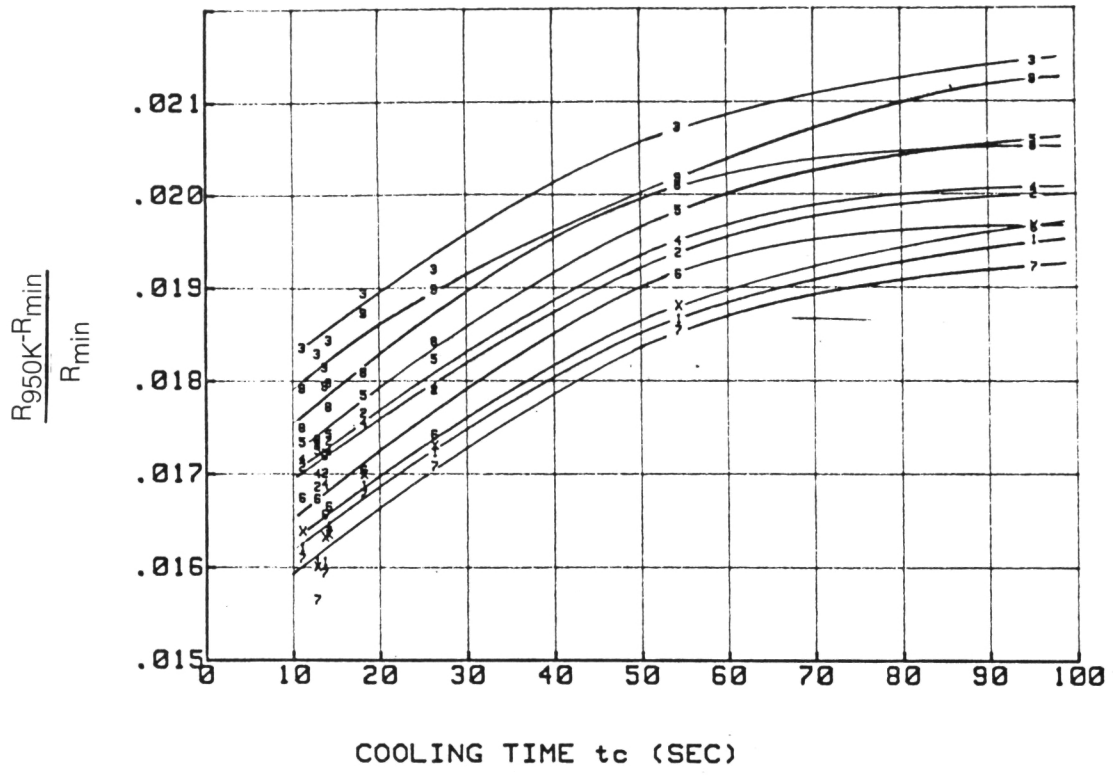

GAGE RESISTANCE CHANGE, FROM 950K TO MINIMUM-RESISTANCE TEMPERATURE, VERSUS t_c, THE COOLING-TIME PARAMETER, FOR EACH OF THE TEN GAGES ON THE BURNER LINER DURING COOL-DOWN TESTS BEFORE THE COMBUSTOR TESTS.

R_{950K} = GAGE RESISTANCE AT 950K

R_{min} = MINIMUM GAGE RESISTANCE OBSERVED DURING EACH COOL-DOWN TEST

THE SYMBOL USED FOR EACH DATA POINT IS THE GAGE NUMBER, FOR GAGES 1 THROUGH 9. SYMBOL X IS GAGE 10.

84–4–18–23

FIG. 22 NORMALIZED GAGE RESISTANCE RATIO FOR COMBUSTOR GAGES BEFORE TESTS

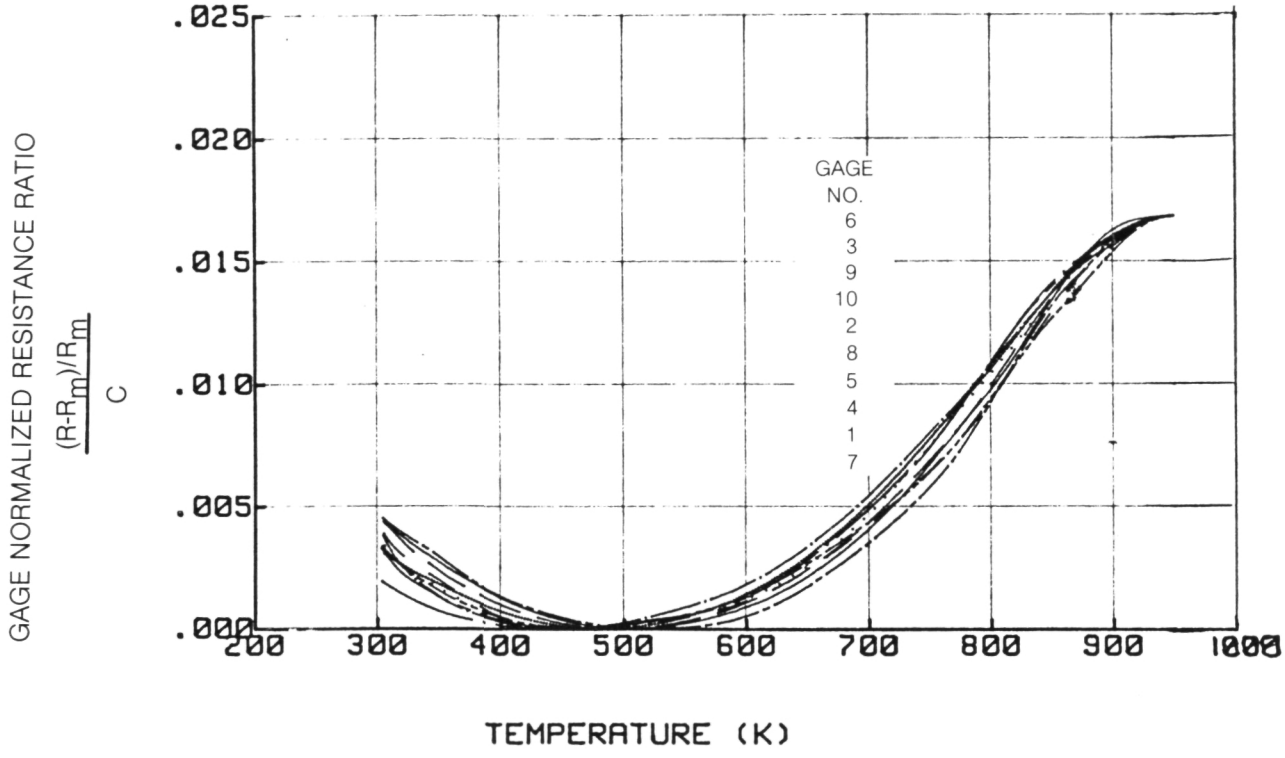

GAGE NORMALIZED RESISTANCE RATIO VERSUS TEMPERATURE DURING RAPID COOLING (t_c =11.1seconds) FROM 950K, FOR THE TEN GAGES ON THE BURNER LINER, BEFORE THE COMBUSTOR TESTS.

R = GAGE RSISTANCE

R_m = MINIMUM RESISTANCE IN EACH TEST

C = SCALING FACTOR FOR EACH GAGE

84–4–18–24

Fig. 23, in which resistance-versus-temperature tracking during rapid cooling is presented for ten gages before the combustor test (Fig. 22) and for the seven surviving gages after the combustor tests (Fig. 23). The curves are normalized by dividing the fractional resistance change by a scaling factor C, chosen for each gage after the first test so that all curves in Fig. 22 pass through 0.0165 at 950K. The values of C are listed in Table 7. Gage No. 2 was arbitrarily designated as the reference gage so that the value of C for gage No. 2 is 1.00.

The test results shown in Fig. 22 and Fig. 23 confirmed that the behavior of any one gage was repeatable from before to after combustor tests. It is this repeatability that makes the use of Kanthal A-1 gages feasible at temperatures up to 950K. The difference between the curves of Fig. 22 and Fig. 23 is plotted in Fig. 24 for each gage. The differences are remarkably small considering that the two tests are separated in time by two months and in life history by four burner tests. At 950K only gage no. 5 shows a difference larger than 250 parts per million. This gage was overtemperatured five times to 1038K during the burner testing, as described later. Maximum differences are found at temperatures between 650K and 900K, ranging from a negative 220 parts per million (Gage 5 again) to a positive 950 parts per million (Gage 1).

The eight reference Kanthal A-1 gages on the two gage-factor test bars were also tested for resistance versus temperature while rapidly cooled from 950K to room temperature (t_c = 12 seconds). These cooling tests were performed after each bar had accumulated two hours at 960K and one complete sequence of gage factor tests to 950K. The resulting curves are shown in Fig. 25. The scaling factor C for each gage is included in Table 7. The resistance versus temperature curves in Fig. 25 fall within the same envelope as the curves for the burner liner gages (Fig. 23). The test bar temperature scaling factors in Table 7 scatter within the same range (1.00 $\pm$ 0.07) as the scaling factors for the burner liner gages.

FIG. 23 NORMALIZED GAGE RESISTANCE RATIO FOR COMBUSTOR GAGES AFTER TESTS

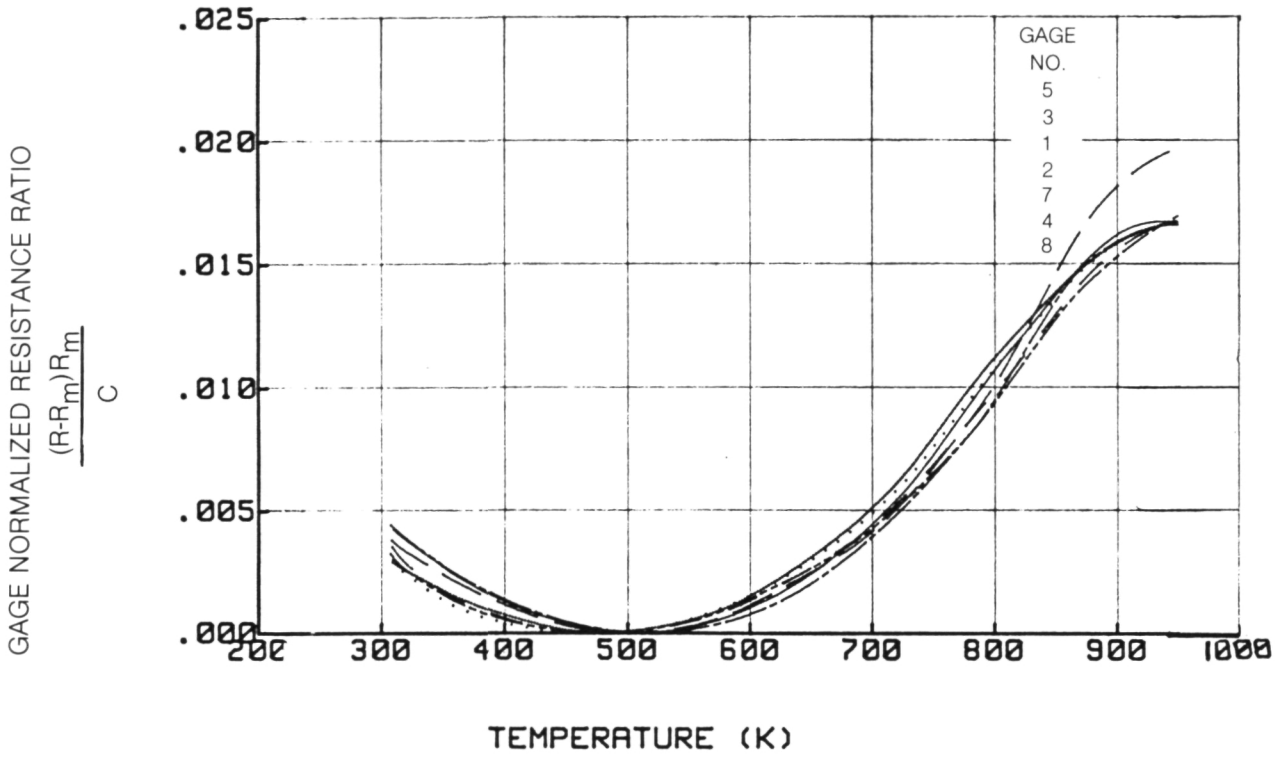

GAGE NORMALIZED RESISTANCE RATIO VERSUS TEMPERATURE DURING RAPID COOLING (t_c = 12.0 seconds) FROM 950K, FOR THE SEVEN GAGES ON THE BURNER LINER AFTER THE COMBUSTOR TESTS. THE SCALING FACTOR C FOR EACH GAGE IS THE SAME AS THAT USED IN FIGURE A. THE RESULTS ARE ALL WITHIN THE ENVELOPE OF THE ORIGINAL CALIBRATION CURVES OF FIGURE A, EXCEPT FOR GAGE NO. 5 WHICH EXPERIENCED OVERTEMPERATURES TO 1041K DURING THE COMBUSTOR TESTS.

84–4–18–25

FIG. 24 EFFECT OF COMBUSTOR TESTS ON NORMALIZED GAGE RESISTANCE RATIO

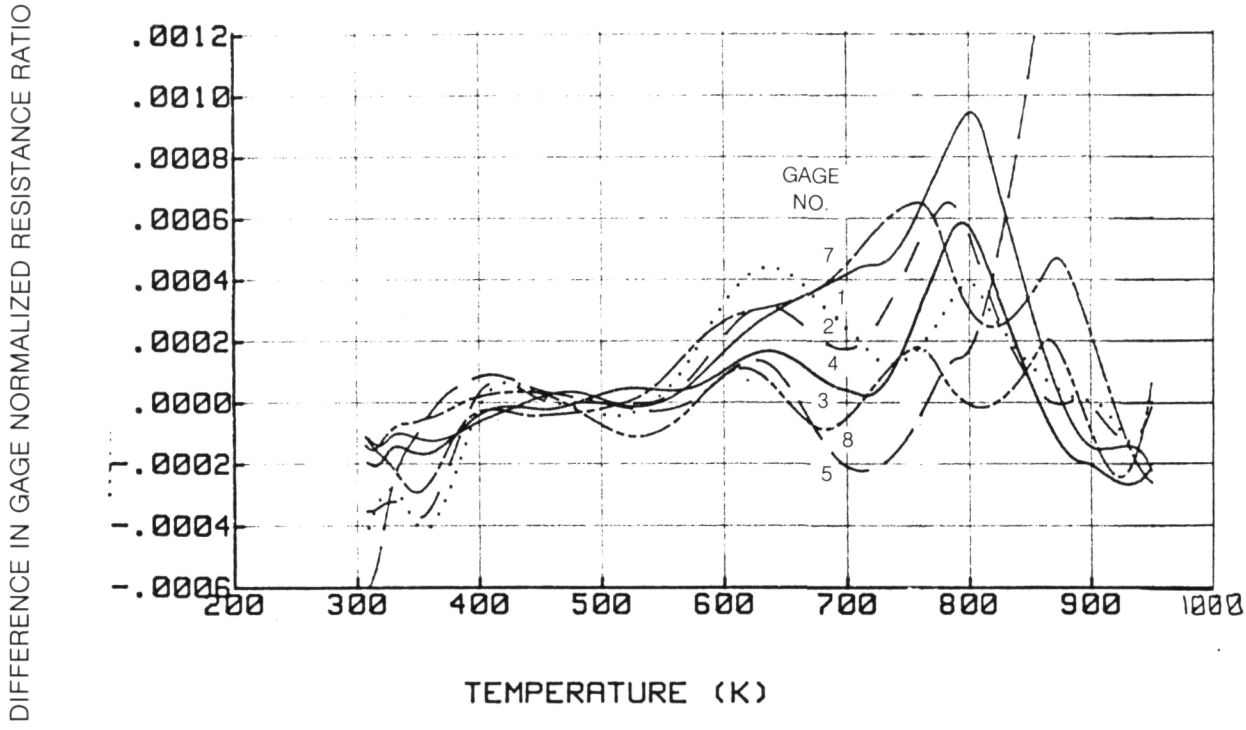

DIFFERENCE IN GAGE NORMALIZED RESISTANCE RATIO VERSUS TEMPERATURE FROM BEFORE TO AFTER THE BURNER TESTS FOR RAPID COOLING FROM 950K. THE DIFFERENCE BETWEEN FIG. 22 AND FIG. 23 IS PLOTTED FOR EACH GAGE.

84-4-18-26

FIG. 25 NORMALIZED GAGE RESISTANCE RATIOS FOR TEST BAR GAGES

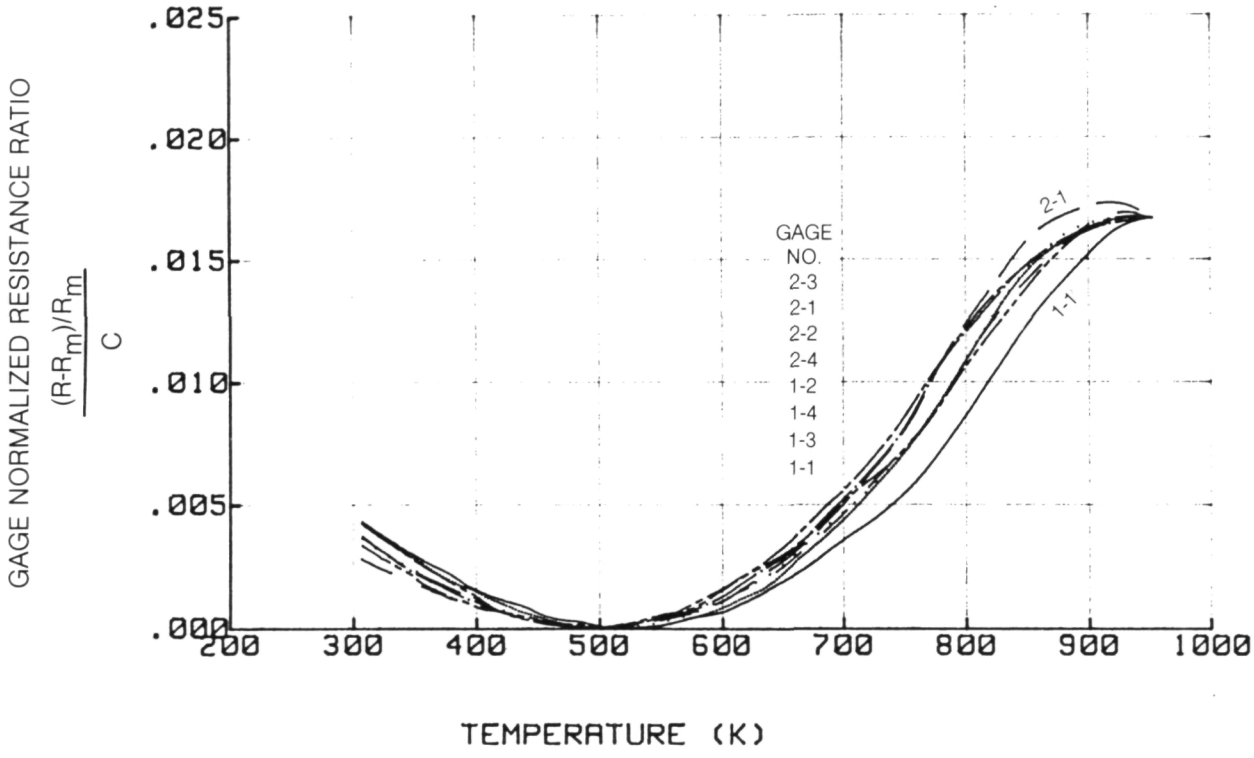

GAGE NORMALIZED RESISTANCE RATIO VERSUS TEMPERATURE DURING RAPID COOLING FROM 950K FOR THE EIGHT GAGES ON THE TWO GAGE-FACTOR TEST BARS. ALL OF THESE CURVES FALL WITHIN THE ENVELOPE OF FIG. 22. THE COOLING-TIME PARAMETER t_c WAS 12 ± 1 SECONDS IN EACH OF THESE TESTS.

84—4—18—27

TABLE 7

Values of Scaling Factor C

Component	Gage No.	C
Burner Liner	1	0.95
Burner Liner	2	1.00
Burner Liner	3	1.08
Burner Liner	4	1.01
Burner Liner	5	1.02
Burner Liner	6	0.99
Burner Liner	7	0.93
Burner Liner	8	1.03
Burner Liner	9	1.03
Burner Liner	10	0.95
Test Bar 1	1-1	1.03
Test Bar 1	1-2	1.02
Test Bar 1	1-3	0.99
Test Bar 1	1-4	1.04
Test Bar 2	2-1	0.99
Test Bar 2	2-2	1.02
Test Bar 2	2-3	1.00
Test Bar 2	2-4	1.01

$$C = [(R_{950K} - R_{min})/R_{min}]/0.0165,$$

where R_{950K} and R_{min} are measured during rapid cooling from 950K (t_c = 12 + 1 seconds).

Upon the completion of the first cooling tests after the burner test, shown in Fig. 23, the instrumented piece cut from the burner liner was subjected to a final series of 24 additional special cooling tests as listed in Table 8. These tests were designed to simulate and bracket specific conditions encountered during one or more of the seven burner cycles. The tests determined the slope of the curve of resistance change (divided by the current value of R_o) versus temperature for each of the seven surviving gages over temperature ranges and cooling rates close to the actual burner test conditions. The slopes are listed in the right-hand columns of Table 8. These slopes were used later when reducing the burner test data as follows: A slope

TABLE 8

RESISTANCE CHANGE VERSUS TEMPERATURE, FOR GAGES ON THE BURNER LINER. TESTS 1 THROUGH 8 WERE CONDUCTED BEFORE THE HIGH PRESSURE BURNER TESTS, AND TESTS 9 THROUGH 40 AFTER.

Test No.	Max. Temp. T3 (K)	Approx. Dwell Time at T3 (Minutes)	Cooling Time t_x T1 to T2 (Sec)	T1 (K)	T2 (K)	$\frac{T_1-T_2}{t_x}$ (K/sec)	$10^6 (r_{T1} - r_{T2})/[Ro \ (T1-T2)]$ parts per million per Kelvin						
							Gage 1	Gage 2	Gage 3	Gage 4	Gage 5	Gage 7	Gage 8
1	950	10	12.8	811	727	6.54	57.9	59.3	62.4	56.5	61.9	61.0	58.8
2	950	10	14.2	811	727	5.92	72.7	68.7	72.0	66.4	68.4	65.3	62.4
3	950	10	13.7	811	727	6.12	64.4	67.6	67.7	60.6	63.1	58.8	57.9
4	950	10	18.2	811	727	4.62	75.0	70.9	72.2	73.4	77.6	73.9	70.9
5	950	10	95.2	811	727	.88	85.8	84.0	89.1	88.1	87.1	86.0	90.9
6	950	10	26.4	811	727	3.19	75.2	70.7	76.7	72.2	78.3	70.4	71.1
7	950	10	54.4	811	727	1.54	80.3	78.1	83.3	81.4	82.2	80.3	82.9
8	950	10	11.1	811	727	7.55	63.9	62.5	67.2	64.6	70.4	69.6	66.7
9	950	10	12.0	811	727	6.98	63.2	62.2	68.4	58.4	67.8	57.4	57.6
10	950	10	13.1	811	727	6.41	59.4	61.2	61.4	53.9	61.3	55.6	59.3
11	950	10	16.6	811	727	5.05	70.1	73.2	74.0	70.1	76.9	63.1	63.3
12	950	10	22.2	811	727	3.79	74.8	77.4	75.3	78.1	83.9	70.8	74.1
13	950	10	30.5	811	727	2.76	80.9	82.1	79.4	82.4	82.6	76.3	78.7
14	950	10	57.6	811	727	1.46	81.5	74.3	83.3	77.1	94.8	80.4	78.7
15	950	10	38.9	811	727	2.16	79.5	76.9	81.1	81.0	89.2	78.9	81.6
16	950	10	12.2	811	727	6.89	59.3	59.4	62.0	60.7	70.2	64.7	65.4
17	819	10	20.0	811	727	4.21	68.7	65.5	65.8	68.8	80.8	65.6	72.1
18	819	20	18.6	811	727	4.53	66.0	65.0	66.4	70.1	83.1	66.9	74.0
19	819	10	113.6	811	727	.74	89.6	90.4	94.5	91.4	103.5	88.6	93.5
20	819	10	19.1	811	727	4.40	66.2	64.8	66.1	69.6	81.9	66.1	72.4
21	819	20	18.0	811	727	4.66	66.6	65.1	66.0	68.4	79.8	64.5	70.9
22	733	10	12.6	733	700	2.63	32.1	29.6	34.8	35.5	52.1	45.2	62.1
23	733	20	9.7	733	700	3.42	31.1	34.2	46.3	57.8	74.1	66.0	84.7
24	733	10	28.6	733	700	1.15	54.6	44.8	59.9	50.1	59.2	55.4	56.2
25	733	20	29.6	733	700	1.12	53.9	48.8	62.6	52.9	71.8	57.4	57.0
26	733	10	9.4	733	700	3.51	30.3	33.6	48.1	52.2	62.6	59.5	74.7
27	733	20	14.7	733	700	2.24	58.8	58.8	64.0	72.1	94.5	71.7	81.4
28	950	10	4.0	811	727	21.21	71.4	69.7	73.4	72.8	82.7	61.1	61.9
29	783	10	19.8	780	700	4.04	43.2	38.0	45.2	45.5	56.2	42.2	52.8
30	783	20	19.7	780	700	4.06	38.8	35.1	39.3	41.5	56.9	50.6	63.6
31	783	10	69.8	780	700	1.15	56.9	54.3	63.9	58.0	70.5	57.3	61.3
32	783	10	18.4	780	700	4.35	45.4	41.5	43.5	50.8	65.6	56.2	70.9
33	1041	10	27.3	1037	819	7.99	29.3	28.3	31.2	34.4	37.2	37.0	44.4
34	1041	10	105.4	1037	819	2.07	30.4	29.0	32.9	31.1	41.3	32.4	36.7
35	1041	10	264.3	1037	819	.89	28.0	30.3	36.0	29.3	41.0	18.7	23.4
36	1041	10	145.3	1037	819	1.50	29.3	39.7	35.8	38.2	35.9	16.1	24.4
37	1041	10	37.4	1037	819	5.83	44.9	46.8	46.7	52.8	57.2	35.3	42.2
38	1041	10	92.2	1037	819	2.36	42.7	44.0	45.1	48.8	55.2	31.4	36.8
39	1041	10	67.5	1037	819	3.23	42.2	45.0	44.8	48.5	56.3	31.4	38.1
40	1041	10	19.5	1037	819	11.17	32.8	29.3	33.6	31.3	26.7	27.6	37.9

interpolated from Table 8 was multiplied by the actual temperature change during the burner test to obtain the quantity $(r_{T2}-r_{T1})/R_o$ in equation 1. In each cooling test, the piece cut from the burner liner was heated to a temperature T3 listed in the table (heating time from room temperature to T3 was about ten minutes), held at T3 for the approximate time indicated, and then cooled to room temperature. The table lists the cooling time for a selected temperature range T1 to T2 in each test, and the fractional change in gage resistance per Kelvin over the interval T1 to T2. The tests are listed in chronological order from top to bottom in the table (test 1 to test 40). The final runs (33 through 40) simulated the overtemperature condfition encountered at location A (Fig. 1) during central burner tests, and represent an attempt to retrieve data from Gage 5, the only survivor of the four at location A.

Gage Factor Versus Temperature

Figures 26 and 27 are plots of measured gage factor versus temperature for the eight Kanthal A-1 strain gages on the two gage-factor test bars. The test procedure for measurement of gage factor was previously described in Section 4.2.5. Inspection of these plots immediately reveals that the gages fall into two classes. Three gages on Bar 1 (gages 1-1, 1-2, 1-3) are in one class and are characterized by very low gage factor at room temperature (1.6 to 2.0), large nonlinearity with strain level (about 10 percent), and large asymmetry with direction of applied strain (about 10 percent difference for tension versus compression). The fourth gage on Bar 1 (gage 1-4) and the four gages on Bar 2 (gages 2-1, 2-2, 2-3, 2-4) are in the second class and are characterized by high gage factor (2.1 to 2.4), generally good linearity with strain (5 percent) and symmetry with respect to direction of applied strain (5 percent). Gage factor trends downward at high temperature in both classes. The behavior of the second class is close to that reported in previous NASA contracts NAS3-22126 and NAS3-23169.

Bar 1 was retested after 200 hours in air at 960K, and Bar 2 was retested immediately after heating to 960K and rapid cooling to room temperature (t_c = 12 seconds) to determine whether heat treatment history was affecting gage behavior. These procedures generally resulted only in small changes in gage factor level or behavior. As shown in Fig. 26, the 200-hour bake changed gage 1-1 from the first class to the second (much higher gage factor and much better linearity) but had no significant effect on the other three gages on Bar 1. The rapid cooling shifted all factors on Bar 2 by small amounts, generally 2 percent to 4 percent downward (Fig. 27). The test of Bar 1 after the 200-hour bake was repeated after removing and reinstalling the bar in the test apparatus to confirm the validity of gage-factor testing procedure. The repeatability (Fig. 26) was good.

FIG. 26 GAGE FACTORS FOR BAR 1 GAGES

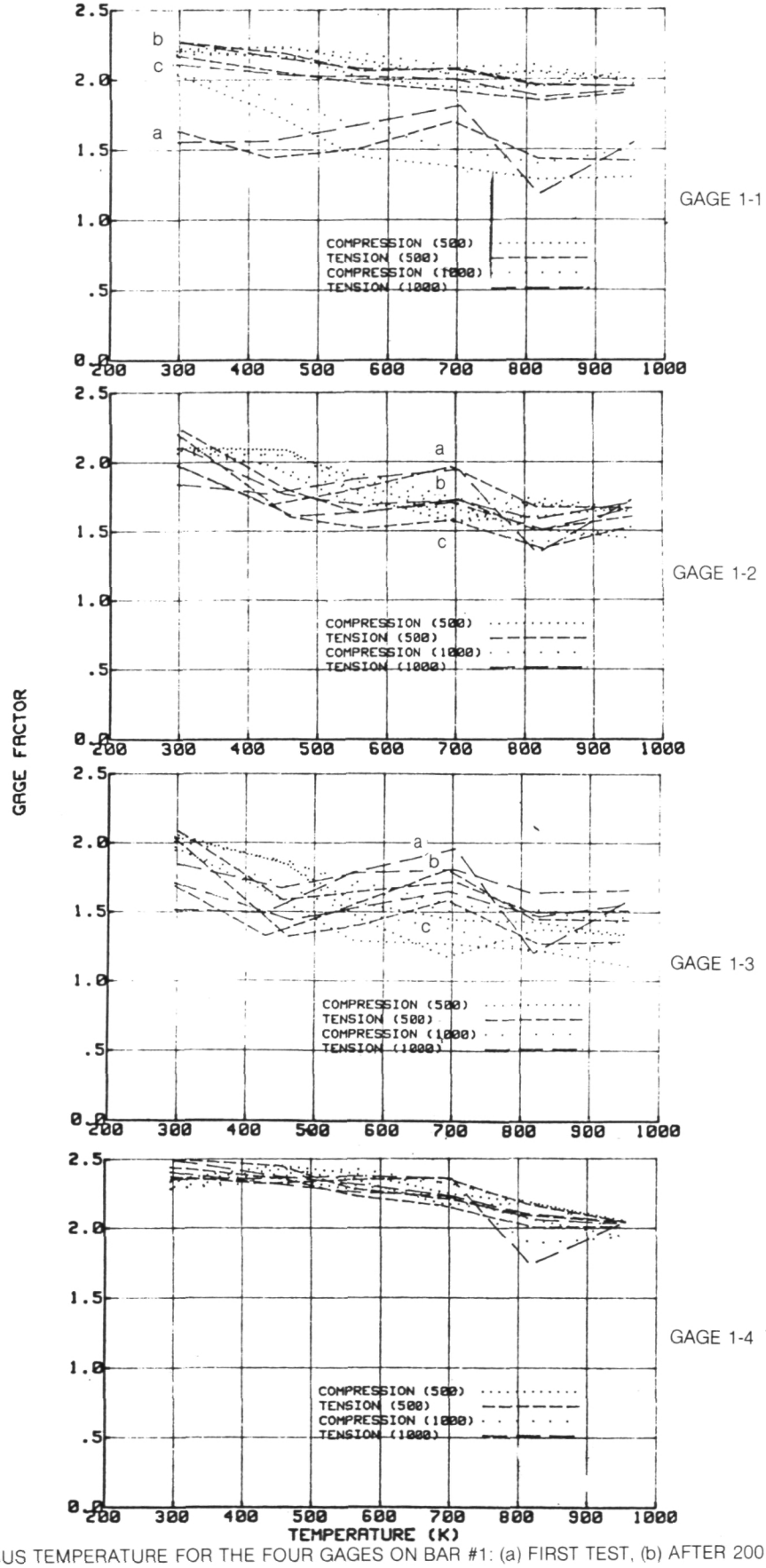

GAGE FACTOR VERSUS TEMPERATURE FOR THE FOUR GAGES ON BAR #1: (a) FIRST TEST, (b) AFTER 200 hours AT 950K (c), REPEAT OF b.

84–4–18–28

FIG. 27 GAGE FACTORS FOR BAR 2 GAGES

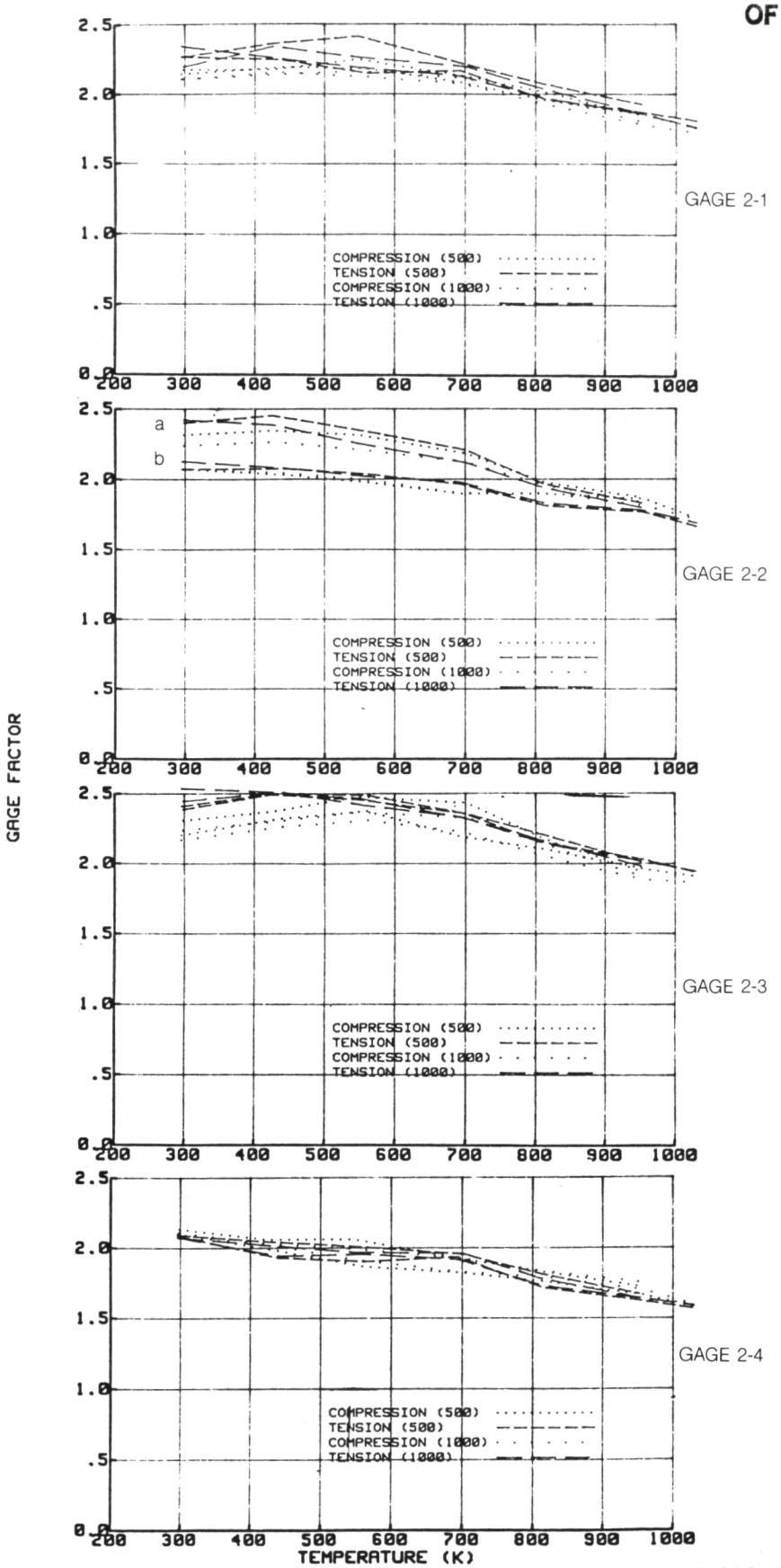

GAGE FACTOR VERSUS TEMPERATURE FOR FOUR GAGES ON BAR #2: (a) FIRST TEST, (b) AFTER RAPID COOLING FROM 950K TO ROOM TEMPERATURE AT $t_c = 12$ sec.

84–4–18–29

Because the burner liner temperature was in the neighborhood of 800K during most of the burner liner testing program, the behavior of gage factor at this temperature was closely examined for the gages on the test bars. Table 9 lists the gage factor for each gage at 800K for each test, averaged over the four strain levels of each test (+500, -500, +1000, -1000 microstrain). At the bottom of Table 9, average gage factor and standard deviation of gage factor are listed for all gages and for each of the two classes of gages. The high gage factor (1.956) and small standard deviation (7.7 percent) of the second class are evident.

The question remained as to which gages on the burner liner belonged to the first class and which belonged to the second class during the burner test. Two possible methods for answering this question were investigated. The first possibility was that the change of gage resistance with temperature (during rapid cooling) might correlate with gage factor, since if any significant mismatch in temperature coefficient of expansion existed then gage-to-gage variations in gage bonding to the surface could affect both gage resistance versus temperature and gage factor. No such correlation was found. For example, comparison of the values of the calibration constant C in Table 7 and the gage factor G in Table 9 shows no systematic relationship. This result may simply mean that mismatch was small. The second possibility was that post-test visual (destructive) inspection of the individual gages would reveal structural features peculiar to one class or another, such as oxidation, cracking of gage wire materials, or incomplete bonding of some gage loops.

The second approach was successfully carried out as follows. A destructive examination was performed for the eight gages on the two gage-factor test bars and the seven gages still functional on the burner liner after the burner tests. The overcoat layer was gradually scraped away, using dental tools, and two kinds of structural defects were found in the ceramic cement layer. One kind of defect occurred only on the three gages of the first class (on test bar 1), and consisted of local voids in the cement, as shown in the photographs in Fig. 28. The voids occur within the area of the strain gage grid along a transverse line near the end loops. This line is the boundary between the two separate applications of cement in the ladder-taping sequence employed during gage fabrication described in Section 4.2.2. No such voids were found in any other gage installations on the test bars or on the burner liner. The unusual behavior of gages 1-1, 1-2, 1-3 (low gage factor and non-linear strain response) was attributed to the presence of the voids, although the detailed mechanism is not clear. It would seem that poor bonding of at least one end loop and one grid wire would be required to produce the observed behavior. The total effect of several voids near the end loops would appear to have produced a similar result.

TABLE 9

Average Gage Factor at 800K (980°F)
(Values are averaged for +500, -500, +1000, and -1000 microstrain)

Bar No.	Gage No.	G
1	1-1	1.40
	1-1	1.95*
1	1-2	1.60
	1-2	1.60*
1	1-3	1.40
	1-3	1.45*
1	1-4	2.10
	1-4	2.10*
2	2-1	2.00
	2-1	1.92**
2	2-2	1.90
	2-2	1.82**
2	2-3	2.15
	2-3	2.10**
2	2-4	1.77
	2-4	1.70**

Category	Average	Std. Dev.
all gages	1.810	.251 (13.9%)
class 1	1.567	.191 (12.1%)
class 2	1.956	.150 (7.7%)

*After 200 Hours at 960K
**After rapid cooling

FIG. 28 PHOTOGRAPH OF VOIDS IN CEMENT OF TEST BAR GAGES

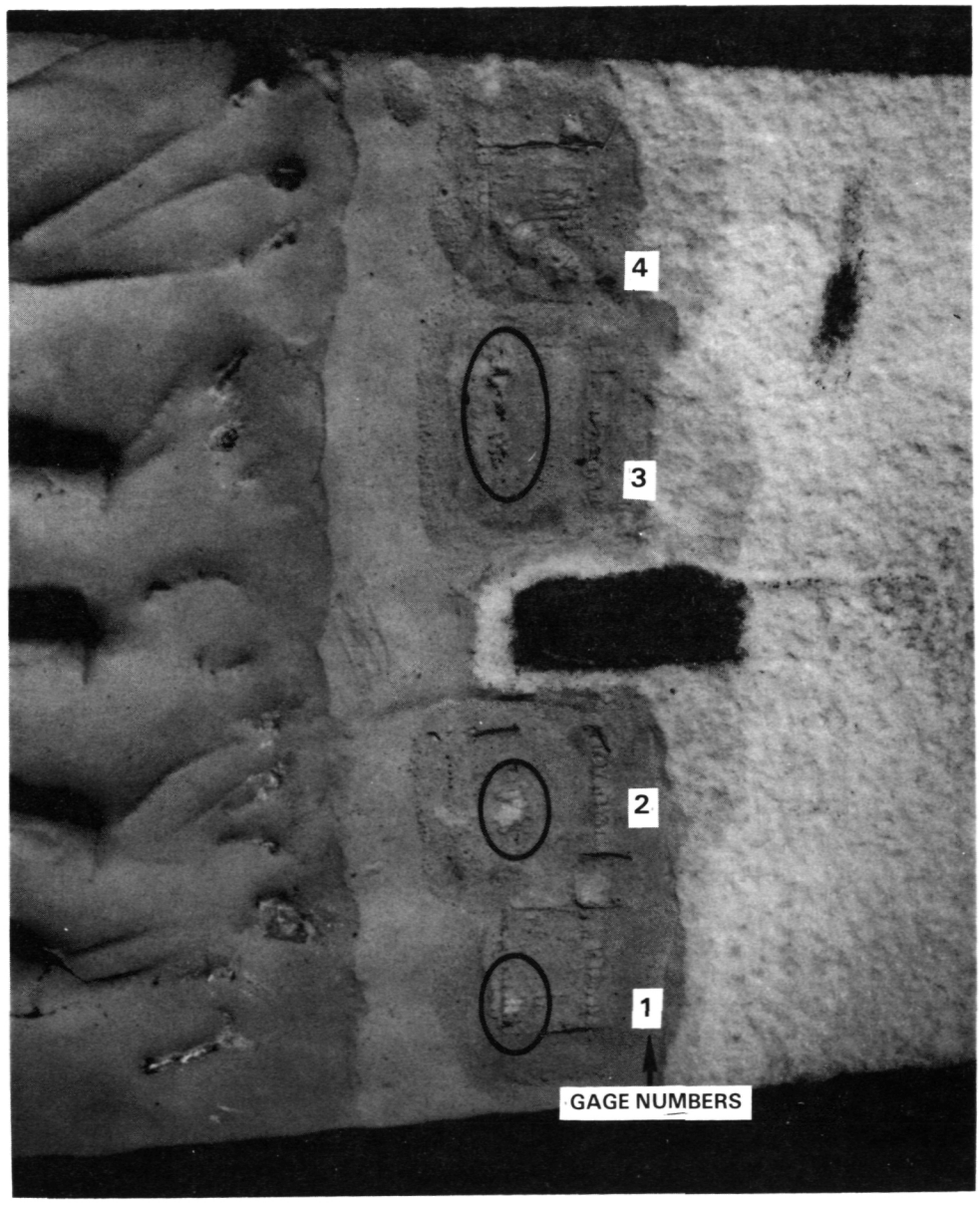

VOIDS IN CEMENT

POST-TEST EXAMINATION OF GAGE-FACTOR TEST BAR NO. 1 REVEALS VOIDS IN THE CEMENT NEAR THE LEFT END LOOPS OF GAGES 1, 2, 3. THE VOIDS (IN THE CIRCLED AREAS) OCCUR ALONG THE TAPE EDGE LINE. THE CEMENT COVERING THE END LOOPS WAS FOUND TO BE SOUND. IN THIS PHOTO, THE LEFT END LOOPS OF GAGE 4 AND THE RIGHT END LOOPS OF 1, 2, 3, 4 ARE VISIBLE WHERE THE CEMENT WAS SCRAPED AWAY DURING EXAMINATION.

The second kind of defect was found only on the burner liner, on gages 5 and 9 at location A. The cement layer under each gage (as revealed by post-test scraping) was found to be powdery and sufficiently non-adherent to the gage wire that the gage was judged to be partially free-floating inside a cement jacket and not systematically subjected to mechanical strain. The burner test data for these gages was reduced along with all other data to determine to what extent any strain was indicated by these gages, and the results are discussed in the next section. It should be noted here that the thermocouples (55 and 56) at this location failed in the first burner test, due to cracking of the cement. After repair of the thermocouples it was found that the temperature at location A exceeded the planned 950K, reaching 1040K (1410°F) during each burner cycle. The ceramic cement has been used successfully in the past to at least 1250K (1800°F), so the overtemperature alone should not have produced failure of the cement. It is believed that the failure was due to some combination of contamination remaining after surface preparation, incomplete mixing or curing of the cement, and too thick an application of cement.

These post-test examinations indicated that the gages on the burner liner were class 2 gages. The following expression, therefore, was used to describe gage factor as a function of temperature, in reducing the data for each gage in the burner liner test (in the temperature range above 700K):

$$G = 2.0 + 0.00078\ (800 - T) \qquad (4)$$

where T is gage temperature, Kelvin. Equation (4) was deduced by inspection of all the data on Figs. 26 and 27 for gages of class 2 (1-4, 2-1, 2-2, 2-3, 2-4). The two-sigma uncertainty, based on Table 9, is about 2 X 7.7 percent or about 16 percent.

5.3.2.3 Results of Burner Tests

Presentation Format

In Table 10, the strain gage data acquired during the burner tests are summarized. The resulting measured strain increments are compared with predicted strain increments in Fig. 29. The data were acquired during seven cycles of burner operation, each cycle consisting of acceleration from an initial idle condition (temperature of the strain gage at a value T2) to a high-temperature operating point (temperature T1), dwell for a few minutes at the high temperature T1, and deceleration to the initial idle condition (temperature returned to T2). Acceleration and deceleration were produced by increasing and decreasing the rate of fuel flow. Inlet air flow temperature

Table 10: Combustor Test Strain Gage Data and Analysis

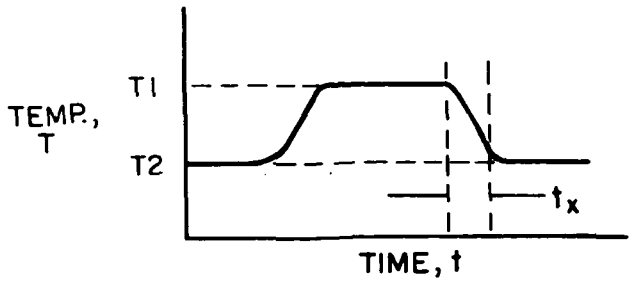

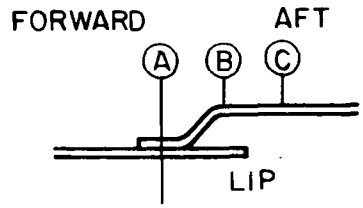

$$e_1 - e_2 = \frac{K}{G_1}(E_1 - E_2) - \frac{1}{G_1}\frac{r_{T1} - r_{T2}}{R_o} - \frac{G_2 - G_1}{G_1} e_2 \qquad (1)$$

Cycle No.		1							
Burner Run No:		3							
Cum. Time At T1:		14 min.							
Cooling time t_x:		77 sec.							
$(TT4)_1$		1261K							
$(TT4)_2$		955K							
TT3		717K							
Location			C			B	A		LIP
Orientation		HOOP	HOOP	AX.	AX.	HOOP	HOOP	AX.	- -
Gage No.		1	2	7	8	3	5	9	-
Thermocouple No.		51	52	51	52	53	55	55	57
T1	(K)	772	769	772	769	783	-	-	1088
T2	(K)	727	727	727	727	727	-	-	844
Predicted e_1	(Microstrain)	556	556	-2044	-2044	2730	-	-	-
Predicted e_2	(Microstrain)	201	201	-699	-699	981	-	-	-
Predicted $e_1 - e_2$	(Microstrain)	355	355	-1305	-1305	1750	-	-	-
$(T_1 - T_2)/t_x$	(K/sec.)	.58	.55	.58	.55	.73	-	-	-
$10^6 (r_{T1} - r_{T2})/R_o(T1-T2)$		59.2	56.9	57.9	60.0	66.6	-	-	-
$10^6 (r_{T1} - r_{T2})/R_o G_1$		1315	1181	1286	1245	1853	-	-	-
$10^6 (E_1 - E_2) K/G_1$		2472	2519	543	2174	2682	-	-	-
$10^6 (G_1 - G_2) e_2/G_1$		3	3	-12	-11	21	-	-	-
$e_1 - e_2$ (Equ. 1, Microstrain)		1154	1335	-731	940	808	-	-	-

Cycle No.		2							
Burner Run No:		4							
Cum. Time At T1:		15 min.							
Cooling time t_x:		57 sec.							
$(TT4)_1$		1244K							
$(TT4)_2$		922K							
TT3		711K							
Location			C			B	A		LIP
Orientation		HOOP	HOOP	AX.	AX.	HOOP	HOOP	AX.	- -
Gage No.		1	2		8	3	5	9	-
Thermocouple No.		51	52	51	52	53	55	55	57
T1	(K)	736	733	736	733	750	-	-	1055
T2	(K)	700	700	700	700	700	-	-	811
Predicted e_1	(Microstrain)	556	556	-2004	-2004	2730	-	-	-
Predicted e_2	(Microstrain)	201	201	-699	-699	981	-	-	-
Predicted $e_1 - e_2$	(Microstrain)	355	355	-1305	-1305	1750	-	-	-
$(T_1 - T_2)/t_x$	(K/sec.)	.63	.58	.63	.58	.88	-	-	-
$10^6 (r_{T1} - r_{T2})/R_o(T1-T2)$		59.3	49.9	60.2	52.0	65.6	-	-	-
$10^6 (r_{T1} - r_{T2})/R_o G_1$		1043	803	1059	838	1609	-	-	-
$10^6 (E_1 - E_2) K/G_1$		1659	2194	-96	1707	2159	-	-	-
$10^6 (G_1 - G_2) e_2/G_1$		3	2	-10	-9	19	-	-	-
$e_1 - e_2$ (Equ. 1, Microstrain)		613	1389	-1145	878	531	-	-	-

Cycle No. 3
Burner Run No: 5
Cum. Time At T1: 17 min.
Cooling time t_x: 40 sec.
$(TT4)_1$ 1255K
$(TT4)_2$ 955K
TT3 710K

Location		C				B	A		LIP
Orientation		HOOP	HOOP	AX.	AX.	HOOP	HOOP	AX.	- -
Gage No.		1	2	7	8	3	5	9	-
Thermocouple No.		51	52	51	52	53	55	55	57
T1	(K)	761	761	761	761	777	1041	1041	1072
T2	(K)	722	722	722	722	722	819	819	833
Predicted e_1	(Microstrain)	556	556	-2004	-2004	2730	-419	911	-
Predicted e_2	(Microstrain)	201	201	-699	-699	981	-172	328	-
Predicted e_1-e_2	(Microstrain)	355	355	-1305	-1305	1750	-247	583	-
$(T_1-T_2)/t_x$	(K/sec.)	.98	.98	.98	.98	1.38	5.55	-	-
10^6 $(r_{T1}-r_{T2})/R_o(T1-T2)$		57.3	54.7	57.0	60.3	62.1	46.1	-	-
10^6 $(r_{T1}-r_{T2})/R_oG_1$		1103	1050	1094	1158	1690	5640	-	-
10^6 $(E_1^1 - E_2^2)$ K/G_1		2070	2265	394	2266	2377	3809	-	-
10^6 $(G_1^1 - G_2^2)$ e_2/G_1		3	3	-10	-10	21	-16	-	-
$e_1 - e_2$ (Equ. 1, Microstrain)		964	1212	-690	1118	666	-1815	-	-

Cycle No. 4
Burner Run No: 5
Cum. Time At T1: 19 min.
Cooling time t_x: 15 sec.
$(TT4)_1$ 1255K
$(TT4)_2$ 955K
TT3 710K

Location		C				B	A		LIP
Orientation		HOOP	HOOP	AX.	AX.	HOOP	HOOP	AX.	- -
Gage No.		1	2	7	8	3	5	9	-
Thermocouple No.		51	52	51	52	53	55	55	57
T1	(K)	761	761	761	761	777	1041	1041	1072
T2	(K)	722	722	722	722	722	819	819	833
Predicted e_1	(Microstrain)	556	556	-2004	-2004	2730	-419	911	-
Predicted e_2	(Microstrain)	201	201	-699	-699	981	-172	328	-
Predicted e_1-e_2	(Microstrain)	355	355	-1305	-1305	1750	-247	583	-
$(T_1-T_2)/t_x$	(K/sec.)	2.60	2.60	2.60	2.60	3.67	14.80	-	-
10^6 $(r_{T1}-r_{T2})/R_o(T1-T2)$		49.8	46.4	53.4	61.6	46.1	14.1	-	-
10^6 $(r_{T1}-r_{T2})/R_oG_1$		956	891	1025	1182	1255	1727	-	-
10^6 $(E_1^1 - E_2^2)$ K/G_1		2019	2267	296	2020	2479	3978	-	-
10^6 $(G_1^1 - G_2^2)$ e_2/G_1		3	3	-10	-10	21	-16	-	-
$e_1 - e_2$ (Equ. 1, Microstrain)		1060	1373	-719	848	1201	2267	-	-

Cycle No. 5
Burner Run No: 5
Cum. Time At T1: 20 min.
Cooling time t_x: 20 sec.
$(TT4)_1$ 1255K
$(TT4)_2$ 955K
TT3 710K

Location		C				B	A		LIP
Orientation		HOOP	HOOP	AX.	AX.	HOOP	HOOP	AX.	- -
Gage No.		1	2	7	8	3	5	9	-
Thermocouple No.		51	52	51	52	53	55	55	57
T1	(K)	761	761	761	761	777	1041	1041	1072
T2	(K)	722	722	722	722	722	819	819	833
Predicted e_1	(Microstrain)	556	556	-2004	-2004	2730	-419	911	-
Predicted e_2	(Microstrain)	201	201	-699	-699	981	-172	328	-
Predicted e_1-e_2	(Microstrain)	355	355	-1305	-1305	1750	-247	583	-
$(T_1-T_2)/t_x$	(K/sec.)	1.95	1.95	1.95	1.95	2.75	11.1	-	-
10^6 $(r_{T1}-r_{T2})/R_o(T1-T2)$		52.8	49.7	54.8	61.1	52.5	26.9	-	-
10^6 $(r_{T1}-r_{T2})/R_oG_1$		1015	955	1054	1172	1432	3295	-	-
10^6 $(E_1^1 - E_2^2)$ K/G_1		2020	2365	296	2217	2528	4305	-	-
10^6 $(G_1^1 - G_2^2)$ e_2/G_1		3	3	-10	-10	21	-16	-	-
$e_1 - e_2$ (Equ. 1, Microstrain)		1002	1407	-748	1055	1075	1026	-	-

Table 10 (Cont'd)

Cycle No.		6							
Burner Run No:		5							
Cum. Time At T1:		22 min.							
Cooling time t_x:		15 sec.							
$(TT4)_1$		1255K							
$(TT4)_2$		955K							
TT3		710K							
Location			C			B	A		LIP
Orientation		HOOP	HOOP	AX.	AX.	HOOP	HOOP	AX.	- -
Gage No.		1	2	7	8	3	5	9	-
Thermocouple No.		51	52	51	52	53	55	55	57
T1	(K)	761	761	761	761	777	1041	1041	1072
T2	(K)	722	722	722	722	722	819	819	833
Predicted e_1	(Microstrain)	556	556	-2004	-2004	2730	-419	911	-
Predicted e_2	(Microstrain)	201	201	-699	-699	981	-172	328	-
Predicted e_1-e_2	(Microstrain)	355	355	-1305	-1305	1750	-247	583	-
$(T_1-T_2)/t_x$	(K/sec.)	2.60	2/60	2.60	2.60	3.67	14.8	-	-
10^6 $(r_{T1}-r_{T2})/R_o(T1-T2)$		49.8	46.4	53.4	61.6	46.1	14.1	-	-
10^6 $(r_{T1}-r_{T2})/R_oG_1$		956	891	1025	1182	1255	1728	-	-
10^6 $(E_1 - E_2)$ K/G_1		1970	2069	296	2118	2427	3476	-	-
10^6 $(G_1 - G_2)$ e_2/G_1		3	3	-10	-10	21	-16	-	-
$e_1 - e_2$ (Equ. 1, Microstrain)		1011	1175	-719	946	1151	1764	-	-

Cycle No.		7							
Burner Run No:		5							
Cum. Time At T1:		24 min.							
Cooling time t_x:		30 sec.							
$(TT4)_1$		1255K							
$(TT4)_2$		955K							
TT3		710K							
Location			C			B	A		LIP
Orientation		HOOP	HOOP	AX.	AX.	HOOP	HOOP	AX.	- -
Gage No.		1	2	7	8	3	5	9	-
Thermocouple No.		51	52	51	52	53	55	55	57
T1	(K)	761	761	761	761	777	1041	1041	1072
T2	(K)	722	722	722	722	722	819	819	833
Predicted e_1	(Microstrain)	556	556	-2004	-2004	2730	-419	911	-
Predicted e_2	(Microstrain)	201	201	-699	-699	981	-172	328	-
Predicted e_1-e_2	(Microstrain)	355	355	-1305	-1305	1750	-247	583	-
$(T_1-T_2)/t_x$	(K/sec.)	1.30	1.30	1.30	1.30	1.83	7.40	-	-
10^6 $(r_{T1}-r_{T2})/R_o(T1-T2)$		55.9	53.1	56.3	60.6	58.9	39.7	-	-
10^6 $(r_{T1}-r_{T2})/R_oG_1$		1073	1019	1079	1162	1605	4856	-	-
10^6 $(E_1 - E_2)$ K/G_1		2069	2266	394	2364	2477	4084	-	-
10^6 $(G_1 - G_2)$ e_2/G_1		3	3	-10	-10	21	-16	-	-
$e_1 - e_2$ (Equ. 1, Microstrain)		993	1244	-675	1212	851	-756	-	-

FIG. 29 PREDICTED AND MEASURED STRAINS

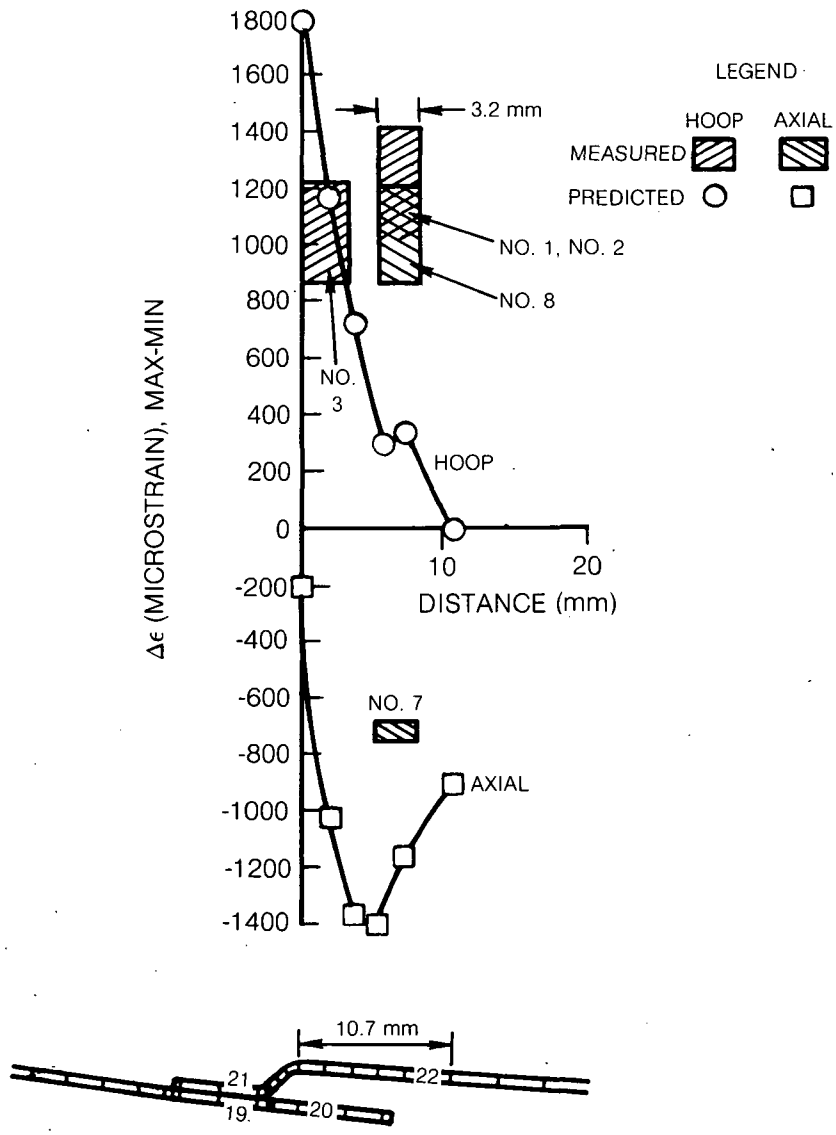

PREDICTED MECHANICAL STRAIN RANGE (USING "AVERAGE" TEMPERATURES) AND MEASURED STRAIN RANGE (USING KANTHAL A-1 GAGES) DURING BURNER CYCLES 4, 5, 6, 7.

84-4-18-31

TT3 was approximately 700K throughout these seven test cycles. At the high-power point the temperature T1 at locations B and C was near 800K, and at location A was near 1040K.

The predicted values of ε_1 and ε_2 were calculated by the analytical technique of NAS3-21836 which was based on a model of the burner liner, the measured temperature at the lip (thermocoule No. 57) listed in Table 10, and the measured temperatures at locations A, B, and C, listed in Table 10 at each operating point.

The measured strain change $\varepsilon_1-\varepsilon_2$ during each deceleration was calculated from the strain gage data and thermocouple data, using equation (1). The correction terms $(r_{T1} - r_{T2})/R_oG_1$ and $(G_2 - G_1)\ \varepsilon_2/G_1$ in equation (1) were evaluated as follows:

(a) Gage factors G_1 and G_2 were calculated from equation (4).

(b) The predicted value of residual strain ε_2 was used in evaluating the correction term $(G_2 - G_1)\ \varepsilon_2/G_1$ in equation (1). This correction term was less than 25 microstrain in every case, and is listed in Table 10.

(c) The correction due to temperature, $(r_{T1} - r_{T2})/R_oG$, was determined as follows. First the temperatures T1 and T2 at each gage location, the deceleration time t_x, and the cumulative time at the high temperature T1 were noted and listed in Table 10 for each gage in each cycle. The cool-down rate, $(T1-T2)/t_x$ was then calculated and entered in the table. Given all this information, interpolation in Table 8 was then used to select an appropriate value of $(r_{T1} - r_{T2})/R_o(T1-T2)$ for each gage in each cycle. The value of $(r_{T1} - r_{T2})/R_oG1$ needed in equation (1) was then calculated by multiplying by (T1-T2)/G1. This value is also listed in Table 10.

Hoop Strain, Measured Versus Predicted

At the forward location (A) the measured hoop strain increments (Table 10) scatter over a range of ±2000 microstrain from test to test confirming that the gages (5 and 9) at this forward location were unreliable after the exposure to severe overtemperature during the first burner cycle (Table 10).

At the center location (B), the measured hoop strain is consistently in the predicted direction (tensile) with magnitude averaging about eighty percent of the predicted 1200 microstrain (Fig. 29). During the final four cycles the two sigma scatter was 268 microstrain.

At the aft location (C) the measured hoop strain is consistently in the predicted direction (tensile) with magnitude larger than the predicted 350 microstrain by a factor of about 3.4. During the final four cycles the two-sigma scatter of all measurements of hoop strain at this location, with gages 1 and 2, was 314 microstrain. The two-sigma scatter for gage 1 alone was notably small: only 52 microstrain.

Axial Strain, Measured Versus Predicted

Measurements of axial strain increments were obtained at the aft location (C) only. No axial gages had been installed at the center location (B), because only small axial strains were expected there. The axial gages at the forward location (A) were open and not repairable after the exposure to severe overtemperature during the first cycle.

The strain increments measured with the two gages at the aft location (C) were surprising in that one gage (no. 7) consistently indicated about 700 microstrain in compression while the other gage (no. 8) consistently indicated about 1000 microstrain in tension. The predicted value was 1200 microstrain in compression. The repeatability of measurements with each gage was excellent (Table 10 and Fig. 29). In fact, during the final four cycles the two-sigma scatter for gage no. 7 was only 52 microstrain and for gage no. 8, 270 microstrain. The indicated difference in axial strain increment at the two locations is believed to be real, and may be associated with circumferential temperature gradients at the liner lip (even though the temperatures at the two gage locations were the same). To help resolve this question thermocouples should be installed at several locations around the periphery of the liner lip in future tests to permit quantitative prediction of nonuniformity in strain.

Summary of Failure Modes

All four gages at the forward location (A) on the burner liner failed during the burner test program, and there were no other failures throughout the program. The four failures occurred during exposure of location (A) to severe overtemperature in the first burner test cycle. The overtemperature was undetected during this first cycle because both thermocouples at this location also failed. The thermocouples were repaired after the second cycle and it was then found that temperatures were above 1040K at this location during every test cycle (Table 10). Since the temperature at locations (C) and (B) on the liner were higher during the first cycles than during any succeeding cycles, it is certain the gages at location (A) were exposed to temperatures above 1040K during the first cycles.

Table 11 describes the failure mode for each of the four failed gages. Three were characterized by a loss of strain signal (open circuit) early in the burner tests. The fourth was characterized by an erratic signal ranging

from +2240 microstrain to -1830 microstrain (gage no. 5, Table V). All of the failures were the result of cracking or disintegration of cement, previously discussed in Section 5.3.2.2.

In the fifth strain gage channel (gage no. 4, Table V), no change in output voltage occurred during the last six cycles of burner testing. Post-test thermal cycling in the laboratory revealed that the gage (like gages 1, 2, 3, 7 and 8) was intact and behaving normally as shown in Fig. 23. Destructive examination showed sound cement and no reason to suspect poor strain transfer. The absence of any output signal during the last six cycles of burner testing was attributed to a malfunction of the data system or a poor connection in the external wiring.

TABLE 11. Summary of Gage Failures

Location	Type	Gage No.	Remarks
Forward (A), right	Hoop	6	Open gage grid occured when cement overcoat cracked at about 1040K (1410°F) in first test in burner. Not repairable.
Forward (A), right	Axial	10	Open gage grid occurred when cement overcoat cracked at about 1040K (1410°F) in first test in burner. Not repairable.
Forward (A), left	Axial	9	Open circuit at splice of third lead (one of two common) occurred at about 1040K (1410°K) in first test in burner. Not repairable. Post-test destructive examination revealed severe crumbling of cement beneath the surface. The gage was loose inside the cement.
Forward (A), left	Hoop	5	Erratic strain readings after exposure at about 1040K (1410°F) in first test in burner. Post-test destructive examination revealed severe crumbling of cement beneath the surface. The gage was loose inside the cement.

6.0 CONCLUSIONS

The following conclusions may be drawn from the results of this test program.

Speckle Photogrammetry

Speckle photogrammetry can be accomplished in the severe environment of a jet burner test stand with high reliability. A major problem was encountered in the form of large, random values of apparent strain generated by the optical inhomogeneities of the hot, high-pressure gases flowing past the combustor under operation. The most likely way to overcome this difficulty would be to record three specklegrams simultaneously from three angular directions and subtract the effects of gas perturbations after data processing. It may be concluded, however, that speckle photogrammetry can be applied to applications where pressures are less than three atmospheres.

Kanthal A-1 Gages

Strain gages made from Kanthal A-1 wire can be successfully employed in burner liner strain measurements provided they are protected from temperatures higher than 977K. Careful attention to the application of ceramic cement is required, especially during the ladder taping sequence, to assure proper functioning of the gages. The individual gages, as installed on the test object, must be subjected to temperature calibration for apparent strain after a minimum of one hour preconditioning at 977K. The removal of a section of a burner for instrumentation and calibration makes this practical if the section can be welded back into place for subsequent testing. Strain measurements must be limited to strain change during rapid cooling of the test section in order to minimize apparent strain corrections and obtain best repeatability. Detailed comparison with computer modeling of strain fields will require more detailed mapping of temperature patterns to assure that assumptions of symmetry are valid.

7.0 REFERENCE

1. Bertodo, R., "Resistance Strain Gauges for the Measurement of Steady Strains at High Temperatures," Proc. Instn. Mech. Engrs. v178, pt 1, no. 34, pg. 907, 1964.

8.0 APPENDICES

8.1 Appendix A

Description of the Experiment Design and Test Plan Formulation

I. Test Facility

The experimental program will be conducted in the UTRC Jet Burner Test Stand (JBTS) on the Cell 1 - East test centerline. The airflow rate satisfying the test conditions will be supplied by an existing 2.7 MPa air supply system and heated by indirect-oil-fired and electrical heaters plumbed in series. A calibrated venturi will be used to meter the flow. The heated air will flow through the facility components including: plenum, space-spools, test section, instrumentation rings, and exhaust "T" section with backpressure valve. Jet A will be the test fuel. It will be delivered to the test cell from underground storage tanks by positive displacement pumps generating pressures up to 10 MPa and metered by a Micro-motion mass flowmeter.

The model combustor will be a louver-cooled, cylindrical combustor with an inside diameter of 12.7 cm and overall length of 41 cm. It consists of a dome (with appropriate fuel injector and igniter mounting bosses) and six air-cooled louvers. The device is constructed from Hastalloy-X with typical material thickness of 0.7 mm. The combustor will be identical to the one designed and operated as part of NAS3-23167, "Aviation-Fuel Property Effects on Combustion." Liner temperature measurements obtained in that program indicate that regions within the limits of the strain gage device (950K) exists along each louver. Laser speckle photography will be used not only to obtain comparative data in these regions but also to measure liner strain in regions where the metal temperature approaches 1100K. This will be accomplished by providing a hole through the outer louver metal to view the inner louver lip.

The combustor model will be concentrically mounted in a section of nominal 15 cm pipe with provision for support arms connected to the dome and a sliding seal at the exit of the combustor. A schlieren-quality fused quartz window mounted on this test section will provide a 7.6 cm diameter viewing area of the liner. This port will be centered on the knuckle of the third louver, midway between the rows of combustion air holes.

II. Test Stand Procedures

The test program will be conducted in the JBTS following standard operating procedures. Each day the data acquisition system will be set up. This activity includes checking the calibration of pressure transducers, verifying reference values of the thermocouple scanners and recording the appropriate facility preparation and checkout activity (opening of proper isolation valves, arming electrical systems, establishing control gas pressure levels, etc.) will be executed.

The test activity will be initiated by establishing the appropriate airflow rate and at several predetermined levels of air temperature. These non-combustion conditions will provide reference values necessary to reduce the photographic data. The combustion tests will begin by igniting the combustor on Jet A fuel. Previous experience indicates that for inlet air temperatures greater than 700K, spontaneous ignition will be achieved. Hence, the fuel flow rate can be sufficiently low to prevent the occurrence of high liner temperature excursions. Liner thermocouples will be monitored while the fuel flowrate, air and preheat and backpressure valves are adjusted to achieve a desired high metal temperature (less than 950K for locations near the resistance-wire strain gauges) and a combustor pressure of 1.3 MPa. It is estimated that one to two minutes of operation will be required to achieve this high-power condition. Three successive sweeps of the data system will be acquired (approximately two minutes duration).

A series of test cycles will be promptly initiated. Each cycle will include a simulated deceleration of a low-power condition, a dwell period to acquire data, a simulated acceleration to the high power condition followed by another dwell to acquire data. The simulated deceleration will be achieved by a fuel flow reduction to a level corresponding to an idle fuel-air ratio. In order to achieve a rapid deceleration, only the fuel flow will be adjusted. The total airflow and inlet air temperature will be held constant while the burner pressure will decrease proportionally to the fuel flow reduction. This approach will permit achieving the simulated deceleration within one minute. A corresponding rapid increase in fuel flow will be followed during the simulated acceleration. Three data points will be acquired in each dwell, resulting in a complete cycle time of approximately five minutes. The fuel flow will be terminated at the conclusion of the cycling and the test rig permitted to cool down. The rig will be subsequently disassembled to permit inspection of the strain gages.

III. Aspects Concerning Speckle Photography of a Burner Liner

1. Laser Power Requirements

The laser power required to photograph a combustor liner may be estimated from photographs recorded with a CW laser of heat blackened Hastelloy. These required in the order of 11 second exposures with a 50 milliwatt laser (HeNe) to properly expose Kodak type 130 plates. This comes to an integrated energy of 0.55 Joules.

Type 130 plates are specially sensitized for HeNe laser wavelength (633 nm) and are not usable at ruby laser wavelength (694 nm). The most suitable plate for ruby laser radiation is AGFA-Gevaert type 10E75 which is five times slower than the type 130 plates. Type 10E75 plates would require about 2.75 Joules for proper exposure.

Preliminary experiments with the UTRC Korad Laser have shown that an open-cavity laser pulse, which has many axial and transverse modes, is adequately coherent for speckle photography. Specklegrams of a blackened Hastelloy X sample were obtained that showed excellent correlation with separate laser pulses. The use of an open cavity laser will greatly simplify laser alignment, improve reliability, and increase the amount of power obtainable. The specklegrams were recorded with Kodak type 120 plates which are eight times slower than 10E75 plates. This indicates an output from this laser of 10 to 20 Joules. It is concluded that this laser will be suitable for the contract work.

2. Exposure Time Requirements

The length of the laser pulse determines the object velocity that may be tolerated during the exposure. If the object moves too rapidly in a transverse direction, the speckles will become blurred and information will be lost. The pulse width from an open cavity ruby laser is generally less than 1 millisec. The speckles to be photographed will be in the order of 20 micrometers minimum in their spatial period. If motion is required to be less than 1/5 that during a 1 millisec interval, this establishes a maximum velocity of 4 mm/sec. The type of motion most likely to occur is vibration at a low frequency. A representative frequency of 10 Hz would have to have an amplitude of less than 0.005 inches peak-to-peak to assure that its peak velocity was less than 4 mm/sec. Estimates of rig stability indicate that this tolerance can easily be met.

3. Pulse Synchronization

A brief study has been conducted of the shutter mounted within the UTRC Telecentric Lens. This shutter has an electronic flash attachment which has

been accessed and to which a connector has been attached. This output consists of a switch that closes when the shutter is fully open, and this type of arrangement has been used before at UTRC to provide the voltage pulse to the Korad laser for firing. An additional circuit will be designed to provide a delayed command to the film plate advance mechanism to avoid double exposure.

4. Remote Changing of Plates

An automatic Photo-Plate Changer made by Spectron Development Laboratories, Inc., has been requested as a capital equipment acquisition and its use is planned on this contract. It will hold 24 plates and will allow plate changing at a rate of 10/min. This unit will easily meet the focal plane tolerance requirements for speckle photography.

5. Burner Viewing Port

Discussions with Aerothermosciences Staff has resulted on the choice of a window and port configuration for the test cell. A commercially available viewing port assembly will be used to assure safe and reliable mounting of the optical quality window. The window will be 1.0 inch thick fused silica, sized to fit into the viewing port. It will be located approximatey two inches from the burner liner to its inner surface. Illumination will be directed toward the window from a mirror lying just outside the lens aperture. This will cause the window reflections to enter the lens at an angle that is outside the acceptance cone defined by the internal aperture of the lens. Only secondary reflections (i.e., window-lens-window) will be able to pass through the lens, and these may be reduced to an acceptable level by anti-reflection coating of the window.

6. Laboratory Checkout of Equipment and Procedures

Specific items that will require laboratory checkout are:

a) the use of the lens-shutter flash-switch to fire the pulsed laser,

b) the use of the pulsed ruby laser, in open cavity configuration, to illuminate the object,

c) the illumination and observation of a cylindrical object surface behind a thick window, and

d) the use of an automatic plate changer to cycle the photographic plates.

Checkout of these systems and operations can be accomplished by the layout of the components on an optical component pallet in the laboratory.

The system can then be used to make specklegram recordings of a simulated section of burner liner behind a window with a pulsed laser. The recordings can be evaluated for speckle correlation and apparent strain. The setup of the components on an optics pallet will serve as a prototype for the arrangement that will be installed at the burner stand.

7. Test Stand Installation and Checkout

A mounting fixture will be fabricated from angle stock to provide a stable support for the optics pallet and to allow positioning at the proper location relative to the test cell. A cover will be fabricated for the optics pallet to keep dirt and oil mist out of the optical components. The laser head, which will be mounted on the optics pallet, will be provided with a dry nitrogen purge to prevent condensation of water on the laser rod or accretion of particles on the mirrors. Such material can be explosively vaporized upon laser firing with a destructive effect to the laser. A solenoid will be used to actuate the lens shutter and fire the laser from a remote distance.

The system will be checked out by first recording specklegrams of the burner at ambient temperature, with and without air flow. These will be developed and examined for correlation. They may also be analyzed subsequently for apparent strain as a check upon the data processing. After the successful recording of specklegrams at ambient temperature, a short sequence of specklegrams will be recorded while the burner is heated to 500K, 700K, and cooled back to 500K, and then back to ambient temperature. These also will be examined for correlation and stored for subsequent data processing. If not, the temperature differences will be made less so that better correlation is obtained.

8. Test Sequencing

In the actual test sequences, the burner will be heated isothermally (by inlet air temperature) from ambient temperature to 700K with a short dwell time at each intermediate temperature to establish equilibrium. The dwell time may be only a matter of 10 seconds, depending upon the thermal inertia of the burner. After a recording has been made at 700K, the fuel will be introduced at a low level and it will spontaneously ignite. The inlet air temperature may be reduced at this point to minimize the overall temperature changes before the next specklegram is recorded. At this point, the test cycling will begin and the fuel flow will be used to cycle the burner temperature through the desired sequences. Specklegrams will be recorded before, after, and at the middle of each heating and each cooling phase for detailed monitoring of the cyclic strains. These phases will be of one minute duration so that the laser capacitor bank may be recharged in time for the mid-point recording.

There will be no dwell at the mid-point recordings, but rather, they will depend upon the short exposure (about one millisecond) to stop any motion. The total number of specklegrams for any run will be limited to 24 by the capacity of the plate changer.

A minimum of four plates will be required before cycling so that with six recordings per cycle, detailed study of the cyclic stresses will be limited to three cycles.

Alternative tests will also be conducted in which the number of specklegrams per cycle will be two, one before the heating phase and one before the cooling phase. With this program, ten cycles may be examined. The strain difference between the high and low temperature states of the burner may make it impossible to extract strain data between these pairs, but data may be obtained on the strain history from cycle to cycle by comparison of subsequent high temperature specklegrams and subsequent low temperature specklegrams. Finally, tests can be conducted with only one specklegram per cycle so that a total of twenty cycles can be examined.

9. Data Processing

After the testing has been completed and suitable sets of specklegrams have been obtained, the optics equipment will be removed from the test stand and the specklegrams will be processed for strain data. Biaxial strain measurements will also be made in the unobstructed central area at a number of locations including the weld region, the knuckle, the region downstream of the knuckle, and the louver lip (through the viewing hole). Use will be made of the semi-automated readout features that are currently being added to the UTRC Heterodyne Photocomparator. Data will be logged on an HP 85 computer and provisions will be available for plots of strain versus burner coordinates.

IV. Resistive Strain Gage Experiment Design and Test Plan

1. Overview

Ten Kanthal A-1 1/8" resistive static-strain gages will be installed on a JT12D burner liner and demonstrated in the UTRC Jet Burner Test Stand. The gages will measure hoop strain at three locations (A, B, C, which are the weld region, the top of the knuckle, and above the end of the louver lip) along the outer wall of the liner, and axial strain at two of these locations (A, C). the region instrumented is centered on the third segment knuckle (location B). The region is one of principal interest to structures analysts, since maximum tensile hoop strains are expected at location B, (about +2200 microstrain) and maximum compressive axial strains at C (about -1800 microstrain). The strains are expected to be lower at B and of opposite sign at A.

The region is favorable to resistive static-strain gage measurement by the proposed technique because maximum temperature is expected to be below 950K when the temperature of the inner lip of the liner is at the maximum planned temperature of 1144K (location D).

A region 64 mm in diameter, including locations A, B, C, and D, will be viewed by the laser speckle system. All ten resistive gages will be within the viewed region. A hole 7 mm in diameter through the outer liner will provide a view location D for the laser speckle system.

The ten gages will be arranged in two groups of five. Each group of five will provide measurement of hoop strain at three axial locations (A, B, C) and axial strain at two axial locations (A, C). Measurement of axial strain is omitted at location B, the location where least axial strain is predicted. In this way, 100 percent redundancy of all strain measurements is attained without exceeding the total of ten gages dictated by cost considerations and space limitations. Six Type K thermocouples will be installed close to the strain gages to provide redundant temperature measurements at each location (A, B, C). One additional Type K thermocouple will be attached to the louver lip near location D.

2. Test Cycles

Acceleration and deceleration will be accomplished in one minute and dwell will be from one to five minutes duration. Eight data points will be taken within each cycle to determine the indicated strain versus temperature characteristic within each cycle. Data points will be taken during at least two successive cycles to each selected operating point to assure establishing the strain gage reference calibration condition. Data points will then be taken on several additional cycles to each operating point to characterize the shift of residual strain in the liner with cycling. Two operating points will be investigated, the first providing a maximum indicated temperature between 922K and 950K. The maximum temperature at the low-temperature end of each test cycle will be as low as possible, consistent with stable and repeatable operation of the burner, and will be determined in initial trials. It is anticipated that minimum temperature will be near 590K.

3. Strain Gage Installations

The Kanthal A-1 wire static-strain gage installation to be employed will be the installation that was proved durable in previous P&W-CE burner installations and in NAS3-22126 laboratory tests (at UTRC and P&W-CE) to 977K.

4. Resistive Strain Gage Data Acquisition

For acquisition of resistive strain gage data, it is planned to use the UTRC WISARD (Wide-band System for Acquisition and Recording of Data) system. This system has a main scanner and can incorporate subscanners to accommodate various types of data signals, such as temperature, pressure and strain. The acquisition rate depends on the quantity and type of data to be recorded, but will require about five seconds per reading for the parameters needed in the planned burner test.

The WISARD system has data processing capability to convert to engineering units, compensate for thermal zero shift and provide print and plot data output form.

A strain gage bridge and balance console is to be provided by P&W Commercial Engineering. It is planned to use 1.5 volts excitation in a Wheatstone bridge circuit. This will result in about ~9 mv output for ~10,000 microstrain full scale. Amplifiers (Preston Scientific, Inc.) are used in the WISARD system to increase the signals to the required 9 v input level.

5. Preliminary Calibration of Gages

Commercial Engineering will fabricate the ten Kanthal A-1 wire resistive strain gage systems on a piece cut from the liner, and will fabricate a two reference Kanthal A-1 wire resistive strain gage system on a flat test bar of the same material as the liner.

Commercial Engineering will perform a two-hour prestabilization heat treatment of all strain gage systems at 964K and measure apparent strain versus temperature for all strain gage systems on the piece cut from the burner liner, and measure gage factor versus temperature for the two reference strain gage systems. Apparent strain tests will be conducted at fast cooling cycles simulating the cylical rates to be used during the combustor test.

At the conclusion of this preliminary testing, the piece cut from the liner will be reinstalled by tungsten inert gas welding which will ensure that no portion of the strain gage system will be heated to a temperature above the strain gage prestabilization temperature. The liner will meet FAA patch repair requirements for form, fit, and structural integrity after reinstallation of the gaged piece.

6. Post-Test Analysis

After completion of the combustor tests, a post-test evaluation of the gage system will be conducted, including:

a) visual examination and photographs,

b) measurement of gage loop resistance and resistance to ground at each lead wire,

c) measurement of the apparent strain as a function of temperature (after again cutting the instrumented section out of the liner),

d) failure analysis on any failed strain gages.

8.2 Appendix B

In section 5.3.1, specklegram data was reduced by means of the interferometric photocomparator. The x coordinate of the photocomparator corresponded to the axial direction on the burner and the y coordinate to the circumferential (or hoop) direction. Let the image displacements in these directions be u and v respectively. The photocomparator measures the rate of change of both of these displacements with respect to x and y and results in four values, A, B, C, and D. If partial differentiation is denoted by a superscript variable, the following four equations define the values measured by the photocomparator:

$$A = u^x,\ B = u^y,\ C = v^x,\ D = v^y. \qquad (1)$$

A is the hoop strain and D is the axial strain, however, there may be additional strain in the form of shear equal to (B+C)/2. In-plane rotation, if present, will equal (C-B)/2. For any pattern of strain and shear, there exists a coordinate system in which the shear term will vanish leaving strain that is aligned with the coordinates only. This is called the principal coordinate system and the resulting strains are called principal strains. For two-dimensional strain, the principal coordinate system is related to any other surface coordinate system by rotation about the surface normal. The principal coordinates are also the directions in which the most extreme values of strain will be observed. Thus, two-dimensional strain patterns are most easily understood terms of principal strains and their corresponding orientations. The following is a derivation of the equations for making this conversion.

Refer to Fig. 30 which shows coordinate system x',y' rotated with respect to coordinate system x,y by an angle θ. The vector from the origin O to the point P is invarient with respect to coordinate system, but has different values for its components depending upon the coordinate system into which it is resolved. Let us call these two representations $\{R\}$ and $\{R'\}$ respectively. They are related by a coordinate transformation $[T]$ as follows.

$$\{R\} = [T]\ \{R'\}, \text{ or } \{R'\} = [T]^{-1}\ \{R\} \tag{2}$$

where

$$[T] = \begin{bmatrix} \cos\theta & -\sin\theta \\ \sin\theta & \cos\theta \end{bmatrix},$$

and $[T]^{-1}$ is the inverse of $[T]$, which, because it is a coordinate transformation, equals the transpose of $[T]$. The transformation $[T]$ rotates the primed coordinate system clockwise through the angle θ into the unprimed coordinate system.

If strain is present, the point P will be displaced relative to the origin by a vector $\{\delta\}$. Expressed in terms of the vector $\{R\}$ and the strain matrix $[\varepsilon]$, the displacement becomes

$$\{\delta'\} = [\varepsilon]\ \{R\}\ . \tag{3}$$

If both vectors in Eq. (3) are transformed to the primed coordinate system, the result is

$$\{\delta'\} = [T]^{-1}\ \{\delta\} = [T]^{-1}\ [\varepsilon]\ [T]\ \{R'\}\ . \tag{4}$$

The product of three matrices in the righthand side of Eq. (4) relates to the transformed vectors in the same way that the strain matrix did to the

FIG. 30 AXES FOR COORDINATE ROTATION

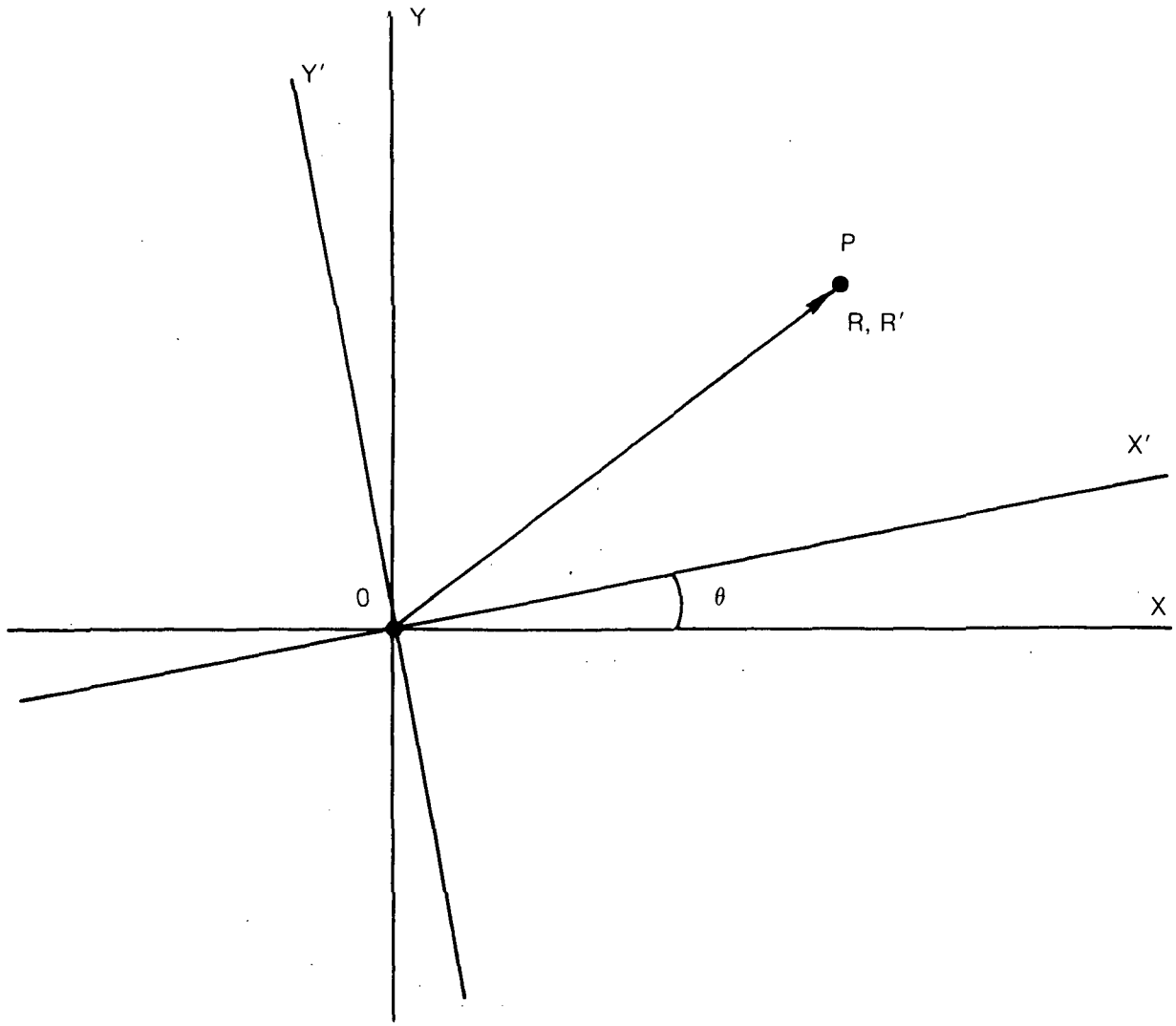

84–4–18–33

untransformed vectors in Eq. (3). It is, therefore, the strain matrix in the primed coordinate system, and we may write

$$[\varepsilon'] = [T]^{-1} [\varepsilon] [T] . \tag{5}$$

This rotates the strain matrix counterclockwise through the angle @@ from the unprimed to the primed coordinates.

When the strain matrix is rotated into its principal coordinate system, the sum of its off diagonal elements will be zero. If the values of [@] are A, B, C, that is,

$$[\varepsilon] = \begin{bmatrix} A & B \\ C & D \end{bmatrix}, \tag{6}$$

then it is possible to derive the following formulae for the angle between the initial and the principal coordinate system:

$$\theta = (1/2) \tan^{-1} (C+B)/(A-D) . \tag{7}$$

Once this is known, the principal strains can be solved as:

$$A' = A \cos^2\theta + (B+C) \sin\theta\cos\theta + D \sin^2\theta . \tag{8}$$

and

$$D' = A \sin^2\theta - (B+C) \sin \cos + D \cos^2\theta . \tag{9}$$

θ is the angle from the original x axis to the x' axis of the principal coordinate system. A' and D' are the x' and y' strains in the principal coordinate system.

When strain values from a number of locations are to be averaged, it is necessary to perform this operation in one coordinate system, in this case the original x,y system of the photocomparator. The result may then be transformed into its own principal coordinate system. Similarly, standard deviations must also be computed in a single coordinate system. Because standard deviations cannot be negative, however, their transformation into a principal coordinate system merely computes the maximum error value they can generate.

Appendix C

Heterodyne Speckle Photogrammetry

The purpose of this appendix is to provide background on the technique of heterodyne speckle photogrammetry for high-temperature strain measurement. Photographs of objects lit by laser light, which may be called specklegrams, have been used since 1970 for measurement of object displacements.[1] The image speckles, which result from diffuse reflection of coherent light, move as if attached to the object surface when that surface is in focus, and they form a high contrast image pattern which uniquely defines each region of the object surface. Specklegrams are commonly recorded as double exposures, before and after an object displacement.

Evaluation of a double-exposure specklegram is commonly done by passing a narrow, converging beam of light through a small region of the specklegram and observing the optical Fourier Transform (often called a halo) displayed where the beam comes to focus. Lateral displacements between the speckle patterns resulting from the two exposures generate in fringes in the transform plane that uniquely define the speckle displacement. The difference between speckle displacements at neighboring regions can generally be related to strain.

The double-exposure specklegram technique has limitations, however. First, the displacement range is limited by the need to measure fringes in the transform plane. The displacement must be large enough to generate at least one or two fringes but cannot be so large as to generate more than about twenty five. Thus strain measurement can be hampered by large bulk displacements that accompany the object deformation. A dual-plate technique, where singly exposured plates are overlayed to generate halo fringes, was developed to deal with this problem.[2] Next, the accuracy with which halo fringe spacing and orientation may be measured is limited to one or two percent. This requires specklegrams to be recorded with low f/number lenses in order to obtain high resolution of object displacements. On the other hand, such lenses reduce depth of focus and cause errors due to defocusing.

Heterodyne readout of halo fringes was proposed in 1980 as a method of overcoming many of the limitations of conventional specklegram techniques.[3] Halos from separate specklegram plates are combined in an interferometer to obtain the halo fringes, which are set into continuous motion by a Doppler shift between the two beams of the interferometer. Fringes are read as the phase of electonic signals obtained by photodetectors in the output plane. The accuracy of fringe measurement can be improved by one to two orders of magnitude in this way. Because the heterodyne interferometer compares the image of one specklegram with that of the other, the system can be referred to as a heterodyne photocomparator.

Heterodyne interferometry is well suited to strain measurement from pairs of single-exposure speckle photographs. A system has been developed at UTRC for this purpose, and it has been discussed in the literature.[4] This system has measured strain patterns from photographs of Hastelloy X samples at temperatures up to 873°C in laboratory setups.

References

1. Archbold, E., J.M. Burch, and A.E. Ennos, "Recording of In-Plane Surface Displacement by Double-Exposure Speckle Photography", Optica Acta 17(1970)883.

2. Adams, F.D. and G.E. Maddux, "Dual Plate Speckle Photography", USAF Technical Memorandum, AFFDL-TR-75-92.

3. Smith, G.B. and K.A. Stetson, "Heterodyne Readout of Specklegram Halo Interference Fringes", Appl. Opt. 19(1980)3031.

4. Stetson, K.A., "The Use of Heterodyne Speckle Photogrammetry to Measure High-Temperature Strain Disbributions", Holographic Data Nondestructive Testing, D. Vukicevic, Ed., Proc. SPIE 370(1983)46.